Order Number 9003201

An integrated computer-aided engineering approach for engine cylinder block analysis using HEXA8 finite elements

Lee, Seungkuh, Ph.D.

The University of Michigan, 1989

U·M·I
300 N. Zeeb Rd.
Ann Arbor, MI 48106

AN INTEGRATED COMPUTER AIDED ENGINEERING APPROACH FOR ENGINE CYLINDER BLOCK ANALYSIS USING HEXA8 FINITE ELEMENTS

by
Seungkuh Lee

A dissertation submitted in partial fulfillment
of the requirements for the degree of
Doctor of Philosophy
(Mechanical Engineering)
in The University of Michigan

1989

Doctoral Committee :

Professor Noboru Kikuchi, Co-Chairperson
Professor Donald J. Patterson, Co-Chairperson
Professor Joe G. Eisley
Professor Richard A. Scott

To my dearest parents,
and
To my wife, Yoon-Mi,
and
our children, Jane and Paula-Jihoon

ACKNOWLEDGMENTS

I wish to express my sincere thanks and gratitude to my advisors, Professor Noboru Kikuchi and Professor Donald J. Patterson, for their profound guidance and continuous encouragement during my study at The University of Michigan. Their invaluable suggestions and endless desire to pursue new ideas in engineering mechanics and computational mechanics has been a great inspiration at various stages of this work.

I also would like to extend my special thanks to the members of my advisory committee, Professor Joe G. Eisley and Professor Richard A. Scott, for serving on my doctoral committee and for their generous suggestions and constructive criticism.

This study is supported by Daewoo Heavy Industries, Ltd., Inchon, Korea through their grant: DRDA-388719. I would also like to thank the company for their kind consideration which allowed me to study in the United States. Especially, Dr. Youngkook Kang and Dr. Nagyoung Chang at the company gave me their incessant encouragement.

I would also like to thank the Mechanical Engineering Program of The University of Michigan for their warm academic environment and CAEN (Computer Aided Engineering Network) for their support of excellent computing facilities, especially the Calma VAX Laboratory, which made it possible to complete my work.

Special acknowledgement is due to my colleague, Dr. Byeong Cheon Koh for his enthusiastic help. Significant help and encouragement of Mr. Ho Sung Lee in the experimental work is gratefully acknowledged. I am also indebted to my colleagues and friends for their invaluable suggestions and encouragement; Dr. Somnath Gosh, Mr. Toshikazu Torigaki, Dr. Helder Rodrigues, Mr. Byung Bae Yoon, Mr. Jose Miranda Guedes, Mr. Weng-Lang Tsai, Mr. Akira Tezuka, Mr. Gerald High, Mr. Yasu Umezu, Dr. Toshimichi Fukuoka, Mr. Katsu Suzuki, Dr. Nobuki Yukawa, Mr. Shinji Nishio, Mr. Jieh-Yeng Sun, and those whom I share many emotional moments and memory with. My special acknowledgement goes to Mr. Gene McNay, who read and corrected my script with patience.

Finally, I sincerely thank my beloved wife, Yoon-Mi for her extreme self-sacrifice and support, and our beautiful children, Jane and Paula Jihoon, for their patience, support and the joy they brought me.

TABLE OF CONTENTS

LIST OF FIGURES

Figures

LIST OF TABLES

LIST OF APPENDICES

CHAPTER I

INTRODUCTION

With the advent of high speed computers, engineers have a tool to solve the mathematical equations which represent the thermal and mechanical behavior of complex engine structures. In particular, the finite element method allows computer simulation of the mechanical and thermal behavior of various engine components in the design stage.

Since the finite element method was first applied to engine analysis in 1972[1], numerous results have been published[2-10]. It has been shown that the finite element method is capable of modeling complex structures, such as engine cylinder blocks, accurately. Finite element modelling allows a particular design to be evaluated and improved without building a prototype.

As market needs change, the engine industry is faced with the task of developing new engines to meet such needs in a timely fashion, and at the lowest possible cost. Therefore, it is increasingly necessary to reduce analysis costs in the process of designing an engine and to integrate various analysis procedures. There are several categories of analysis, including stress, dynamic and thermal analyses. In past research, different finite element models of an engine have been used for each of these analyses. An engine has been modeled, in general, using either 8-node or 20-node solid elements for the thermal and stress analyses, while it was modeled using 4-node plate and shell elements for dynamic

analysis. This approach was inefficient because different finite element models of the same structure had to be developed. In order to reduce the time and the cost for analysis and simulation of a particular design, it is essential to reduce the duplication of effort required to develop different finite element models for different analyses. One solution is to integrate various activities such as design layout, geometric modelling, and design analysis based on a common geometric description. Solid modeling is a popular method to define geometry. Commercially available software packages allow the solid model to be manipulated to form detailed design and finite element meshes.

In generating finite element meshes, it is necessary to generate three-dimensional solid elements without changing the basic geometric representation used by the solid modeler. 8-node hexahedral(HEXA8) elements or 4-node tetrahedral(TETRA4) elements are the simplest elements to fulfill this requirements. This approach, using simple solid elements to develop a three-dimensional solid finite element model of a rather complex geometrical structure, is rapidly replacing conventional model development methods which use higher order finite elements such as 20-node hexahedral(HEXA20) elements. A significant time saving may be realized by using the simplest element to generate a finite element model. The HEXA8 element is one of the best candidates to be used in this regard.

Therefore, a finite element model of a complex structure such as an engine cylinder block is developed using simple, HEXA8 finite elements. These elements are simplified in order to achieve shorter computing time necessary to form the stiffness matrices as well as to increase accuracy for stress, and vibration analyses by examining the theories of mechanics and heat conduction for structures.

Even though it is more economical to use HEXA8 elements in developing a model for a complex geometry such as a cylinder block, they should not be used unless they can provide a sufficiently accurate solution. HEXA8 elements perform poorly in bending

dominated problems for thin shell-like structures in both stress and vibration analyses. To overcome this poor performance of HEXA8 elements, reduced integration methods have been applied to form the element stiffness matrices.

There have been some studies[21,22] to evaluate the stiffness matrix of HEXA8 elements. The method used in these studies is to "under-estimate" stiffness by applying a reduced integration method, i.e., one point integration is applied for the HEXA8 elements. However, this is not totally satisfactory, since this can activate spurious, non-physical modes. These are called hourglass modes in the literature. To eliminate these non-physical modes, an hourglass control method must be applied. By combining reduced integration with hourglass control, the HEXA8 elements can be used to accurately model a complex structure.

In chapter 2, the newly developed directional reduced integration (DRI) technique is applied to formulate element stiffness matrices, and to improve the accuracy of the finite element approximation for dynamic problems. To do this, the directional reduced integration technique with hourglass control studied in [20] is extended to dynamic problems. Results using this new formulation are compared with results obtained using traditional beam and plate elements.

In chapter 3, a finite element model of a diesel engine cylinder block is developed. It is analyzed using NIKE3D program[24] and its related codes[23,25,26], developed by John Hallquist at the Lawrence Livermore National Laboratory after substantial modification of these programs for the present study. The changes to NIKE3D involved the modification of the HEXA8 solid element by using the directional reduced integration method with hourglass control. It will be shown that these modifications provide reasonably accurate solutions to the eigenvalue analysis of a diesel engine cylinder block.

The computed results are compared with experimental modal analysis results. Dynamic characteristics of the cylinder block are discussed based on the computational results.

Although directional reduced integration with hourglass control can provide fairly accurate solutions, there is still some unacceptable error. This error may be due to either an inappropriate finite element mesh or to the numerical integration scheme used for time integration to solve the dynamic problem. To minimize such errors, the adaptive finite element method is introduced. It can be used to improve the approximation in the space and/or time frames in the present study. Therefore, the selection of an appropriate finite element idealization and choice of an effective time integration scheme are closely related.

In chapter 4, adaptive finite element methods are presented to reduce errors due to poor discretization. Based on the error, which is presented in chapter 2, we introduce adaptive methods and discuss how these are applicable to analyses of an engine structure.

When a time integration scheme is applied to solving dynamic problems, error is introduced during the integration process of the problem. It is known that the truncation error is a function of the time step used. Therefore, it is desirable to select a time step size at each time step which will minimize or reduce such error. Thus, a variable time stepping algorithm is considered in chapter 5.

There have been many time integration schemes developed to solve dynamic problems[59,60,66,76]. These methods have been verified and have been successfully applied in many different types of dynamic problems. Since NIKE3D employes the implicit Newmark-β method, our investigation is focused on implicit methods.

Most of numerical studies show a steady and rapidly increasing growth of error as the time step size increases. Stability and accuracy requirements suggest that it is important to control the error as well as to control the time step size for stability. Several variable-step

integration procedures have been proposed for both explicit methods[57, 58, 48, 59], and implicit methods by [60, 65, 63]. However, it is recognized in the literature that no satisfactory general approach is available. Furthermore, it is a difficult task to assess what the error will be for multi-degree-of-freedom systems for which the solution consists of a priori unknown combinations of modal response. It has become evident that there is a great need for an algorithm that can calculate the optimum time step in an automatic fashion during the solution process. Such an algorithm should reduce a significant amount of error while maintaining computational efficiency.

The method described in this work has many similarities to time step selection in the literature. It is based upon a local truncation error control technique using truncation error measure. However, it is modified to improve the accuracy and to reduce the possibility of instability that might occur during the time step size adjustment. It will provide a relatively fast and reliable solution by improving upon the effectiveness of traditional step size change techniques.

In chapter 6, an experimental modal analysis of a diesel engine cylinder block is performed. This analysis is conducted in order to obtain the dynamic characteristics of the cylinder block structure of the Daewoo-M.A.N. D0846HM diesel engine in the W. Lay Automotive Laboratory. Results obtained from modal analysis are used to verify the reliability and accuracy of the finites element analysis on the cylinder block which is discussed in chapter 3. The objective of experimental modal analysis, or modal testing, is to determine the modal parameters, which consist of; the modal frequencies, the modal damping, and the mode shapes. This chapter is concerned with these major parts of the experimental modal analysis.

CHAPTER II

VIBRATION OF ENGINE STRUCTURE

2.1 Equation of System

Suppose that the following vibration problem is considered for a given elastic structure subject to a body force **f** and a surface traction **t** on Γ_T, which is a part of the boundary Γ of the structure Ω :

$$\rho \frac{\partial^2 \mathbf{u}}{\partial t^2} + C\frac{\partial \mathbf{u}}{\partial t} - \mathrm{div}\Sigma(\mathbf{u}) = \rho \mathbf{f} \quad \text{in } \Omega, \tag{2.1}$$

$$\mathbf{n}\cdot\Sigma(\mathbf{u}) = \mathbf{t} \quad \text{on } \Gamma_T,$$

$$\mathbf{u} = \mathbf{g} \quad \text{on } \Gamma_D,$$

where C is a damping coefficient per unit volume, ρ is the mass density, $\Sigma(\mathbf{u})$ is the stress tensor due to the displacement **u**, **n** is the unit vector normal to the boundary, Γ_T is the traction boundary, **g** is the constrained displacement specified on the boundary $\Gamma_D = \Gamma - \Gamma_T$, and div is the divergence operator defined in the domain Ω. For simplicity, let us assume that C=0 in the following development. If linear elasticity is assumed, the stress tensor $\Sigma(\mathbf{u})$ is related to the linearized strain tensor $\varepsilon(\mathbf{u})$:

$$\Sigma(\mathbf{u}) = \mathbf{D}\cdot\cdot\varepsilon(\mathbf{u}) - \Sigma_0, \tag{2.2}$$

where **D** is the 4th. order tensor of elastic properties, Σ_0 is the initial stress and (··) represents a double inner product, i.e., $\mathbf{D}\cdot\cdot\varepsilon = D_{ijkl}\varepsilon_{kl}$. The linearized strain $\varepsilon(v)$ due to an arbitrary displacement v by :

$$\varepsilon(v) = \frac{1}{2}\ \{\ (\text{grad } v)^T + \text{grad } v\ \}, \tag{2.3}$$

where grad is the gradient operator and $(.)^T$ is the transpose of (.).

As a first step, let a weak form be obtained at an arbitrary time $t \in (0,\tau)$ by multiplying an arbitrary test function such that $v = 0$ on Γ_D and by integrating over the domain Ω :

$$\int_{\Omega} (\ v\cdot\rho\ \frac{\partial 2\mathbf{u}}{\partial t2} - v\cdot\text{div}\Sigma(\mathbf{u}))d\Omega = \int_{\Omega} v\cdot\rho f\ d\Omega\ . \tag{2.4}$$

Applying the divegence theorem to the second term yields:

$$\int_{\Omega} (v\cdot\rho\ \frac{\partial 2\mathbf{u}}{\partial t2} + (\text{grad } v)\Sigma(\mathbf{u}))d\Omega = \int_{\Omega} v\cdot\rho f\ d\Omega\ + \int_{\Gamma_T} v\cdot t\ d\Omega, \tag{2.5}$$

after applying the boundary condition on Γ_T.

Defining:

$$(\mathbf{u},v) = \int_{\Omega} v\cdot\rho u\ d\Omega, \tag{2.6}$$

$$a(\mathbf{u},v) = \int_{\Omega} \varepsilon(v)\cdot\cdot\mathbf{D}\cdot\cdot\varepsilon(\mathbf{u})\ d\Omega, \tag{2.7}$$

$$L(v) = \int_{\Omega} \varepsilon(v)\cdot\cdot\Sigma_0\ d\Omega + \int_{\Omega} v\cdot\rho f\ d\Omega + \int_{\Gamma_T} v\cdot t\ d\Gamma, \tag{2.8}$$

and denoting $\dot{\mathbf{u}} = \frac{\partial \mathbf{u}}{\partial t}$ and $\ddot{\mathbf{u}} = \frac{\partial^2 \mathbf{u}}{\partial t^2}$, the weak form is given by

$$\mathbf{u} \in V: (\ddot{\mathbf{u}}, \mathbf{v}) + a(\mathbf{u},\mathbf{v}) = L(\mathbf{v}), \forall \mathbf{v} \in V_o, \tag{2.9}$$

at $t \in (0,\tau)$, where V_o is the set of admissible displacements for the homogeneous boundary condition $\mathbf{g}=\mathbf{0}$ on Γ_D, while V is the admissible set for a general $\mathbf{g}$. The initial condition is assume on the displacement and velocity as follows:

$$\mathbf{u} = \mathbf{u}_o \text{ and } \dot{\mathbf{u}} = \dot{\mathbf{u}}_o \text{ at } t = 0. \tag{2.10}$$

In summary, the equations of vibration are given by:

$$\mathbf{u} \in V : (\ddot{\mathbf{u}}, \mathbf{v}) + a(\mathbf{u},\mathbf{v}) = L(\mathbf{v}), \forall \mathbf{v} \in V_0 \text{ at } t \in (0,\tau), \tag{2.11.a}$$

$$\mathbf{u} = \mathbf{u}_o \text{ and } \dot{\mathbf{u}} = \dot{\mathbf{u}}_o \text{ at } t = 0,$$

or

$$a^*(\mathbf{u},\mathbf{v}) = L(\mathbf{v}), \tag{2.11.b}$$

where

$$a^*(\mathbf{u},\mathbf{v}) = (\ddot{\mathbf{u}}, \mathbf{v}) + a(\mathbf{u},\mathbf{v}).$$

Suppose that V_h is a finite element approximation of V and suppose that V_{oh} is a finite element approximation of V_o. Let $\mathbf{v}$ be an arbitrary element of V, and let $\mathbf{v}_h$ be its global finite element approximation. V_h then consists of all such approximations. More precisely, in an arbitrary finite element Ω_e, $\mathbf{v}_h$ is spanned by its nodal values $\{V_\alpha\}$ and the shape functions $\{N_\alpha\}$, $\alpha=1,2...,N_e$:

$$\mathbf{v}_h(\mathbf{x},t) = \sum_{\alpha=1}^{N_e} V_\alpha(t) N_\alpha(\xi), \tag{2.12}$$

where N_e is the total number of nodes in an element Ω_e, and ξ , i.e. (ξ_1, ξ_2, ξ_3), is the coordinates in the master element Ω_M defined by, for example, a cube (-1,1)x(-1,1)x(-1,1) for a three dimensional structure. If 8-node trilinear elements, which are called HEXA8 element in this work, are used, the shape functions $N_\alpha(\xi)$ are given by:

$$N_\alpha(\xi)=\frac{1}{8}(1+\xi_{1\alpha}\xi_1)(1+\xi_{2\alpha}\xi_2)(1+\xi_{3\alpha}\xi_3),$$

where $(\xi_{1\alpha},\xi_{2\alpha},\xi_{3\alpha})$ are the coordinates of the eight corner nodes in the master element, Ω_M. If isoparametric relationship is assumed for geometry,

$$\mathbf{x} = \sum_{\alpha=1}^{N_e} \mathbf{x}_\alpha N_\alpha(\xi), \tag{2.13}$$

where $\mathbf{x}_\alpha$ are the coordinates of the eight corner nodes in the physical coordinate system.

A semi-analytic finite element approximation of the vibration problem (2.1) is formally written as:

$$\boldsymbol{u}_h \in V_h : (\ddot{\boldsymbol{u}}_h, v_h) + a(\boldsymbol{u}_h, v_h) = L(v_h), \ \forall\ v_h \in V_{oh} \text{ at } t \in (0,\tau),$$

$$\boldsymbol{u}_h = \mathbf{u}_{oh} \text{ and } \dot{\boldsymbol{u}}_h = \dot{\mathbf{u}}_{oh} \text{ at } t=0, \tag{2.14}$$

where $\mathbf{u}_{oh}$ and $\dot{\mathbf{u}}_{oh}$ are the finite element interpolations of the initial displacement $\boldsymbol{u}_o$ and the initial velocity $\dot{\boldsymbol{u}}_o$, respectively.

Using an integration scheme for the finite element approximation, which will be further discussed in the next section, Eq.(2.14) can be written in the following form :

$$[M]\{\ddot{u}_h\} + [K]\{u_h\} = \{P\}. \tag{2.15}$$

Eq. (2.15) may be solved by the unconditional stable, one-step, Newmark-β time integration scheme

$$\ddot{u}_h^{n+1} = \frac{\Delta u_h}{\beta \Delta t^2} - \frac{\dot{u}_h^{n}}{\beta \Delta t} - \frac{1}{\beta}\left(\frac{1}{2} - \beta\right)\ddot{u}_h^{n}, \tag{2.16.a}$$

$$\dot{u}_h^{n+1} = \dot{u}_h^{n} + \Delta t\,(1-\gamma)\ddot{u}_h^{n} + \Delta t\,\gamma\,\ddot{u}_h^{n+1}, \tag{2.16.b}$$

$$x^{n+1} = x^{n} + \Delta u_h, \tag{2.16.c}$$

where Δt is the time step size and β and γ are the free parameters of integration.

For the transient dynamic problem, Eq. (2.15) may be written as a time difference equation as follows:

$$[M]\{\ddot{u}_h^{n+1}\} + [K]\{\Delta u_h^{n+1}\} = \{P(x^n)\}^{n+1} - \{F(x^n)\}, \tag{2.17}$$

where

$[M]$: lumped mass matrix,

$[K]$: stiffness matrix,

$\{P(x^n)\}$: External Load,

$\{F(x^n)\}$: Internal Load,

u_h^{n+1} : displacement $= x^{n+1} - x^n$,

$\ddot{u}_h^{n+1}$: acceleration at time n+1.

Eq. (2.17) leads to:

$$[K^*]\{\Delta u_h^{n+1}\} = \{P(x^n)\}^{n+1} - \{F^*(x^n)\}, \tag{2.18}$$

where

$$[K^*] = [K] + [M]/\beta \Delta t^2, \text{ and}$$

$$\{F^*\} = \{F\} - [M]\left(\frac{\dot{u}_h^{\,n}}{\beta\Delta t} + \frac{1}{\beta}\left(\frac{1}{2} - \beta\right)\ddot{u}_h^{\,n}\right).$$

2.2 Finite Element Formulation Based on Directional Reduced Integration with Hourglass Control

In this section we shall discuss the finite element approximation of the term $a(u_h, v_h)$ which yields the stiffness matrix [K] using the directional reduced integration method with hourglass control.

As mentioned previously, the HEXA8 finite element has been reluctantly used by analysts because of poor accuracy for bending dominated problems due to the shear locking phenomenon. As an alternative, TETRA10 or HEXA20 have been used to achieve better accuracy. However, the use of these elements increase nodal degrees of freedom as well as bandwidth of [K]. Thus, in this work, we shall use the HEXA8 finite element in order to reduce computation time required. The accuracy of the approximation is also significantly improved so that this element is almost comparable to the higher order elements.

It is noted that there are several integration schemes to construct the stiffness matrix, such as full integration, reduced integration and selective reduced integration. The full integration scheme has been widely used because the "stability" is always guaranteed for well-posed problems in the sense that it leads to no nonphysical hourglass modes. However, full integration scheme can cause shear locking phenomenon in bending

dominated problems. To resolve this difficulty, the reduced integration scheme is introduced, which alsoprovides more efficient formulatation of the stiffness matrix since less number of integration points are required. However, the reduced integration scheme implies instability in the sense that there is a possibility of producing physically unreasonable spurious modes with zero strain energy.

Thus, the element stiffness matrix $\mathbf{K}_e$, obtained by using reduced integration, must be modified by adding a "correcting" term to eliminate these nonsensical zero energy modes:

$$\mathbf{K}_e^{act} = \mathbf{K}_e^{RI} + \mathbf{K}_e^{corr}, \tag{2.19}$$

where $\mathbf{K}_e^{act}$ is the modified element stiffness matrix, $\mathbf{K}_e^{corr}$ is the correction term to $\mathbf{K}_e^{RI}$ obtained by using the reduced integration scheme. It should be noted that $\mathbf{K}_e^{act}$ need not be the same to the one obtained by using the full integration scheme.

To solve the difficulty mentioned above, Koh and Kikuchi[20] suggested that the correction term $\mathbf{K}_e^{corr}$ be added properly to control the hourglassing based on not only mathematical but physical considerations. The correction term should maintain all structural behaviors such as bending and torsion as well as axial deformation. According to their development, the stiffness matrix can be decomposed into several terms relating to the directional behavior of the hexahedral element . Consequently, the actual stiffness matrix $\mathbf{Ke}^{act}$ applied in computation can be written in the form:

$$\mathbf{K}_e^{act} = \mathbf{K}_e^{RI} + \mathbf{K}_e^{\xi_1} + \mathbf{K}_e^{\xi_2} + \mathbf{K}_e^{\xi_3} + \mathbf{K}_e^{\xi_1\xi_2} + \mathbf{K}_e^{\xi_2\xi_3} + \mathbf{K}_e^{\xi_3\xi_1} + \mathbf{K}_e^{\xi_1\xi_2\xi_3}, \tag{2.20}$$

where superscripts ξ_1, ξ_2, and ξ_3 stand for the normalized coordinates in the master element. Furthermore, *every term in Eq.(2.20) can be approximately but explicitly obtained*

without using a quadrature rule to integrate in the parametric space ξ_1, ξ_2, *and* ξ_3, using the information evaluated at the centroid of each element that corresponds to the reduced integration point for the quadrature in the HEXA8 element. In most finite element programs, the stiffness matrix is computed by applying a quadrature rule such as 2x2x2 eight point Gauss integration rule (herein referred as the full integration scheme) for the HEXA8 element. Despite its complication, explicit evaluation of the terms in Eq.(2.20) can be derived as shown in [20]. However, since evaluation is performed based on the quadrature point of the 1 point reduced integration scheme, and since it is explicitly obtained, computation time required is significantly reduced compared to the conventional full integration scheme.

The concept of directional reduced integration can be expressed as follows. If a given structure is thin shell type, and if the direction ξ_3 in the master element approximately coincides to the thickness direction of the shell like structure while the $\xi_1\xi_2$ plane is identified with its tangent plane, the shear strains related to the ξ_3 axis should not generate much contribution to the strain energy. If such an element is subject to plane bending, the shear contribution to strain energy should be minimal, especially in very thin structures. This physical consideration leads the reduced integration should be applied in the plane direction in order not to include the excessive effect from the finite element deformation that yields the shear strains related to the thickness direction. Therfore, reduced integration is applied both in ξ_1 and ξ_2 directions, while the "exact" integration is applied in the thickness direction, i.e., in the ξ_3 direction. This means that the terms related to both ξ_1 and ξ_2 ; $\mathbf{K}_e^{\xi 1}$, $\mathbf{K}_e^{\xi 2}$, $\mathbf{K}_e^{\xi 1 \xi 2}$, $\mathbf{K}_e^{\xi 2 \xi 3}$, $\mathbf{K}_e^{\xi 3 \xi 1}$, and $\mathbf{K}_e^{\xi 1 \xi 2 \xi 3}$ should be "neglected" in forming the stiffness matrix. Similarly, a rod type structure is modeled so that the rod axis is coincided with the ξ_3 axis in the master element, the full integration should be applied both in the r and s direction which form the cross section of the rod, while the reduced

integration must be applied in the t direction that is the axis direction. That is, the terms $\mathbf{K}_e^{\xi 3}$, $\mathbf{K}_e^{\xi 2 \xi 3}$, $\mathbf{K}_e^{\xi 3 \xi 1}$, and $\mathbf{K}_e^{\xi 1 \xi 2 \xi 3}$ are eliminated from the element stiffness matrix.

A major advantage of the Directional Reduced Integration is that any artificial viscosity which was introduced in earlier methods by Hallquist[23,24] can be eliminated. In the directional reduced integration method, by underestimating strain directionally, difficulties of shear related terms are avoided. Thus, a thin and deeply curved structure like an engine cylinder block can be solved using solid elements if the mechanics are correctly reflected in the process to form the stiffness matrix.

Details of such a method can be found in Koh and Kikuchi[20]. Here only a brief description of the method is given. Evaluating the expression of the isoparametric relation of geometry between an arbitrary finite element and the master element :

$$\begin{Bmatrix} x_1 \\ x_2 \\ x_3 \end{Bmatrix} = \begin{bmatrix} l_1.x_1 & l_2.x_1 & l_3.x_1 \\ l_1.x_2 & l_2.x_2 & l_3.x_2 \\ l_1.x_3 & l_2.x_3 & l_3.x_3 \end{bmatrix} \begin{Bmatrix} \xi_1 \\ \xi_2 \\ \xi_3 \end{Bmatrix}$$

$$+ \begin{Bmatrix} \mathbf{c}.x_1+\mathbf{h}_1.x_1\xi_2\xi_3+\mathbf{h}_2.x_1\xi_3\xi_1+\mathbf{h}_3.x_1\xi_1\xi_2+\mathbf{h}_4.x_1\xi_1\xi_2\xi_3 \\ \mathbf{c}.x_2+\mathbf{h}_1.x_2\xi_2\xi_3+\mathbf{h}_2.x_2\xi_3\xi_1+\mathbf{h}_3.x_2\xi_1\xi_2+\mathbf{h}_4.x_2\xi_1\xi_2\xi_3 \\ \mathbf{c}.x_3+\mathbf{h}_1.x_3\xi_2\xi_3+\mathbf{h}_2.x_3\xi_3\xi_1+\mathbf{h}_3.x_3\xi_1\xi_2+\mathbf{h}_4.x_3\xi_1\xi_2\xi_3 \end{Bmatrix}, \tag{2.22}$$

where

$$l_1^T = \frac{1}{8}\{-1, 1, 1, -1, -1, 1, 1, -1\}, \qquad l_2^T = \frac{1}{8}\{-1, -1, 1, 1, -1, -1, 1, 1\},$$

$$l_3^T = \frac{1}{8}\{-1, -1, -1, -1, 1, 1, 1, 1\}, \qquad \mathbf{c}^T = \frac{1}{8}\{1, 1, 1, 1, 1, 1, 1, 1\},$$

$$\mathbf{h}_1^T = \frac{1}{8}\{\ 1,\ 1,\ -1,\ -1,\ -1,\ -1,\ 1,\ 1\},\qquad \mathbf{h}_2^T = \frac{1}{8}\{\ 1,\ -1,\ 1,\ -1,\ -1,\ 1,\ 1,\ -1\},$$

$$\mathbf{h}_3^T = \frac{1}{8}\{\ 1,\ -1,\ 1,\ -1,\ 1,\ -1,\ 1,\ -1\},\qquad \mathbf{h}_4^T = \frac{1}{8}\{\ -1,\ 1,\ -1,\ 1,\ 1,\ -1,\ 1,\ -1\},$$

and the coordinate in each direction are

$$\mathbf{x}_1^T = \{x_{11},x_{12},x_{13},x_{14},x_{15},x_{16},x_{17},x_{18}\},$$

$$\mathbf{x}_2^T = \{x_{21},x_{22},x_{23},x_{24},x_{25},x_{26},x_{27},x_{28}\},$$

$$\mathbf{x}_3^T = \{x_{31},x_{32},x_{33},x_{34},x_{35},x_{36},x_{37},x_{38}\}. \tag{2.23}$$

Its inverse relation can be obtained as

$$\begin{Bmatrix}\xi_1\\ \xi_2\\ \xi_3\end{Bmatrix} = \begin{bmatrix} l_1.x_1 & l_2.x_1 & l_3.x_1\\ l_1.x_2 & l_2.x_2 & l_3.x_2\\ l_1.x_3 & l_2.x_3 & l_3.x_3\end{bmatrix}^{-1} \cdot \begin{Bmatrix}x_1\\ x_2\\ x_3\end{Bmatrix}$$

$$- \begin{bmatrix} l_1.x_1 & l_2.x_1 & l_3.x_1\\ l_1.x_2 & l_2.x_2 & l_3.x_2\\ l_1.x_3 & l_2.x_3 & l_3.x_3\end{bmatrix}^{-1} \begin{Bmatrix} c.x_1+h_1.x_1\xi_2\xi_3+h_2.x_1\xi_3\xi_1+h_3.x_1\xi_1\xi_2+h_4.x_1\xi_1\xi_2\xi_3\\ c.x_2+h_1.x_2\xi_2\xi_3+h_2.x_2\xi_3\xi_1+h_3.x_2\xi_1\xi_2+h_4.x_2\xi_1\xi_2\xi_3\\ c.x_3+h_1.x_3\xi_2\xi_3+h_2.x_3\xi_3\xi_1+h_3.x_3\xi_1\xi_2+h_4.x_3\xi_1\xi_2\xi_3\end{Bmatrix}. \tag{2.24}$$

Since a similar expression to (2.24) can be obtained for a "displacement" vector $\mathbf{v}$:

$$\begin{bmatrix} \mathbf{b}_1.\mathbf{v}_1 & \mathbf{b}_2.\mathbf{v}_1 & \mathbf{b}_3.\mathbf{v}_1 \\ \mathbf{b}_1.\mathbf{v}_2 & \mathbf{b}_2.\mathbf{v}_2 & \mathbf{b}_3.\mathbf{v}_2 \\ \mathbf{b}_1.\mathbf{v}_3 & \mathbf{b}_2.\mathbf{v}_3 & \mathbf{b}_3.\mathbf{v}_3 \end{bmatrix} = \begin{bmatrix} \boldsymbol{l}_1.\mathbf{v}_1 & \boldsymbol{l}_2.\mathbf{v}_1 & \boldsymbol{l}_3.\mathbf{v}_1 \\ \boldsymbol{l}_1.\mathbf{v}_2 & \boldsymbol{l}_2.\mathbf{v}_2 & \boldsymbol{l}_3.\mathbf{v}_2 \\ \boldsymbol{l}_1.\mathbf{v}_3 & \boldsymbol{l}_2.\mathbf{v}_3 & \boldsymbol{l}_3.\mathbf{v}_3 \end{bmatrix} \begin{bmatrix} \boldsymbol{l}_1.\mathbf{x}_1 & \boldsymbol{l}_2.\mathbf{x}_1 & \boldsymbol{l}_3.\mathbf{x}_1 \\ \boldsymbol{l}_1.\mathbf{x}_2 & \boldsymbol{l}_2.\mathbf{x}_2 & \boldsymbol{l}_3.\mathbf{x}_2 \\ \boldsymbol{l}_1.\mathbf{x}_3 & \boldsymbol{l}_2.\mathbf{x}_3 & \boldsymbol{l}_3.\mathbf{x}_3 \end{bmatrix}^{-1} , \tag{2.25}$$

one can obtain

$$\begin{Bmatrix} \mathbf{v}_1 \\ \mathbf{v}_2 \\ \mathbf{v}_3 \end{Bmatrix} = \begin{bmatrix} \mathbf{b}_1.\mathbf{v}_1 & \mathbf{b}_2.\mathbf{v}_1 & \mathbf{b}_3.\mathbf{v}_1 \\ \mathbf{b}_1.\mathbf{v}_2 & \mathbf{b}_2.\mathbf{v}_2 & \mathbf{b}_3.\mathbf{v}_2 \\ \mathbf{b}_1.\mathbf{v}_3 & \mathbf{b}_2.\mathbf{v}_3 & \mathbf{b}_3.\mathbf{v}_3 \end{bmatrix} \begin{Bmatrix} \mathbf{x}_1 \\ \mathbf{x}_2 \\ \mathbf{x}_3 \end{Bmatrix}$$

$$+ \begin{Bmatrix} \mathbf{a}.\mathbf{v}_1+\mathbf{g}_1.\mathbf{v}_1\xi_2\xi_3+\mathbf{g}_2.\mathbf{v}_1\xi_3\xi_1+\mathbf{g}_3.\mathbf{v}_1\xi_1\xi_2+\mathbf{g}_4.\mathbf{v}_1\xi_1\xi_2\xi_3 \\ \mathbf{a}.\mathbf{v}_2+\mathbf{g}_1.\mathbf{v}_2\xi_2\xi_3+\mathbf{g}_2.\mathbf{v}_2\xi_3\xi_1+\mathbf{g}_3.\mathbf{v}_2\xi_1\xi_2+\mathbf{g}_4.\mathbf{v}_2\xi_1\xi_2\xi_3 \\ \mathbf{a}.\mathbf{v}_3+\mathbf{g}_1.\mathbf{v}_3\xi_2\xi_3+\mathbf{g}_2.\mathbf{v}_3\xi_3\xi_1+\mathbf{g}_3.\mathbf{v}_3\xi_1\xi_2+\mathbf{g}_4.\mathbf{v}_3\xi_1\xi_2\xi_3 \end{Bmatrix} , \tag{2.26}$$

where

$$\mathbf{a} = \mathbf{c} - (\mathbf{c}.\mathbf{x}_1)\,\mathbf{b}_1 - (\mathbf{c}.\mathbf{x}_2)\,\mathbf{b}_2 - (\mathbf{c}.\mathbf{x}_3)\,\mathbf{b}_3, \text{ and}$$

$$\mathbf{g}_i = \mathbf{h}_i - (\mathbf{h}_i.\mathbf{x}_1)\,\mathbf{b}_1 - (\mathbf{h}_i.\mathbf{x}_2)\,\mathbf{b}_2 - (\mathbf{h}_i.\mathbf{x}_3)\,\mathbf{b}_3 \text{ , i=1, 2, 3, and 4.} \tag{2.27}$$

Approximating the differential relation between $\mathbf{x}$ and ξ by:

$$\begin{Bmatrix} \frac{\partial}{\partial \xi_1} \\ \frac{\partial}{\partial \xi_2} \\ \frac{\partial}{\partial \xi_3} \end{Bmatrix} = \begin{bmatrix} \frac{\partial x_1}{\partial \xi_1} & \frac{\partial x_2}{\partial \xi_1} & \frac{\partial x_3}{\partial \xi_1} \\ \frac{\partial x_1}{\partial \xi_2} & \frac{\partial x_2}{\partial \xi_2} & \frac{\partial x_3}{\partial \xi_2} \\ \frac{\partial x_1}{\partial \xi_3} & \frac{\partial x_2}{\partial \xi_3} & \frac{\partial x_3}{\partial \xi_3} \end{bmatrix} \begin{Bmatrix} \frac{\partial}{\partial x_1} \\ \frac{\partial}{\partial x_2} \\ \frac{\partial}{\partial x_3} \end{Bmatrix}$$

$$\approx \begin{bmatrix} l_1.x_1 & l_2.x_1 & l_3.x_1 \\ l_1.x_2 & l_2.x_2 & l_3.x_2 \\ l_1.x_3 & l_2.x_3 & l_3.x_3 \end{bmatrix}^T \begin{Bmatrix} \frac{\partial}{\partial x_1} \\ \frac{\partial}{\partial x_2} \\ \frac{\partial}{\partial x_3} \end{Bmatrix}, \qquad (2.28)$$

differentiation with respect to the coordinate system **x** is approximated by

$$\begin{Bmatrix} \frac{\partial}{\partial x_1} \\ \frac{\partial}{\partial x_2} \\ \frac{\partial}{\partial x_3} \end{Bmatrix} \approx \begin{bmatrix} l_1.x_1 & l_2.x_1 & l_3.x_1 \\ l_1.x_2 & l_2.x_2 & l_3.x_2 \\ l_1.x_3 & l_2.x_3 & l_3.x_3 \end{bmatrix}^{-T} \begin{Bmatrix} \frac{\partial}{\partial \xi_1} \\ \frac{\partial}{\partial \xi_2} \\ \frac{\partial}{\partial \xi_3} \end{Bmatrix}. \qquad (2.29)$$

Thus, the bilinear and trilinear terms in ξ are differentiated in **x** as

$$\begin{Bmatrix} \frac{\partial}{\partial x_1} \\ \frac{\partial}{\partial x_2} \\ \frac{\partial}{\partial x_3} \end{Bmatrix} (\xi_2\xi_3) \approx \begin{bmatrix} l_1.x_1 & l_2.x_1 & l_3.x_1 \\ l_1.x_2 & l_2.x_2 & l_3.x_2 \\ l_1.x_3 & l_2.x_3 & l_3.x_3 \end{bmatrix}^{-T} \begin{Bmatrix} \frac{\partial}{\partial \xi_1} \\ \frac{\partial}{\partial \xi_2} \\ \frac{\partial}{\partial \xi_3} \end{Bmatrix} (\xi_2\xi_3)$$

$$= \begin{bmatrix} l_1.x_1 & l_2.x_1 & l_3.x_1 \\ l_1.x_2 & l_2.x_2 & l_3.x_2 \\ l_1.x_3 & l_2.x_3 & l_3.x_3 \end{bmatrix}^{-T} \begin{Bmatrix} 0 \\ \xi_3 \\ \xi_2 \end{Bmatrix} , \qquad (2.30)$$

etc.

Applying these relations, the first derivatives of **v** in **x** can be approximately obtained in terms of ξ. Furthermore, noting that polynomials in ξ in the master element Ω_M can be explicitly integrated if the Jacobian of the transformation is approximated in a polynomial form of ξ, the element stiffness matrix due to the bilinear form of $a_e(.,.)$, where subscript 'e' denotes the integration domain which is now restricted in Ω_M instead of the whole domain Ω, can be approximated *without applying a quadrature rule.*

2.3 Estimation of Approximation Error in Space

In finite element approximation there are several types of errors, such as interpolation error, integration error, and boundary approximation error. Among these errors, the finite element interpolation error is considered to be the dominant one. Once one can estimate the amount of finite element interpolation error in a particular finite element

model, it is possible to determine accuracy of the approximation and then it becomes possible to apply adaptation processes to reduce such error.

It is noted that the finite element approximation error is, in general, bounded by the interpolation error in the elliptic boundary problem. This means that if the interpolation error is reduced by adapting finite element models, the amount of the finite element approximation error is also automatically reduced. A popular choice of an error measure which can estimates the amount of approximation or interpolation error in each finite element, is represented in terms of the norm related to the strain energy. The mean square of the strain energy generated by the difference between the exact solution and its finite element approximation or its finite element interpolation is the quantity representing the amount of the error for the adaptive method. Details of the method to evaluate such a quantity can be found in Kikuchi[40] and Kikuchi and Torigaki[42].

For the present problem it is necessary to modify the method in [40] , since it is a dynamic problem of a linearly elastic structure. In this problem, there is a quasi-orthogonality property of the approximation error of the semi-analytic finite element approximation (that is the finite element approximation of (2.14) in space but the exact evaluation of the differentiation in time) of the original problem (2.11), yielding the identity:

$$(\ddot{u}_h - \ddot{\mathbf{u}}, u_h - \mathbf{u}) + a(u_h - \mathbf{u}, u_h - \mathbf{u})$$

$$= (\ddot{v}_h - \ddot{\mathbf{u}}, v_h - \mathbf{u}) + a(v_h - \mathbf{u}, v_h - \mathbf{u}) \quad \text{, at any time t, for every } v_h. \tag{2.31}$$

If the error of a finite element approximation at time t is defined by:

$$e^2 = (\ddot{u}_h - \ddot{\mathbf{u}}, u_h - \mathbf{u}) + a(u_h - \mathbf{u}, u_h - \mathbf{u}), \tag{2.32}$$

it may follow from (2.31) that an error indicator that can estimate the amount of the approximation error is defined by the quantity:

$$e_I^2 = (\ddot{v}_h - \ddot{u},\ v_h - u) + a(v_h - u,\ v_h - u), \tag{2.33}$$

using the interpolation v_h of the solution u of the original problem (2.11). Although the following inequality holds for the elliptic (i.e. static) problem:

$$e \le e_I, \tag{2.34}$$

it may not be valid for the present problem. However, from the physical consideration of the nature of the dynamic problem that the energy is conserved, the error indicator e_I is a strong and natural candidate of the quantity that represents the amount of the approximation error. Following this, an error measure in each finite element Ω_e is now defined by

$$E_e^2 = (\ddot{v}_h - \ddot{u},\ v_h - u)_e + a_e(v_h - u,\ v_h - u). \tag{2.35}$$

It is noted that :

$$e_I = (\Sigma E_e^2)^{1/2} < (NE)^{1/2}\ \text{Max Ee}, \tag{2.36}$$

where NE is the total number of finite elements in a model.

Now we shall discuss how to compute error measure E_e. To do this, note that the relation of differentiation of two coordinate systems for the finite element approximation in space is given by

$$\begin{Bmatrix} \frac{\partial}{\partial \xi_1} \\ \frac{\partial}{\partial \xi_2} \\ \frac{\partial}{\partial \xi_3} \end{Bmatrix} = \begin{bmatrix} \frac{\partial x_1}{\partial \xi_1} & \frac{\partial x_2}{\partial \xi_1} & \frac{\partial x_3}{\partial \xi_1} \\ \frac{\partial x_1}{\partial \xi_2} & \frac{\partial x_2}{\partial \xi_2} & \frac{\partial x_3}{\partial \xi_2} \\ \frac{\partial x_1}{\partial \xi_3} & \frac{\partial x_2}{\partial \xi_3} & \frac{\partial x_3}{\partial \xi_3} \end{bmatrix} \begin{Bmatrix} \frac{\partial}{\partial x_1} \\ \frac{\partial}{\partial x_2} \\ \frac{\partial}{\partial x_3} \end{Bmatrix} \approx \begin{bmatrix} J_{11} & J_{12} & J_{13} \\ J_{21} & J_{22} & J_{23} \\ J_{31} & J_{32} & J_{33} \end{bmatrix}^T \begin{Bmatrix} \frac{\partial}{\partial x_1} \\ \frac{\partial}{\partial x_2} \\ \frac{\partial}{\partial x_3} \end{Bmatrix}. \qquad (2.37)$$

Since the interpolation errors for the hexahedral 8-node element are given by:

$$v_h - u = \frac{1}{2} [(1 - \xi_1^2) u_{\xi_1\xi_1} + (1-\xi_2^2) u_{\xi_2\xi_2} + (1-\xi_3^2) u_{\xi_3\xi_3}],$$

$$(v_h - u)_{\xi_1} = \frac{1}{2} [-2 \xi_1 u_{\xi_1\xi_1} + (1 -\xi_2^2) u_{\xi_1\xi_2\xi_2} + (1 - \xi_3^2) u_{\xi_1\xi_3\xi_3}],$$

$$(v_h - u)_{\xi_2} = \frac{1}{2} [-2 \xi_2 u_{\xi_2\xi_2} + (1 - \xi_3^2) u_{\xi_2\xi_3\xi_3} + (1 - \xi_1^2) u_{\xi_2\xi_1\xi_1}],$$

$$(v_h - u)_{\xi_3} = \frac{1}{2} [-2 \xi_3 u_{\xi_3\xi_3} + (1 - \xi_1^2) u_{\xi_3\xi_1\xi_1} + (1 - \xi_2^2) u_{\xi_3\xi_2\xi_2}],$$

(2.38)

where

$$u_{\xi_1\xi_1} = \frac{\partial^2 u}{\partial \xi_1^2} \quad \text{and} \quad u_{\xi_1\xi_2\xi_2} = \frac{\partial^3 u}{\partial \xi_1 \partial \xi_2^2}, \text{ etc.}$$

Thus the interpolation errors in the first derivatives in the physical coordinate system (x_1,x_2,x_3) are given by using the relation:

$$\begin{Bmatrix} (v_h - u)_{x1} \\ (v_h - u)_{x2} \\ (v_h - u)_{x3} \end{Bmatrix} = \begin{bmatrix} J_{11} & J_{12} & J_{13} \\ J_{21} & J_{22} & J_{23} \\ J_{31} & J_{32} & J_{32} \end{bmatrix}^{-1} \begin{Bmatrix} (v_h - u)_{\xi 1} \\ (v_h - u)_{\xi 2} \\ (v_h - u)_{\xi 3} \end{Bmatrix}, \qquad (2.39)$$

and Eq. (2.38). Since the interpolation error of $(v_h\text{-}u)_{\xi 1}$ and others are given in Eq. (2.38), the interpolation error of $(v_h\text{-}u)_x$ and others can be written in terms of the second derivatives of the exact solution **u** with respect to the global coordinate system **x** by applying the relation:

$$\begin{aligned} u_{\xi 1 \xi 1} &= (J_{11}\, u_{x1} + J_{12}\, u_{x2} + J_{13}\, u_{x3})_{\xi 1} \\ &= J_{11}\, \xi_1\, u_{x1} + J_{12}\, \xi_1\, u_{x2} + J_{13}\, \xi_1\, u_{x3} + J_{11}\, u_{x1\xi 1} + J_{12}\, u_{x2\xi 1} + J_{13}\, u_{x1\xi 1} \\ &= J_{11}^2\, u_{x1x1} + J_{12}^2\, u_{x2x2} + J_{13}^2\, u_{x3x3} \\ &\quad + 2(J_{11}J_{12}\, u_{x1x2} + J_{12}J_{13}\, u_{x2x3} + J_{13}J_{11}\, u_{x3x1}), \text{ etc.} \end{aligned} \qquad (2.40)$$

Since the components of the Jacobian matrix $J_{11},....,J_{33}$ are proportional to the finite element size, the interpolation error is also proportional to it. It is noted that the second derivatives of the exact solution **u** which is unknown a priori, must be estimated only by using the finite element approximation $\mathbf{u}_h$. There are several ways to estimate the second derivatives, see the details in[40].

The term $\ddot{\mathbf{v}}_h - \ddot{\mathbf{u}}$ are computed by applying Newmark-β approximation (2.16) of the interpolation error $\mathbf{v}_h - \mathbf{u}$.

2.4 Test of DRI for Dynamic Problems

2.4.1 Computer Program

The directional reduced integration method is extended to dynamic problems and its accuracy is tested using several examples in which the analysis program FEM3D, an in-house finite element code, is used. Then it is implemented in NIKE3D[24]. The preprocessing routine for generating hourglass control parameters, which controls integration over a region specified by user, has been implemented in INGRID[25] which is a preprocessor to NIKE3D.

All programs developed here are available on VAX11-780 and APOLLO DN3000/DN4000.

2.4.2 Numerical Examples

To test the accuracy of the finite element solution of dynamic problems, the following examples are selected for the free vibration problem which yield the eigenvalue analysis:

- Beam model with one end clamped,

- Plate model with one side clamped, and

- Fabricated panel model.

Specifically, the test cases are intended to examine the accuracy of DRI with hourglass control by solving eigenvalue problems. It is noted that several static problems were tested

to examine the solution accuracy of DRI in [20]. Thus, in this work numerical testing is limited to vibration problems.

In solving examples selected, the discretization of the examples are performed using regular HEXA8 elements of right angles. In most structural problems, however it is not possible to generate finite element meshes using only such elements when structures of complicated 3-D geometry is solved. In such a case, freely-shaped HEXA8 elements may used to describe geometry. The accuracy of solution using such freely-shaped elements is geneally worse than the one using regular HEXA8 elements. However, it is shown that the accuracy of solution does not decrease even in such cases when directional reduced integration is used toformulate HEXA8 finite elements[20].

EXAMPLE 1. (Cantilever Beam)

A 3-D cantilever beam is modeled in four different discretizations. Its geometry and material properties are given in Fig.2.1. For all discretizations, the reduced integration with hourglass control is applied only to the longitudinal direction when element stiffness matrices are formulated.

Eigenvalues obtained for the different discretizations are shown in Table 2.1 and mode shapes for the case of 64 elements are also given in Fig.2.2. As the total number of element increases, in general, the solution by DRI with hourglass control converge to the one obtained using Euler's beam theory. Convergence was achieved in all the test cases.

In these test cases, relatively accurate eigenvalues are obtained in the lower modes. Remarkable improvement is achieved in higher modes about the y-direction if discretization in the x-direction is doubled. In the third test case, in which discretization in the y-direction is doubled while numbers of discretization in x and z directions are kept same as the second

discretization, improvement is not achieved compared to the second case. In the final test case, in which the mesh density in all directions is doubled as shown in Fig.2.1, solution errors dropped to less than 1 % and the eigenvalues of the higher modes in both the x- and y-direction are improved and agree more closely to those obtained using Euler's beam theory.

Numerical tests of DRI using four different discretizations suggests that if we apply the same discretization to both the x and y directions, the stiffness in the x direction is getting softer in the case where the aspect ratio of the cross section is larger than one. In Table 2.1, errors in each mode are shown. The maximum error of the eigenvalues in the bending modes is less than 10 % up to the 6th mode. It seems that the solution accuracy of dynamic analyses is not as good as that of the static analyses as seen in Koh and Kikuchi[20]. However, although solution accuracy obtained by using the hourglass control algorithm is relatively low for higher modes, it can be applied to the 3-dimensional dynamic analysis of a large structure at a cheap cost if only the lower modes are of interest.

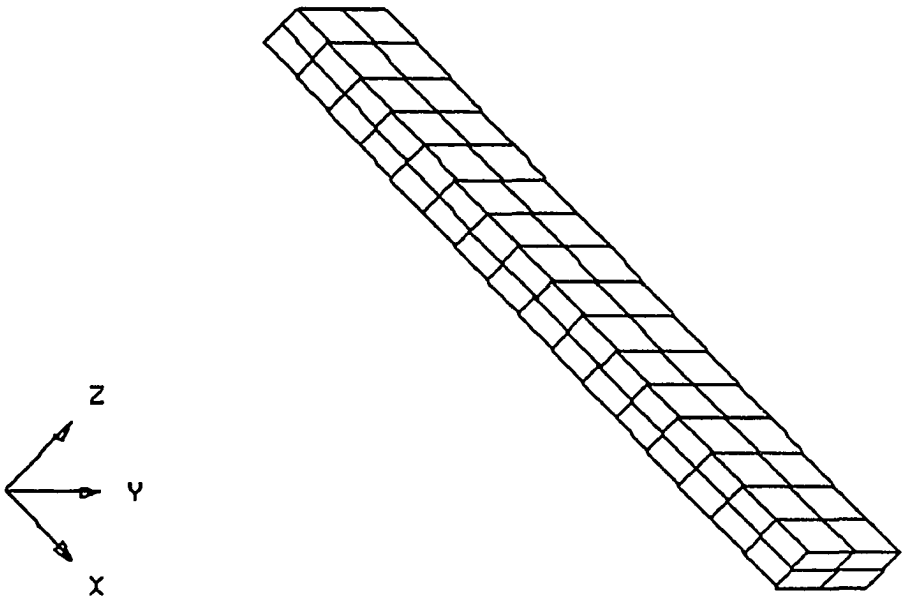

E=2.068E11Pa,Poisson's Ratio = 0.3, Density = 7800 kg/m^3,

Dimension 0.5b x 0.25t x 4L (m), total element : 64

Fig. 2.1 Properties and Undeformed Configuration of Cantilever Beam

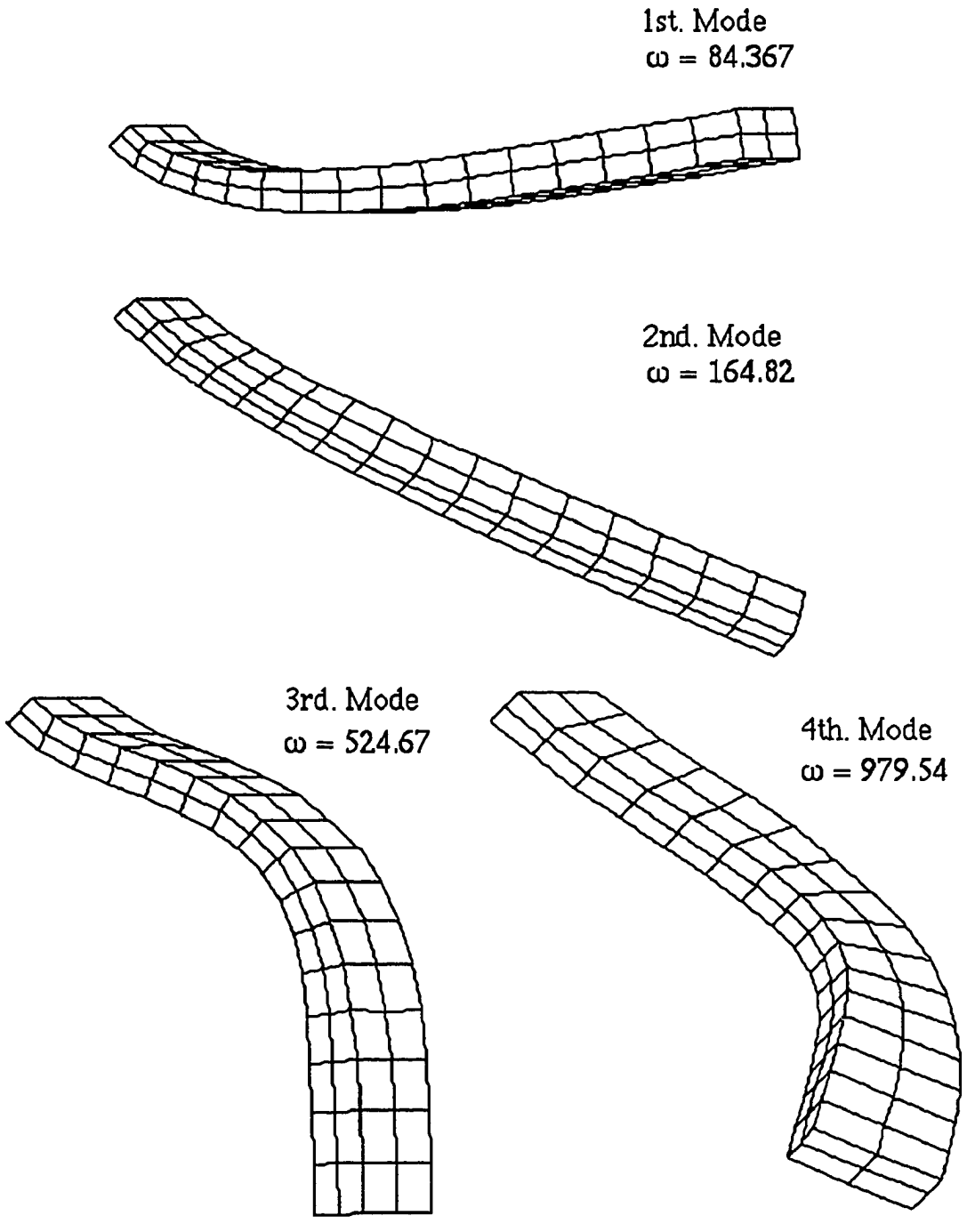

Frequency in Hz

Fig. 2.2 Mode Shapes of Cantilever Beam Model (64 Elements)

Table 2.1 Natural Frequencies of Cantilever Beam

Unit : Rad/sec

Case	1	2	3	4	Euler	Type of
Mode No.	8 Elem. 1 x 1 x 8	16 Elem. 1 x 2 x 8	32 Elem. 2 x 2 x 8	64 Elem 2 x 2 x 16	Beam	Mode
1	0.28512	0.28384	0.27001	0.26892	0.25559	1.bending y-d.
2	0.53843	0.53643	0.53519	0.53363	0.51176	1.bending x-d.
3	2.0212	1.8093	1.9175	1.7168	1.6019	2.bending y-d.
4	3.2043	3.1876	3.2009	3.1848	(torsional)	1.torsion z-d.
5	3.6050	3.2572	3.5851	3.2415	3.1966	2. bendingx-d.
6	6.3862	5.2649	6.3833	5.0085	4.48512	3. bendingy-d..

EXAMPLE 2.(Plate Model)

A plate clamped on one side was selected to study the dynamic characteristics of the 3-D solid model formulated by using the directional reduced integration with hourglass control. The dimensions and properties of the model are shown in Fig. 2.3. The model analyzed here was discretized in 4 different ways. The hourglassing will be controlled in both longitudial directions and not controlled in the thickness direction. Results were verified by comparing them with the solution obtained by NIKE3D using the Hughes-Liu plate element.

Eigenvalues for different models are shown in Table 2.2 and compared to the solution of NIKE3D. In the first two test cases, in which the number of divisions in the thickness direction is only one, solutions are not as accurate as those of plate theory. As

seen in Table 3, eigenvalues up to the third mode are quite accurate with error less than 10%. In the next two test cases, where the thickness direction was discretized in 2 divisions, the solutions are more accurate and comparable to that of plate theory. Mode shapes of the model using 124 elements are shown in Fig.2.4.

It is noted that HEXA8 elements and QUAD4 plate/shell elements have the same number of the degrees of freedom in each element. Each QUAD4 element needs a transformation matrix between the global coordinate system and the local one defined for each finite element. Thus, after forming the element stiffness matrix of QUAD4 in the local coordinate system, it must be transformed into the global one, before being assembled into the global stiffness matrix. This means that many computational steps are required for plate/shell elements. Roughly speaking, six to eight HEXA8 elements require the same amount of computing time as one QUAD4 element to form the global element stiffness matrix. This means that using solid HEXA8 elements to form a finite element stiffness matrix is not as expensive as using QUAD4 shell elements.

Table 2.2 Natural Frequencies of One-Side-Clamped Plate

Unit : Rad/sec

Mode No.	HEXA8 Element		Plate Element (NIKE)	
	32 Elem.	128 Elem.	16 Elem.	64 Elem.
1	270.65	274.95	265.18	268.56
2	615.01	643.74	616.65	640.63
3	1521.0	1636.3	1545.0	1619.6
4	1723.0	2041.1	1834.5	2006.7
5	1876.2	2090.0	2126.1	2287.6

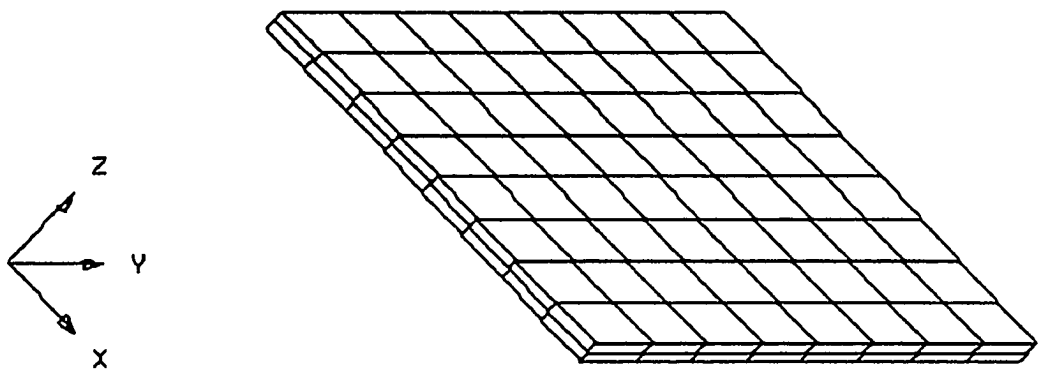

Young's Modulus : 2.07E11 Pa, Poisson's ratio: 0.3, Density :7800 kg/m^3
Dimesnion : 1B x 1B x 0.025t (m)

Fig. 2.3 Properties and Undeformed Configuration of Plate Model

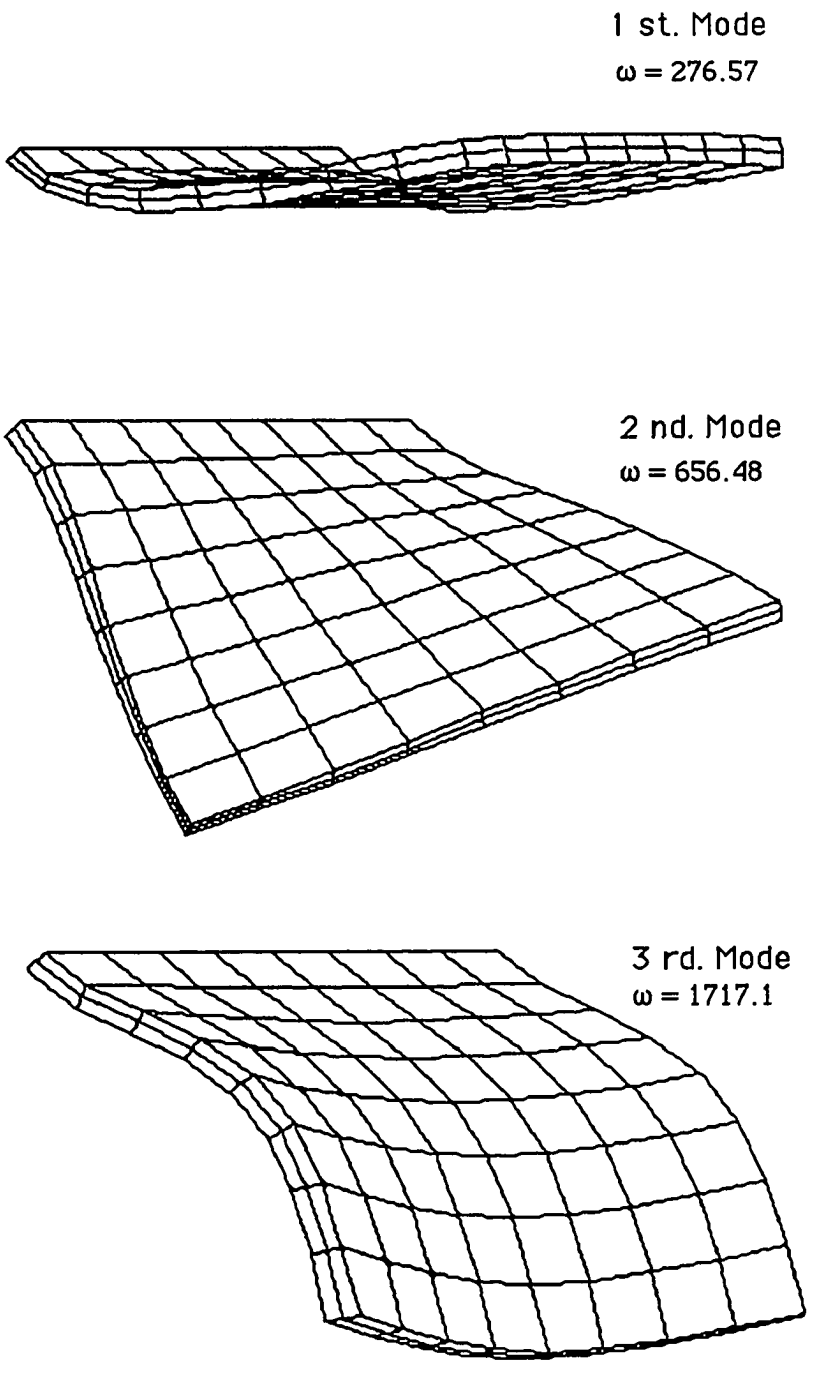

Frequency in Hz

Fig. 2.4 Mode Shapes of Plate Model (128 Elements)

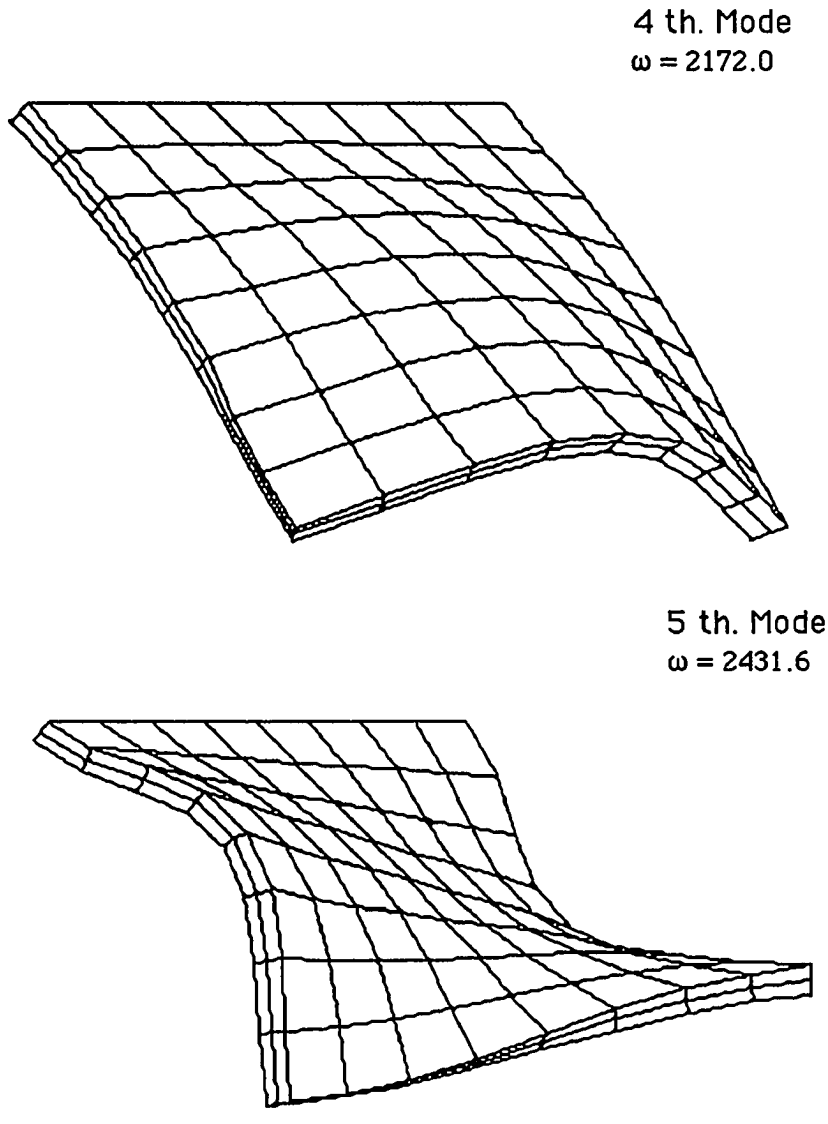

Frequency in Hz

Fig. 2.4 Mode Shapes of Plate Model (128 Elements)

EXAMPLE 3 (FABRICATED PANEL MODEL)

In the third example, a simple fabricated panel structure model was used. Unlike a simple beam or a simple plate structure we are expecting to see more complexity, showing some characteristics of real, complex, structures like an engine cylinder block. In this example, 3 different discretizations of the model, which are shown in Fig. 2.5., are analyzed and compared using NIKE3D with the Hughes-Liu shell element. Eigenvalues obtained using HEXA8 elements with DRI are listed in Table 2.3 and are compared to the solution obtained using the Hughes-Liu shell elements.

Eigenvalues for different models are shown in Table 2.3 and compared to the solution obtained using NIKE3D. As the number of elements increases, the solution generally becomes better.

Table 2.3 Natural Frequencies of T-Shape Fabricated Beam Model

Unit : Rad/sec

Mode No.	HEXA8 Element		Plate Theory	Euler's Beam Theory
	Model 1	Model 2		
1	0.012166	0.012760	0.011269	0.012177
2	0.014064	0.014467	0.015426	0.015064
3	0.025479	0.026167	0.025908	0.026385
4	0.037692	0.039750	0.035137	
5	0.065169	0.069358	0.061186	

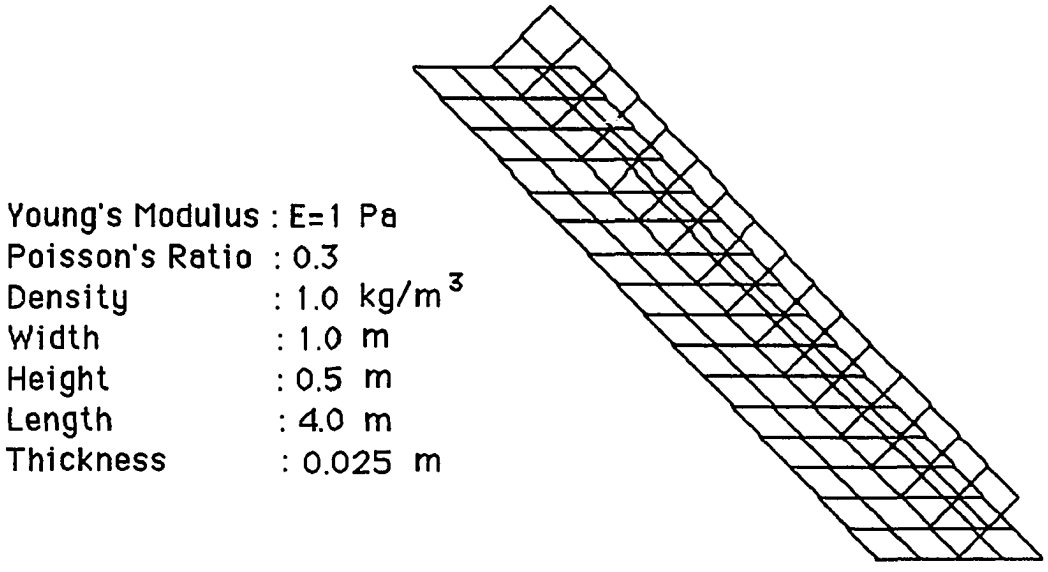

Young's Modulus : E=1 Pa
Poisson's Ratio : 0.3
Density : 1.0 kg/m^3
Width : 1.0 m
Height : 0.5 m
Length : 4.0 m
Thickness : 0.025 m

Plate Model

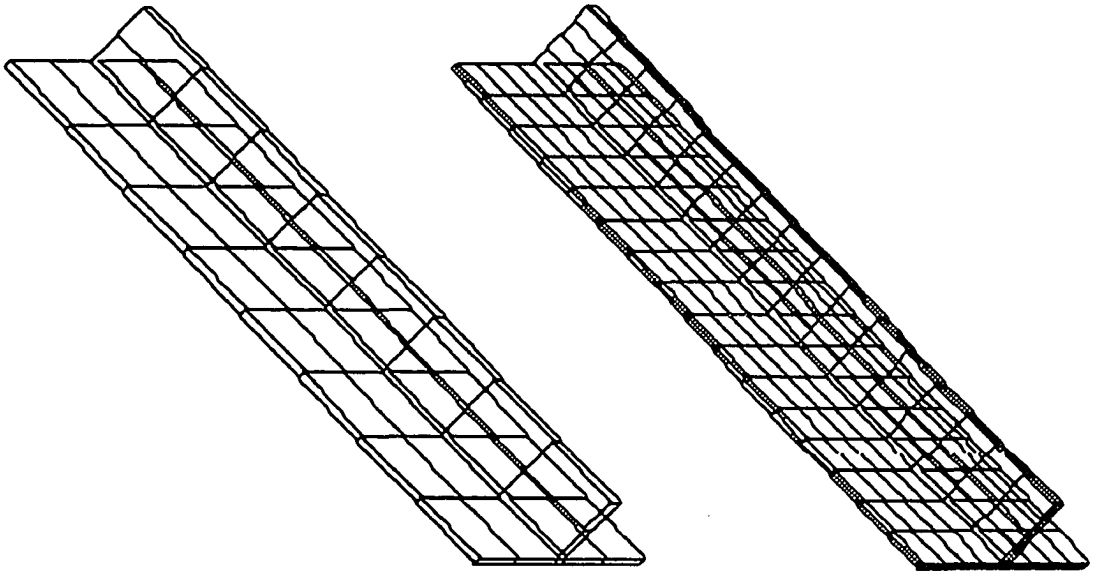

Brick-Element Model 1

Brick-Element Model 2

Fig. 2.5 Discretization of T-Shape Beam Model

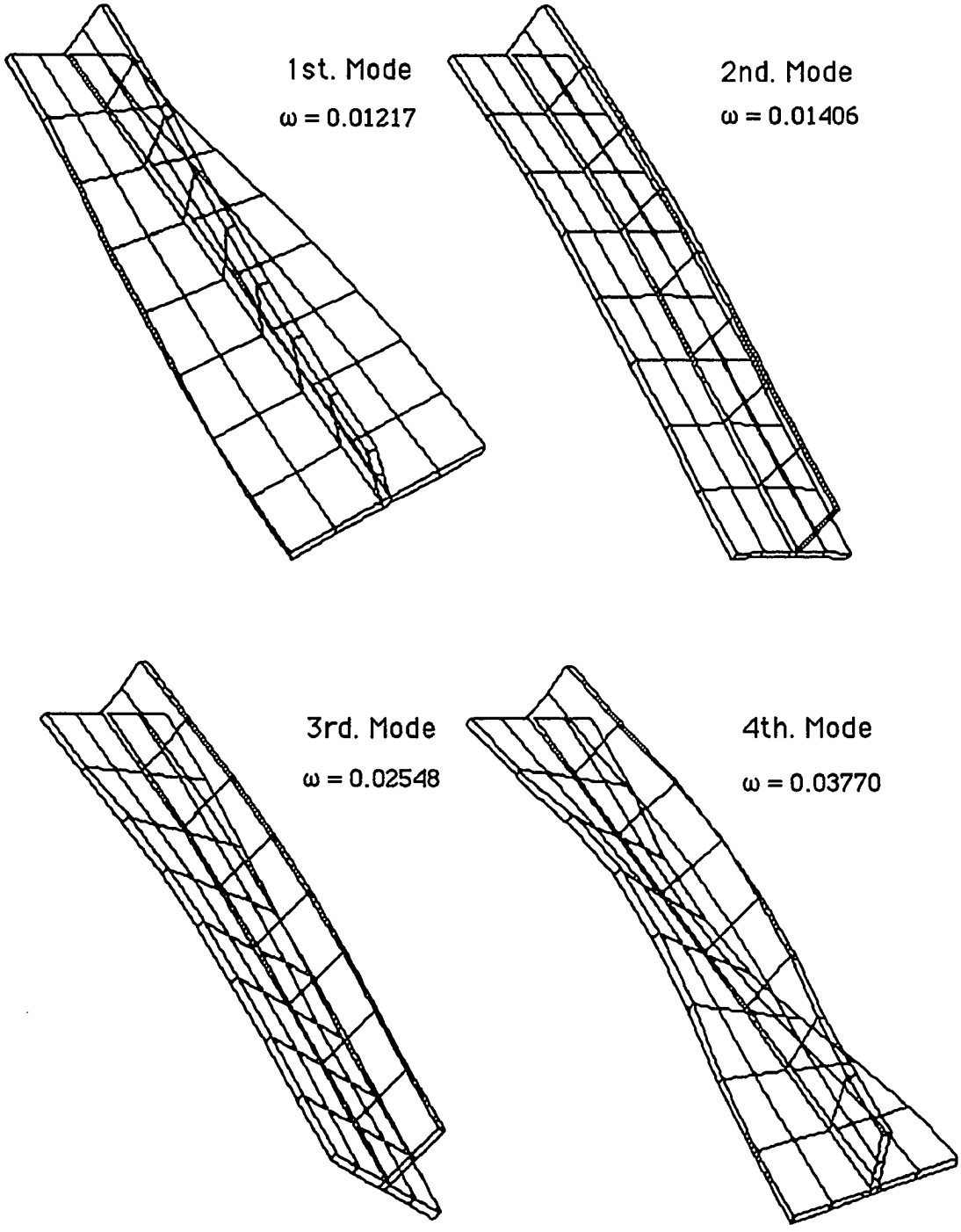

Frequency in Hz

Fig. 2.6 Mode Shapes of T-Shape Beam Model (Brick Element Model #2)

CHAPTER III

FINITE ELEMENT ANALYSIS OF DIESEL ENGINE CYLINDER BLOCK

3.1 Introduction

Over the last two decades, diesel engine development and manufacturing have seen unprecedented technological changes. Global competition has made life cycle cost, quality and reliability more important than ever. Therefore, diesel engine manufactures can no longer afford prolonged, expensive, product development time usually required in the design-test-redesign sequence of the past practices. These factors along with an increasing emphasis on thermal efficiency, higher outputs, and higher operating temperatures, put considerable responsibility on the designers. Such needs have caused the component/system analysis process to become an important ingredient in the design of a diesel engine. To analyze a complex diesel engine system and its subsystem, one of the most valuable tools is the finite element method.

With the advent of large, high speed computers, the finite element method is commonly used in industry to solve the structural and thermal equation systems which describe the complex behavior of engine structures. In particular, finite element analysis allows the performance of engine components to be predicted in the design stage.

The scope of finite element analysis goes beyond just stress and thermal analyses. Finite element analysis is also necessary in order to improve complex component systems whose performance is dependent on their mutual interaction under the thermal and mechanical loads.

As early as 1972, researchers used finite element analysis to study the dynamic characteristics of simple engine components and demonstrated reasonable agreement with experimental results[1]. This information was later published in 1975[2]. In 1979 it was shown that complex structures such as an engine block could be modelled accurately[3]. Subsequent work has shown good correlation with experimental results[4,5,6]. In past research, numerical modelling of the structure of an engine has been performed using at least two different models, one for static and thermal analysis, and a separate model for dynamic analysis[9,10]. Engine stress and thermal analyses typically employ finite element models composed of either 20-node solid elements, while for dynamic analysis 4-node plate and shell elements are commonly used. This approaches is inefficient because different finite element models of the same structure must be developed.

In order to reduce the time and the cost for analysis and simulation of a particular design, it is essential to reduce the duplication of effort required to develop different finite element models for these different analyses. Therefore, a finite element model of an engine has developed using simple HEXA8 finite elements formulated with the directional reduced technique. These elements are optimized in order to shorten computation time required to form the stiffness matrices, as well as to increase accuracy for stress, thermal and dynamic analyses.

In this chapter, earlier works are reviewed to show how development of modelling and analysis of engines has progressed. A new unified approach to thermal, stress and dynamical analysis is presented.

3.2. Nature of Engine Design Analysis

3.2.1 Basic Design Concept

In order to improve the performance of a new diesel engine program, it has been suggested that the basic design process be conducted without being influenced by conventional design concepts and biases. Some clear targets that might guide the design are as follows:

1) High output with low fuel consumption,

2) Light weight and compact size,

3) Excellent reliability and durability, and

4) Low production and maintenance costs.

Within these constraints, basic design parameters are selected such as bore size, stroke, engine rated speed, number of cylinders, combustion system characteristics, type of cycle. Once these parameters have been selected and combined with other functional requirements such as, power, size, weight, etc., the basic design forcing function in a diesel engine can be established. Additionally, engine sound levels are affected by the dynamic characteristics of the structure and radiation effectiveness of its structure.

With these basis, the conceptual design can be processed. In the initial design stage, a graphical design facility can create a conceptual design at minimal man power cost. The finite element method can then be adopted for all thermal, stress, vibration analyses in order to achieve an optimal design. Specifically in the design analysis process, the finite element method allows an analyst to study the behavior of the engine and its various components in

their operating environment, which helps to optimize the design prior to actual prototype development.

Finite element analysis has been used for many years and offers many advantages. The principal advantage of the method is the reduction of in the development time and the ability to analyze main engine structure and components without having to fabricate them. This allows an assessment of several design alternatives in a relatively short amount of time, and at a relatively small additional costs.

3.2.2 Structural Analysis of an Engine Structure

In order to meet the constraints set up prior to manufacturing, the structure of an engine must be optimized both statically and dynamically. Moreover, due to high combustion pressures, the structure radiates considreable noise, which needs to be reduced where possible. Successful design of quieter engines depends upon an understanding of the vibration mechanisms within the engine structure, and of the way in which those vibration-generated noises are transmitted to the environment.

When forces are applied to the engine structure by the combustion process and mechanical interactions, small, abrupt movements occur which physically displace the external surfaces peripherally (forced vibration) and cause the structure to vibrate in resonance in a large number of normal modes (damped natural vibration). Many of these normal modes involve motion at a right angle to the plane of the surface, which in turn forces the air in contact with it to move. At low frequencies, the air moves without significant pressure variations being generated, and little energy is imparted to the air. At higher frequencies, sufficient pressure may be built up by the vibration to cause significant sound power to be radiated. At higher frequencies still, the surfaces of the

structure vibrate in a very large number of normal modes, each making a contribution to the total sound radiated by the engine. Since the structural response of the running engine to the cylinder pressure development depends upon the natural modes of the cylinder block, the whole engine block should be examined by either eigenvalue analysis or forced response analysis with fluctuating forces being applied to the top face of the piston. Of cause the pressure force is applied to cylinder head also. This tends to lift the from the block. The head itself adds considerable stiffness to the head/block structure[11-19].

Previous studies show that there are several types of mode shapes which may be classified as follows[11-13]:

- Global bending and torsional modes. In some cases rigid body modes due to poor structural support,
- Local modes in which mainly the bearing supports move, and
- Skirt panel modes, where the predominant movement is in the bottom of the block.

In general, the global modes, like the bending and torsional modes, are excited at the lower frequency ranges, while the local and skirt panel modes are excited at higher frequency ranges. These mode shapes show that the stiffness along the cylinder block varies from the top, which is very stiff even without the cylinder head, to the bottom which is relatively flexible.

It should be emphasized that the vertical stiffness is important from a strength point of view, but the horizontal stiffness is the main factor contributing to noise radiation. This means that the bottom of the engine structure radiates noise with very small displacements at high frequencies. This excites the oil pan and transmits vibration to the automotive body.

This is due to the fact that vibration normal to the crankcase is mainly produced by bending in the horizontal plane.

3.2.3 Finite Element Modeling Approach

Three basic types of finite element model have been considered for engine analysis;

a) 3D Solid Element Model,

b) 3D Solid and Shell Element Model,

c) Shell and Beam Model.

Finite element models built primarily of solid elements should yield the most accurate solutions, but incur significant penalties in terms of computer time and problems of mesh generation. Solid and shell elements can be combined in a hybrid model. Solid elements can be used to modes areas of complex solid geometry and shell elements can be used for more shell-like regions such as crankcase panels and the like. These models offer some time and cost reduction over the all-solid models. The models including shell and beam elements are constructed with no solid elements. The beam elements are used to supply additional stiffness arising from geometric features such as stiffening ribs. Generation of these models involves considerable experience to achieve valid geometrical approximations, but they may offer cheaper running costs.

Among these conventional model types, solid elements are usually chosen for stress and temperature analyses. However, the preferred elements for vibration prediction on engine blocks have been the plate and shell elements since out-of-plane motion, which is the major motion in engine vibration, is controlled by an accurate bending stiffness formulation. Care should be taken, when using plate elements to model cylinder block

structures, in that great attention must be paid to accurate definition of plate intersections, where, physically, structures are more of a solid nature.

It should be noted that in vibration analysis for noise prediction, the outer surface out-of-plane motion is of prime importance. When solid elements are used the accuracy of this out-of-plane motion is inadequate since the bending stiffness of high aspect ratio 3D solid elements is very poor. Thus, many researchers have used plate and shell elements exclusively to model an engine structure for dynamic analysis.

In the engine modeling process, the first step is to identify the major static components. Typical static components are the cylinder head, gasket, cylinder block and crankcase of an engine. Then, the engine structure can be subdivided into more manageable subcomponents. Further subdivision into several subassemblies is also possible.

In a conventional design analysis process, at least two separate finite element models for an engine structure are required to simulate the engine both statically and dynamically. Consequently, an systematic and unique approach to engine modelling will be introduced.

3.2.3 New Modeling Technique using 3-D Solid Finite Element

To reduce the time and the cost for analysis and simulation of a particular design, it is essential to reduce the duplication of effort required to develop different finite element models for different analyses.

One tool used to strive toward these objectives involves the integration of various design activities such as design layout, geometric modelling, and design analysis based on a common geometric description. The use of solid modeling is a popular method to define

geometry and is easily extended to geometric and structural analysis. The use of a solid modeler enables an engineer to develop model geometry, while the mesh generator included in such software packages help to automate the task of creating nodes and elements from the geometric description of the design.

In generating finite element meshes, it is necessary to consider a consistent way to generate three-dimensional solid elements without changing the basic geometric representation used by the solid modeler. To do this, 8-node hexahedral elements or 4-node tetrahedral solid elements are a natural choice. This approach of using a three-dimensional solid finite element model for a rather complex geometrical structure is rapidly replacing more conventional model development methods which use higher order finite elements such as 20-node hexahedral elements. A significant time savings may be realized by using the simplest element to generate a finite element model. The 8-node hexahedral element is assumed to be one of the best choices to generate meshes in this regard.

Therefore, a finite element model of a complex structure such as an engine has been developed using simple HEXA8 finite elements. These elements are optimized in order to achieve a shorter computing time to form the stiffness matrices as well as increased accuracy for stress, thermal, and vibration analyses as shown in chapter 2.

In chapter 2, the practical applicabilities of the Directional Reduced Integration(DRI)technique, developed by Koh *et. al.*, has been tested successfully, and has proven to be a more efficient method than other methods like the selective reduced integration method, to achieve accurate results in three dimensional analysis. Therefore, DRI allows us to solve structural problem modeled with 3D solid elements. DRI is insensitive to the element rotation and solves shear related difficulties. Even a thin and deeply curved structure like an engine cylinder wall can be solved with the continuum approach using DRI as well as the plate and shell structures.

3.3 Finite Element Model of Cylinder Block

3.3.1 Preparation of Finite Element Model of Cylinder Block

The finite element modeling and analysis are performed on a Daewoo-M.A.N. D0846HM Diesel Engine. Finite element generation is carried out using INGRID, which was developed at the Lawrence Livermore Natxonal Laboratory[25]. In order to supply NIKE3D[24] parameters for the directional reduced integration method, with which finite element formulation is performed within NIKE3D, INGRID has been modified to generate these data from the geometry.

The structure is divided into several parts, a group of 6 cylinders, a cylinder block, a flywheel housing and the bearing caps. The cylinder block is made of cast iron and it is not symmetric. The block has a great number of stiffening ribs. To ease the work of modelling, we take advantage of the representative nature of only a few key parts of the cylinder block. As far as the cylinder block is concerned in this analysis, the main point is to represent the mass distribution of the cylinder block and the stiffness of cylinder block wall carefully. The displacement and vibration characteristics of the lower block are considered to be more important than those near the top of the structure. The upper part of cylinder block is much stiffer than the bottom. Thus, the lower part of block and its bearing housing are modeled more closely than are the upper part of the engine.

The finite element model of the diesel engine block for the study is shown in Fig.3.1. This finite element model consists of 5640 nodes and 2828 HEXA8 elements.

3.3.2 Structural Check of Model

Finite element predictions are uncertain without confirmation of the accuracy of the model. These predictions depend upon the analyst's judgement when constructing the finite element model as well as the capability of the code used for analysis.

To check the integrity of the model, the mass of the finite element model is compared to the actual component being modeled before beginning computations. Actual mass data is listed in Table 3.1 and compared with the mass which is computed in a routine of NIKE3D based on input geometry data. As seen in Table 3.1, the total acual mass is 197.7kg which includes the mass of 6 cylinder liners, while the computed mass was 201 kg. The total mass of the cylinder block was found by actual measurement to be 1.6% less than the figure obtained from the computer model. The finite element model corresponded to the nominal blueprint dimensions.

Table 3.1 Physical Data of D0846HM Diesel Engine

Unit : kg

Item	Quantity	Unit Mass
Cylinder Block Assembly (without Bearing Cap)	1	188.2
Cylinder Liner	6	9.5
Cylinder Head	3	64.8
Flywheel Housing	1	40.95
Crankshaft Assembly	1	66.7

3.4 Vibration Analysis of Diesel Engine Cylinder Block

3.4.1 Objects of Vibration Analysis

In this work, our attention was focused on the free vibration analysis. Therefore, it is not within the scope of this paper to analyze the stresses under more complex boundary conditions such as combustion forces. Such an extention is reserved for a future study.

Identification of the free vibration model of the engine structure is important for the following reasons:

- An understanding of the mechanisms of vibration may be obtained, which may suggest potential design improvement.
- Free modal data provides a powerful mechanism for the validation of finite element models.
- When used in conduction with radiated noise spectra, a knowledge of modal frequencies and shapes aides the synthesis of design improvements.

Assessment of free vibration results is basically split into two stages. The first is the validation of the analysis, achieved by standard checks such as ensuring that rigid body mode frequencies are at least two orders of magnitude lower than the first non-rigid mode.

The second stage of the assessment is the comparison of mode shapes and frequencies, preferably against experimental data. It is very difficult to identify equivalent mode shapes, for any but the first two or three modes by visual inspection. The comparison with experimentally obtained data is a severe and useful check on the validity of the finite element model. If both the total mass and the free vibration modes agree well, then it may be assumed that the model is accurate in terms of the important mass/stiffness distributions.

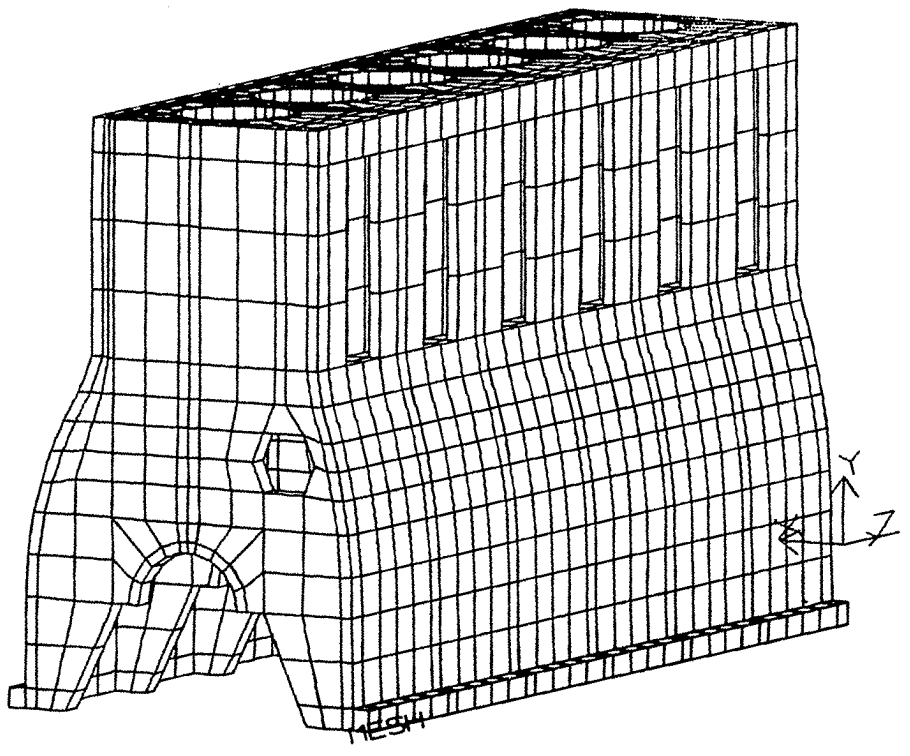

Fig. 3.1 Finite Element Model of Diesel Engine Cylinder Block

3.4.2 Free Vibration Analysis for Correlation with Modal Testing

A reliable model can be obtained, when one modifies the finite element model in order to correlate the computed modal frequencies with the measured ones. In this section, the analysis is performed in order to match the lower two eigenvalues to the ones from the modal testing of real engine structure before more detailed analysis is performed.

For this analysis, the finite element formulation is performed using the directional reduced integration with hourglass control. DRI is applied to the finite element formulation for the lower part of cylinder block, both skirt panels and the block partition plates. Through the correlation study, the finite element model is modified and refined, to obtain the final model to be used in later analyses.

A correlation study is carried out to determine modal characteristics of Daewoo-M.A.N. D0846HM diesel engine block, as well as to verify the finite element model whose lowest modes correspond to the ones obtained from modal testing of the engine [see chapter 6 and appendix 2 for the details of this method].

The experimental set-up, excluding the flywheel housing, was mounted on a rigid bed plate and supported by a ball at each corner. The structural influence of a supporting structure can be avoided by using small ball supports in order to simulate simply supported boundary conditions. The frequency response for this configuration is obtained as shown in Fig. 3.2, and the mode shapes at the lower two frequencies are shown in Fig. 3.3.

The first resonant frequency measured in this test was 199.67 Hz. The second resonant frequency was 430.0 Hz.

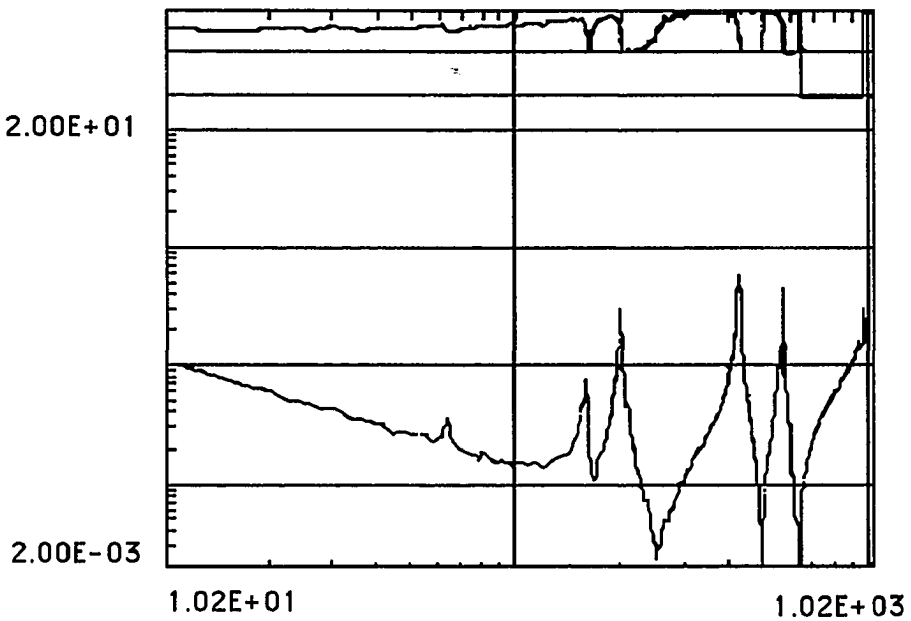

Fig. 3.2 Frequency Response Plot from Modal Testing

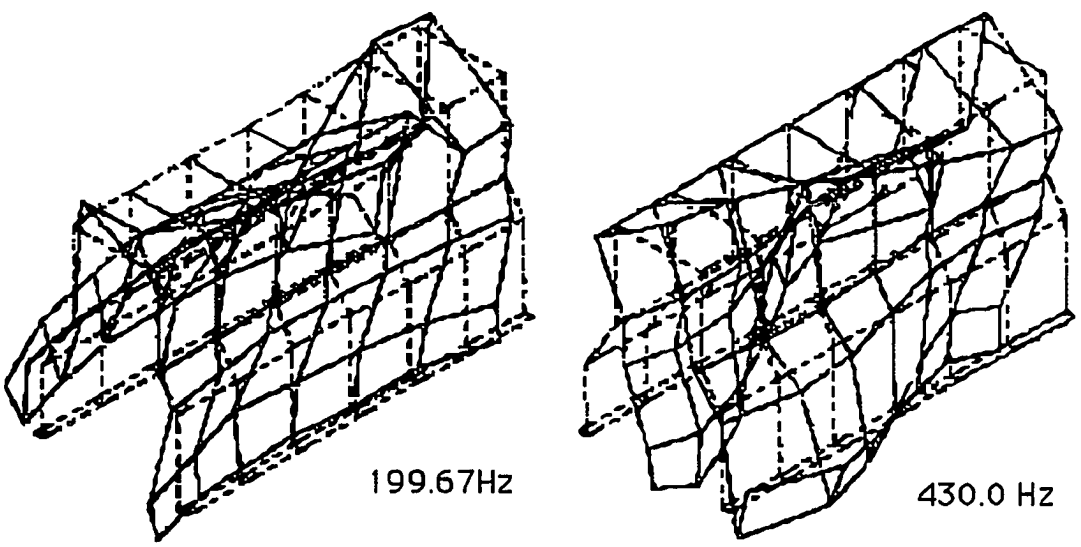

Fig. 3.3 Mode Shapes from the Modal Testing Results

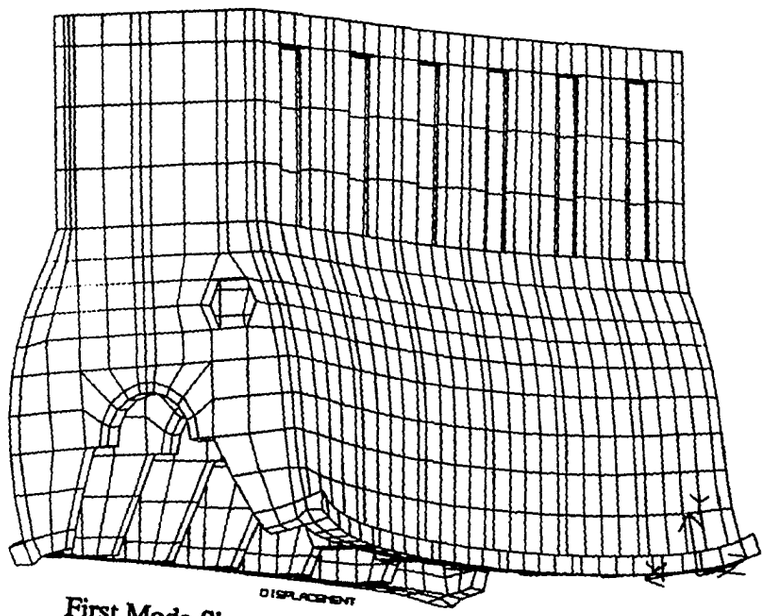

First Mode Shape of Cylinder Block(211.9Hz)

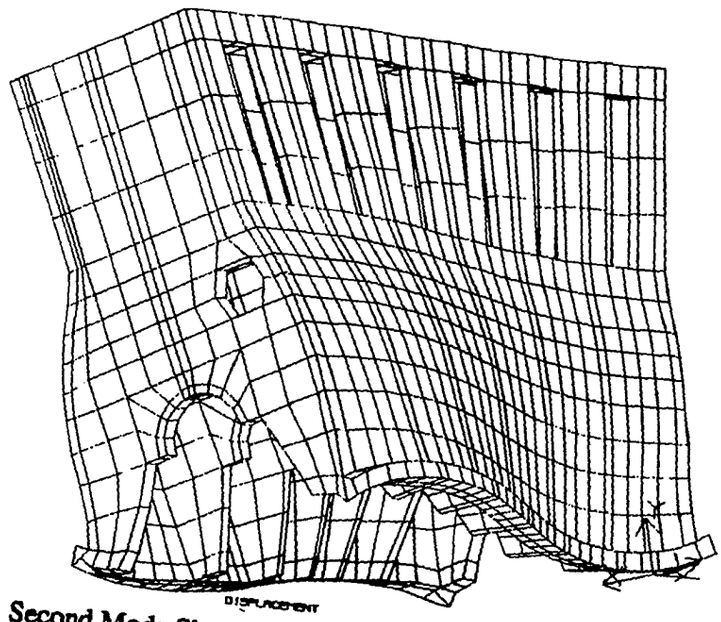

Second Mode Shape of Cylinder Block(484.2Hz)

Fig. 3.4 Mode Shapes of Cylinder Block under Simply Supported Boundary Condition

Table 3.2 Eigenvalues from Finite Element Solution and Modal Testing

Unit : Hz

Mode No.	Finite Element	Modal Testing	Remark
1	211.9	199.67	1. Bending Mode
2	484.2	430.0	Torsional Mode
3	___	573.5	2. Bending Mode

In the finite element analysis, simply supported boundary conditions were assumed to simulate the actual boundary conditions imposed by ball supports. This helped to achieve improved correlation with the results from modal testing, in which the results were compared according to the experimental set-up configurations [See chapter 5, for detailed configuration of experimental set-up's and its difference]. The eigenvalues from the finite element analysis are listed in Table 3.2. The results show that the two lowest frequencies are 211.9Hz and 484.2 Hz for the model are close to 199.67Hz and 430.0Hz which were observed experimentally. The Mode shapes of two lower modes are shown in Fig.3.4. These mode shapes of cylinder block are close to the ones obtained from modal testing as seen in Fig 3.3 and Fig 3.4. The finite element solution are greater than the experimental ones by 6% for the first mode and 11% for the second mode, repectively. Even though DRI with hourglass control evaluates the stiffness matrix of HEXA8 elements than the conventional integratiuon scheme, it is recognized that it is sometime difficult to eliminate such errors. This might be improved by some treatmenets; increasing elements of the model

and applying adaptive method. However, in view of reducing the size of the computational memory space and time, this model may be acceptable to be used for further analysis.

3.5 Dynamic Characteristics of Diesel Engine Cylinder Block

The finite element model of the cylinder block obtained from the correlation study may be used with confidence to study the dynamic characteristics of the given engine. A more detailed analysis of the cylinder block structure is presented in this section.

In the previous study, simply supported boundary conditions were assumed. However, when simply supported boundary conditions are assumed, some spurious rigid body motions can not be avoided. It can be difficult to determine whether some mode is rigid body or not. Since the experimental measurement of the cylinder block was limited to obtaining only the three lower modes of free vibration, the boundary condition could be changed to fixed boundary condition, in which the displacements are fixed and the rotations are allowed to move.

For this analysis, the finite element formulation was performed using the directional reduced integration with hourglass control as before. DRI was applied to the finite element formulation for the lower part of cylinder block, both skirt panels and the block partition plates.

It has been known that whole range of vibration modes are related to the vibration characteristics of various parts of the engine as known in the literatures. In particular, the highest frequency modes of vibration make the greatest contribution to the noise radiation. Even though the mechanism of the noise generation is not considered, the modes of the noise transmitting structures in the cylinder block are important to reduce the vibration level at certain modes which dominate most of noise transmitting through the strucure.

From the eigenvalue analysis of the engine block, only the first 11 modes were obtained due to the space limitations of the computer used in this study. The eigenvalues from the finite element analysis are listed in Table 3.3. The results show that the two lowest frequencies are 214.2Hz and 378.9 Hz. The mode shapes of modes 8,9, and 10 are shown in Fig.3.5. While it would be dersirable to look at higher modes, only modes of 8 to 11 ,whose frequency levels are greater than 1000Hz, were in this study.

The structural components on the external surfaces of the engine which radiate most of the engine noise are the crankcase panels, waterjacket panels, side covers, and sump. Many of these have numerous flexual modes of vibration, which are able to radiate noise efficiently above a certain frequency. This frequency is dependent oon the size of the engine. Typically it is approximately 1000 Hz for a mid-sized engine.

Table 3.3 Natural Frequencies From Finite Element Solution under Fixed Boundary Condition

Unit : Hz

Mode	Frequency	Mode	Frequency
1	214.2	7	801.5
2	378.9	8	1038.4
3	430.6	9	1193.0
4	462.5	10	1207.0
5	503.3	11	1257.9
6	725.1	12	—

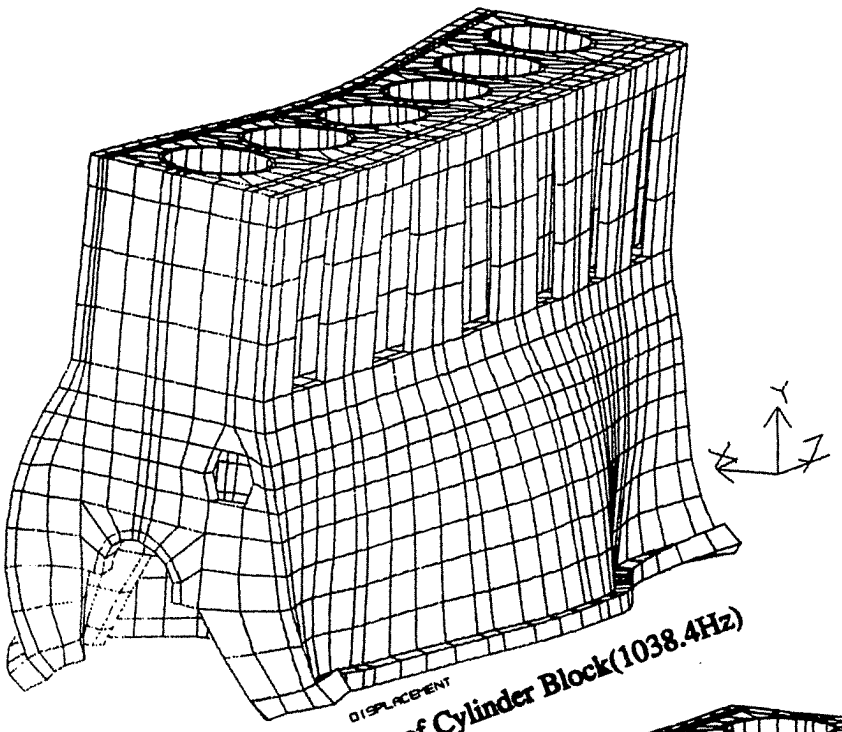

9th. Mode Shape of Cylinder Block(1038.4Hz)

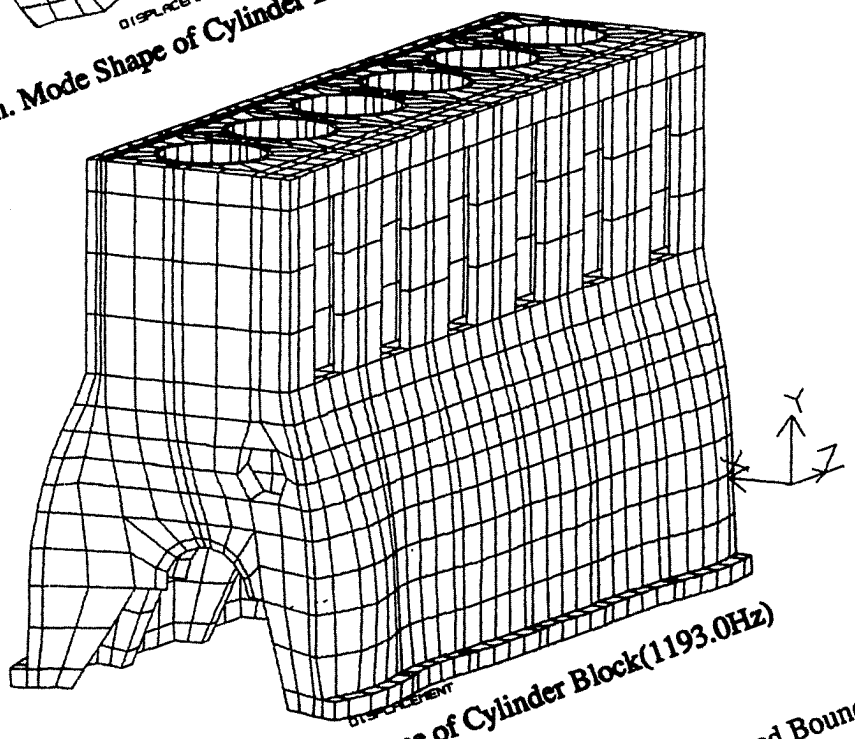

10th. Mode Shape of Cylinder Block(1193.0Hz)

Fig. 3.5 Mode Shapes of Cylinder Block under Fixed Boundary Condition at Four Corners

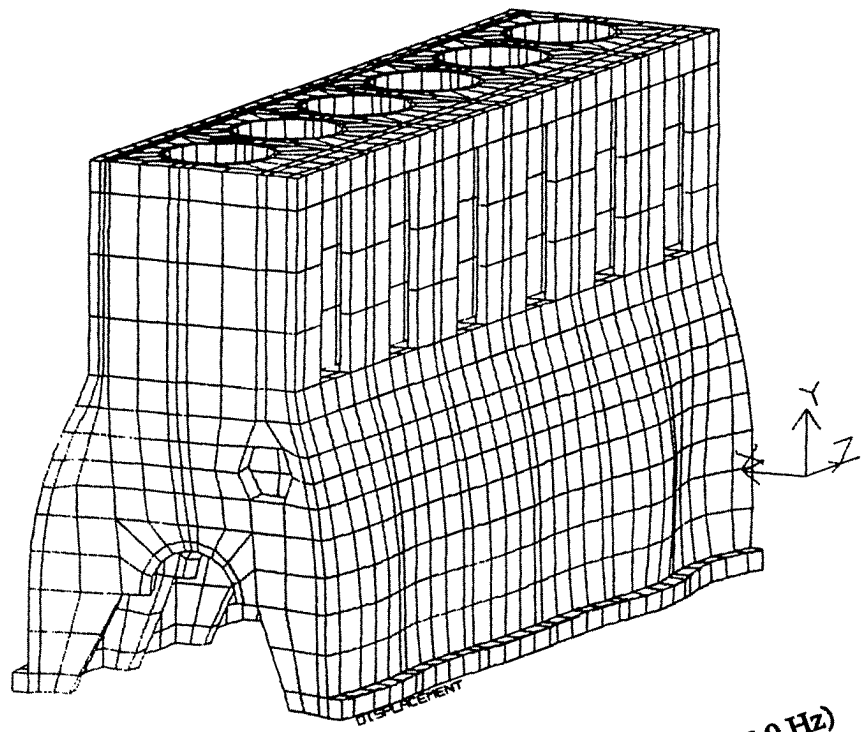

11th. Mode Shape of Cylinder Block(1207.0Hz)

Fig. 3.5 Mode Shapes of Cylinder Block under Fixed Boundary Condition at Four Corners(Continued)

The crankcase and water jacket vibrate in a series of modes. At high frequencies, a group of closely-related mode shapes appear, with only small differences in mode shape and natural frequencies between the members of each group. The normal modes which appear in mode shapes from the results are:

- Crankcase bending modes with torsion of cylinder block,
- Fundamental crankcase panel mode. With respect to any reference panel, the adjacent panels on that side of the engine, and the panel opposite on the other side of the engine, move 180 degree out-of-phase to the reference panel.
- Skirt-flapping modes on long-skirted crankcases.

Most of these modes are capable of radiating a significant amount of the noise from a conventional mid-sized engine.

The normal modes described above are fundamental to the response of the structure to mechanical impacts as well as to the cylinder pressure development. The distortion of the crankcase and cylinder block castings excites forced vibrations and resonant vibrations in the oil pan and valve-gear covers.

3.6 Conclusion

A finite element modeling and analysis of a diesel engine cylinder block was performed. Also, basic dynamic characteristics of the cylinder block are discussed before the detailed analysis was carried out.

To reduce the time and the cost for analysis and simulation of a particular design, it is essential to reduce the duplication of effort required to develop different finite element models for different analyses. The HEXA8 element is used to generate meshes. This approach of using a HEXA8 finite element model of a rather complex geometrical structure is more efficient to reduce system size than conventional model development methods which use higher order finite elements such as 20-node hexahedral elements.

Using a finite element model of the engine cylinder using HEXA8 elements, it was attemted to show that once the engine vibration problem is solved accurately, HEXA8 elements can be used for further thermal and stress analyses. Consequently, engine analysis is optimized with respect to shorter computation time required to form the stiffness matrices, and increase accuracy for stress and dynamic analyses.

The finite element model of a diesel engine cylinder block was analyzed using this newly developed directional reduced integration with hourglass control. It was shown that a fairly accurate eigenvalues were obtained when the results were compared with experiments. A significant time saving was realized by using the simplest element to generate a finite element model.

CHAPTER IV

APPLICATION OF ADAPTIVE FINITE ELEMENT METHODS TO VIBRATION ANALYSIS

4.1 Introduction

The adaptive method has been introduced in this decade to improve accuracy of finite element approximations based on *a posteriori* error estimates. Since Oliveira published his paper on mesh optimization in 1968, there have been many investigation on adaptive finite element methods. Earlier adaptive finite element method and mesh optimization were based on the variational principles together with mathematical programing methods for optimization[29,30,31,32]. Quasi-optimum meshes were attempted without utilizing 'a posteriori' error which can be computed from approximate solution. In 1976, Babuska and Rheinbolt[35,79] developed a mathematical theory of the adaptive finite element methods. They applied an estimated upper bound error as defined by interpolation error to the adaptive methods. Since Zienkiewicz *et. al.* [82] introduced of the adaptive method to engineering community in 1982, the adaptive finite element method was quickly accepted by engineers.

Recently, the adaptive finite element method has been introduced to some CAE system. However, most of the adaptive methods currently in use are still primitive in terms of user friendliness and the method used to achieve the desired accuracy. Therefore, in

order for the adaptive method to provide valuable information in the design analysis process, adaptive finite element method should be equipped with more up-to-date capabilities.

The adaptive methods can be applied not only to static problems but also to vibration problems. The main reason why the adaptive method is attractive in vibration problem, or transient problem, is its capabilities of controlling the amount of approximation error introduced by finite element methods. The finite element discretization can be optimized by relocating nodes(r-method), subdividing elements(h-method), and by increasing the degree of the polynomials for approximation of finite element methods(p-method). Details of each techniques are discussed in [40,42]. In most vibration problems, h-adaptive method is more efficient and applicable than r-adaptive method.

There was some discrepancy between the finite element solutions and actual test results of the cylinder block. In order to reduce these discrepancies, we employ an adaptive finite element method. When a large structure like an engine block is solved, we have to determine how to efficiently refine elements and manage such data. If a conventional direct method is used, one has to deal with the increase in bandwidth caused by introducing new nodes during mesh refinement. In order to use the adaptive method in a design analysis process of large structure, such a problem should be resolved.

In this chapter, some vibration problem is solved using adaptive methods. An additional investigation is made into the mesh refinement process, especially the h-method, in conjunction with space index mesh generation scheme.

4.2 Adaptive Methods in Vibration Problems

4.2.1 Selection of Error Measure

Most computational overhead of the adaptive method involves error estimation and the subsequent remeshing operation is a major task of adaptive finite elements. At every time step we estimate the error at all grid points and minimize this error by remeshing the structure. As the new mesh is created, then its initial values are obtained by interpolating data from the previous mesh points.

As mentioned before, there are several adaptive schemes and mesh moving strategies based on approximate error measures.Several different error indicators and methods of implementation are possible. The error estimate E_e of eq. (2.35) for each element is used to control the motion of the mesh and the refinement or coarsing strategy.

4.2.2 The r- Adaptive Method

The r-method, first investigated by Oliveira[31], is based on the design of optimal finite element grids. If the error measure of each element, E_e, is determined, we can consider a problem to minimize the maximum finite element error of the domain with the design variables of nodal coordinates as following:

$$\text{Min Max } E_e . \tag{4.1}$$

The necessary condition of Eq.(4.1) requires that the error in each element be constant, that is:

$$E_e = \text{constant for every element.} \tag{4.2}$$

Once the error measure E_e is computed, the strategy of nodal relocation can be set up. There are several versions of relocating scheme of nodes. In general, the new location of the n-th node can be defined such that

$$x_n = \Sigma\, x_e^c\, (E_e / A_e) / \Sigma\, (E_e / A_e) \tag{4.3}$$

where the summation is taken over the finite elements connecting to n-th node, x_e^c is the coordinate of the centroid of Ω_e and A_e is the area. Relocation and finite element analysis with new discretization are repeated until the condition of Eq.(4.2) is met. The schematic view of the relocation scheme according to (4.3) is shown in Fig.4.1.

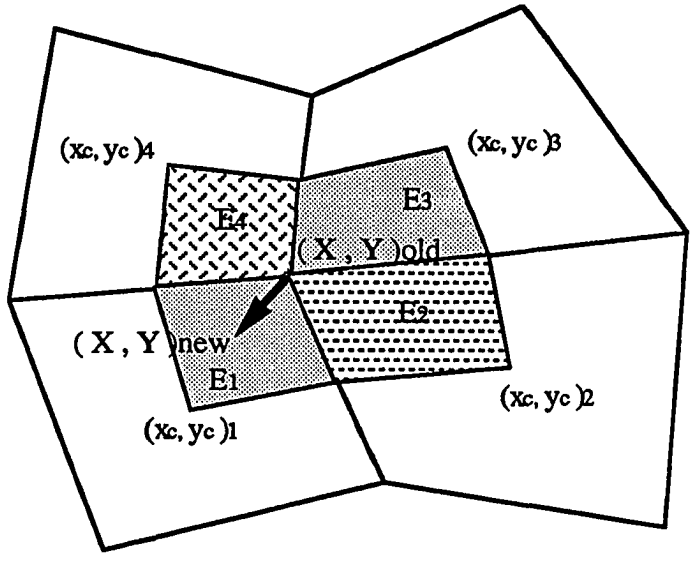

Fig. 4.1 Schematic View of the Node Relocation Scheme

It has been noted that the relocation scheme in r-adaptation method cannot represent the necessary condition Eq.(4.2) appropriately if the neighboring elements are too distorted[42]. In order to solve this difficulty, a computational geometry, which has only rectangular elements, is prepared for node relocation as seen in Fig. 4.1. Indeed, the parametric (transformation) relation between the physical and computational geometry can be obtained by using a mapping mapping method.

The procedure for node relocation is as follows:

1. evaluate the error in the physical domain according to Eq.(2.35),
2. perform node relocation in the indexed space (computational domain) according to Eq.(4.3),
3. then find the new node location by applying the transformation relation.

4.2.3 The h- Adaptive Method

The h-method, originally studied by Sewell and Babuska, is the method in which refinement is performed by subdividing elements, which have a large amount of error, into much smaller ones. Using the adaptive grid, analysis is performed again to compute the error measure in each finite element, and the subdivision process of finite elements is repeated. Even though the necessary optimality condition is never satisfied by h-adaptation, the absolute value of the difference of the maximum and minimum error measure decreases considerably as well as the value of the maximum error measure. Furthermore, the amount of finite element approximation error can be reduced. These are limitations of the h-method.

The h-method adaptive remeshing scheme illustrated in Fig.4.4 is used. In the figure, numbers denote the relative amount of approximation error in each element. When one element has a relative error of 2, and the other element have relative error of 1, then the element of amount 2 will be subdivided.

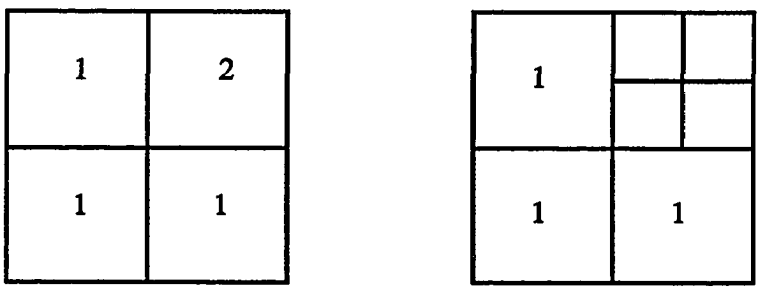

(a) before remeshing (b) after remeshing

Fig. 4.2 Remeshing Scheme in h-Adaptive Method

In this case, the parametric space is used to generate subelements just the same as in the r-adaptive method. Since it is quite difficult to identify additional constraint condition, and to generate additional nodes and element connectivities in 3-D space. This method is computationaly expensive relative to the r-method.

4.3 New Adaptive Mesh Generation Technique

4.3.1 Representation of Geometry

The first step, in this section, is representing a 3-D surface. The boundary of the desired geometry is defined using several cubic curves. 3-D surface can be generalized

from those cubic curves to bicubic surfaces defined by cubic equations of two parameters, s and t. Varying both parameters from 0 to 1 defines all points on a surface patch. If one parameter is assigned a constant value and the other parameter is varied from 0 to 1, the result is cubic curve. As with curves, we will work only with the parametric equation for x, denoted by x(s,t).

One form used to represent x(s,t) is:

$$x(s,t) = SC_x T^T, \tag{4.3}$$

where $S=[\ s^3\ \ s^2\ \ s\ \ 1\ ]$, $T=[\ t^3\ \ t^2\ \ t\ \ 1]$. This is called the algebraic form of the representation, because C_x gives the coefficients of the bicubic polynomials. There is also a C_y and C_z which gives the coefficient of y(s,t) and z(s,t). However, there are several form to define C's. The following simple blending function[86] is used to interpolate 3-D surfaces:

$$r = (1-\xi)r(0,\eta) + \xi\, r(1,\eta) + (1-\eta)r(\xi,0) + \eta\, r(\xi,1)$$

$$- (1-\xi)(1-\eta)\, r(0,0) - (1-\xi)\eta\, r(0,1) - \xi(1-\eta)\, r(1,0) - \xi\eta\, r(1,1). \tag{4.3}$$

4.3.2 Base Mesh Generation

For adaptive mesh generation, the idea employed by the INGRID mesh generation package, which generates complete input files for the codes NIKE3D and DYNA3D, will used. Geometries are described primarily by using index space concepts which came from the program INGEN[25].

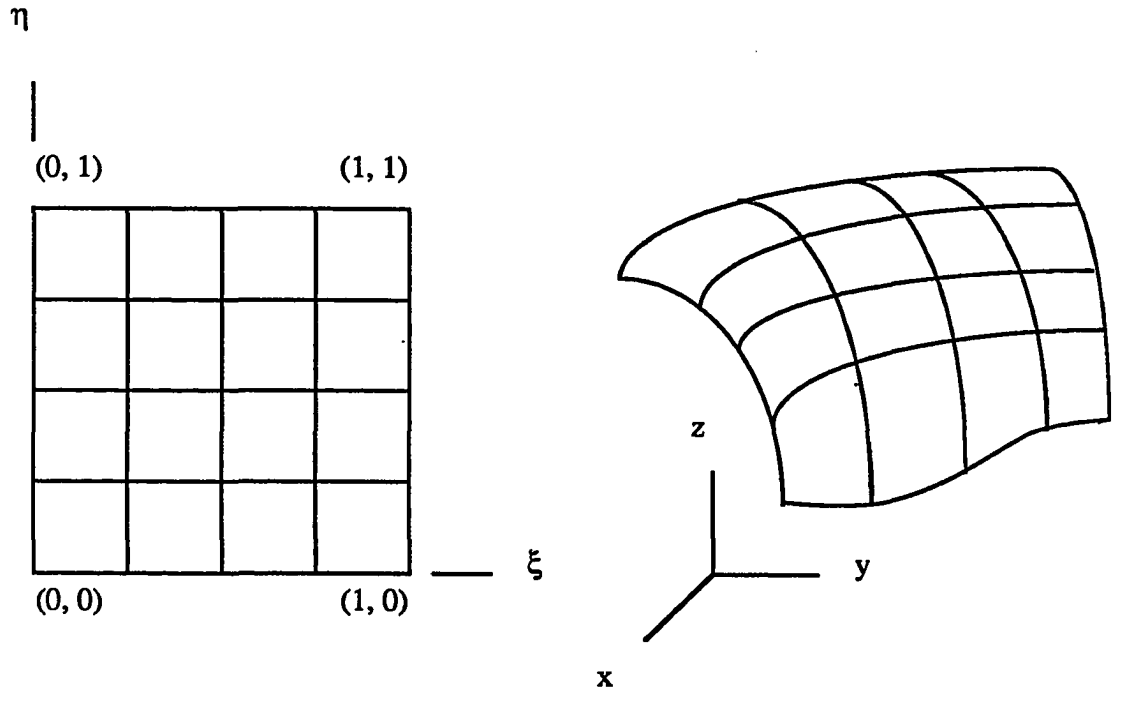

Fig. 4.3 Transformation for a Surface

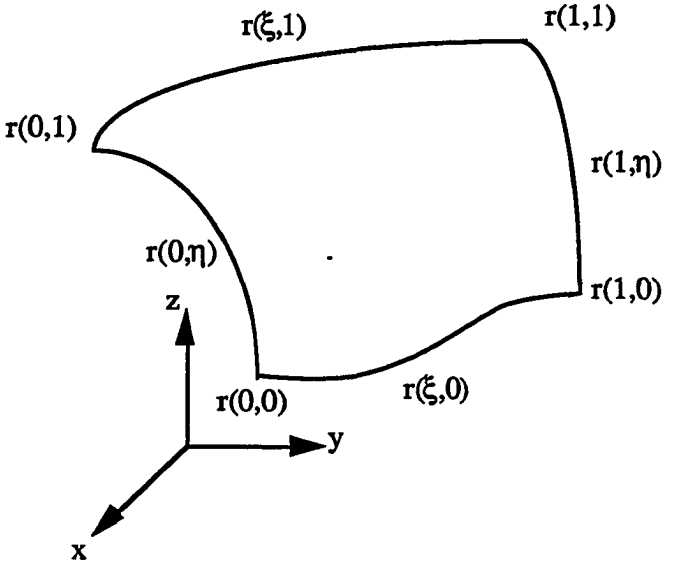

Fig. 4.4 Coons Blending Function

An index space is a three-dimensional discrete coordinate system with integer greater than or equal to 1 in each of the three directions. The three discrete coordinates are labeled I, J, K axes respectively. Each point in the index space, (i, j, k), represents a nodal point. Element are defined as a group of adjacent nodes in the index space.

In an index space, a region can be defined. A region is any rectangular or cubic block of nodes. A region is usually defined by a block of nodes in an index space. Second higher definition id part. A part is a collection of regions which can be grouped and generated conveniently in an index space. The final model is a collection of parts. Each part has its own index space and independent of other parts. Parts are connected together either by global coincident node removal, slide surfaces, or other constraints.

4.3.3 Adaptive Mesh in a Time Dependent Problem

The time dependent problem differs from the steady-state problem, in that irregularities in the solution may migrate over the grid during a given time interval. The grid thus has to adapt itself continuously to meet the accuracy requirements of the solution. If some changing feature of the solution is lost at an intermediate step, then this loss may be unrecoverable in future solution steps. Time dependent problems require that, besides a refinement capability, we also have an unrefinement capability. In general, we require that only groups of elements that were refined before can be unrefined. The error of a group of elements is equal to sum of the errors of the elements in that group.

4.4 Practical Considerations for the h-Method

4.4.1 Initial Mesh

The initial mesh is generated in parametric space. In parametric space, the coordinates are expressed by index numbers. The coordinates, (n_s,n_t), in parametric space have the following relationship with space index number(N_s, N_t):

$$N_s = N_i + \chi_s \cdot n_s \quad , n_s = 1,2,....NS_{max} \quad ,$$

and

$$N_t = N_j + \chi_t \cdot n_t \quad , n_t = 1,2,....NT_{max} \quad .$$

where χ_s and χ_t are allowable subdivision numbers in one element in s and t directions, respectively when QUAD4 elements are used. Also, NS_{max} and NT_{max} are maximum node numbers in s and t direction of the initial grid. Thus, some nodal points in index space may not be occupied by initial grid, acting as fictious nodes.

4.4.2 Consecutive Steps for Refining Elements

Assume at this point that we have identified an element that can be refined without violating any topological constraints. Then the actual processing of the refinement is very simple.

1. Once the finite element solution is achieved using the initial mesh or previous mesh and the error measure for each element is computed, then these error measures for each element are averaged. Using some fraction of averaged error measure, the appropriate division level is determined for each element

when the amount of error of that element is larger than a specified fraction of the averaged error.

2. In Fig.4.5, the node and element numbering sequence is illustrated when remeshing of grid is needed according to the level of error. Initial space indices are generated according to the maximum level of subdivision. Initial mesh is generated based on those space indices, thus, some indexed coordinates are not active.

3. Generate new element and node numbers in the index space. In general, there are active numbers corresponding to the nodes of real mesh and inactive numbers not occupied by mesh in the index space. We choose the element and node numbering sequence as illustrated in Fig.4.5. Then element numbers are sorted in order.

4. Compute the connectivities of the elements. This can be easily deduced from the activeness data array of elements according to space indices. These element connectivity data are sorted in order to achieve better efficiency.

5. Adapt the connectivities of the surrounding elements. Whereas the surrounding elements pointed to one single element, they will now point to the four subelements. Then, nodal constraints are determined.

6. Interpolate solution over the new nodes.

Certain situations are treated as exceptions. For example, if an element is successively refined, but its neighbor is not designated to be refined on either pass, then we force the coarser refinement of the neighbor to ensure a smoother mesh grading and to simplify the data structure[see Fig 4.6]

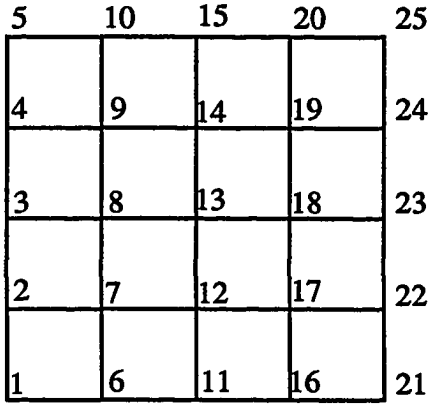

(a) Index Space

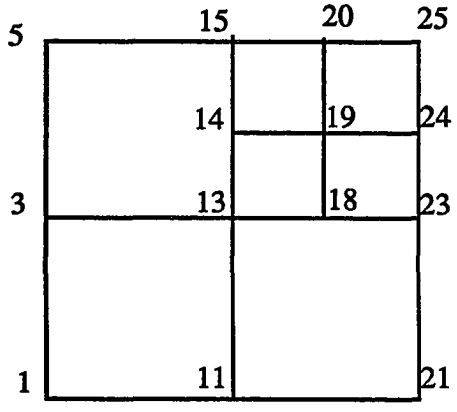

(b) Node Numbering in Index Space

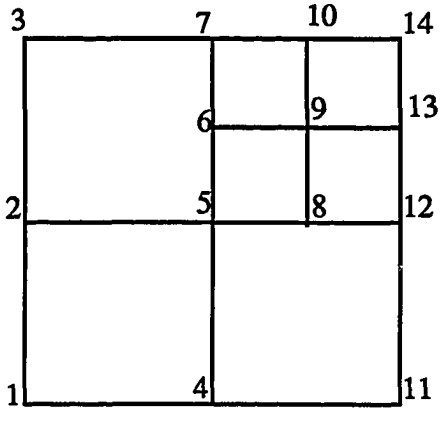

(c) Final Node Numbering of
Adaptive Mesh in Parametric Space

Fig. 4.5 Numbering Sequence of Elements and Nodes in the h- Adaptive Method

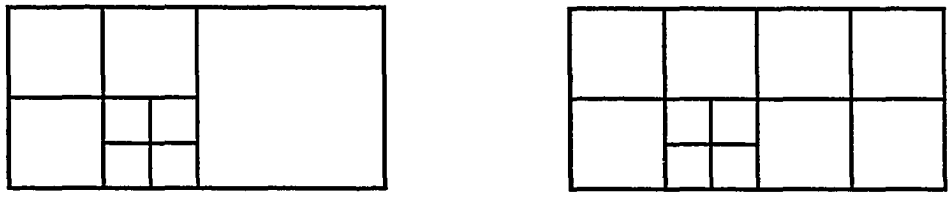

Rejected Accepted

Fig. 4.6 Refinement of a Neighbor Elements to Avoid Multiple Constraints

Going through these steps, one sees that we have updated or created all items of the original data structure. Moreover, the initial data was sufficient to all these operations on a local basis, i. e. no loop over the mesh nodes or elements was necessary to do the operations. In addition, no data about the refinement history of the element was necessary.

In this refinement scheme, refinement element data structures have following data associated with neighbor elements, such as element number, refinement level, neighbor element, and constrained node data. Here, the refine level indicates the level of refinement of an element, e.g., 0=unrefined, 1=refined once, 2=refined twice, etc.

This h-mesh generation scheme can be generalized to the 3-D case with minor modification. This scheme is quite helpful to generate a mesh for 3-D complicated structure and reduce the extraction time of data.

4.4.3 Constraint Conditions

An essential part of the refinement strategy is that, in order to satisfy continuity over the boundaries of the elements, some nodes need to be constrained. First we describe how constrained nodes are identified using the current data structure. Secondly, we show how the node array is used to identify the degree of freedom of an element. Finally, we show how the element matrices are computed and adapted to reflect the elements.

4.4.3.1 Identification of Constraints

When the level of a neighbor of an element is lower that the level of the element, then the element has a constrained node on that side. The actual node that is constrained can be identified by looking for the connection number by which the first element is connected to the neighbor. Depending on whether the connection number is smaller or greater than four, we can conclude which node is constrained.

4.4.3.2 Consideration of Constrained Conditions in the Element Matrices

The variable of constrained node of the element is equal to the average of the two corner nodes which possess the constrained nodes. Actually, the location of the constrained node of the element may not be found as the average of the physical location of the two corner nodes. Once we have constrained node data, we compute the element matrices in usual way. In order to reflect the constraints, the shape function of constrained node is equal to 1/2 at the physical location of node 2. Thus, we have following penalty matrix for constrained conditions when QUAD4 elements are used:

$$p = \begin{bmatrix} 1 & \frac{1}{2} & \frac{1}{2} \\ \frac{1}{2} & \frac{1}{4} & \frac{1}{4} \\ \frac{1}{2} & \frac{1}{4} & \frac{1}{4} \end{bmatrix}. \qquad (4.5)$$

4.5 Application of the Adaptive Method to the Vibration Problems

Adaptive methods are used to solve a cantilever beam modeled with 8 node hexahedral elements. The beam is loaded under a sine function of unit magnitude. It is known that although a large time increment Δt is assumed, the Newmark-β method will provide a fairly good solution which is close to the exact solution. Thus, in this example, we will investigate how an adaptive method will improve solution of dynamic response and see what kind of adaptive method is preferred in solving a vibration problem.

The finite element discretization of the model is shown in Fig.4.7. At each time step, the error of each element is calculated. The problem is solved by the r-method using 4 elements and 8 elements respectively, and is solved by the h-method using an initial discretization of 4 elements. According to the error measure, the finite element model is remeshed based on both the r-method and the h-method and then, reanalyzed. In the h-adaptation one-time subdivision for each element is performed.

Results of solutions by the r-method are listed on Table 4.1 and 4.2 and Fig. 4.8. Results of solutions by the h-method are shown in Fig. 4.9. The responses of the beam using both r- and h- method at each time step are shown in Fig. 4.10.

As shown in Table 4.1 and 4.2, in the r-adaptation, the maximum error measure is reduced satisfying the optimality condition at each time step, while the total amount of error remains unchanged. Consequently, the r-adaptive mesh is achieved at each time step as

shown in Fig. 4.8. If r-adaptation is applied several times at each time step the mesh may converge close to the optimal mesh at a given number of nodes and elements. In the h-adaptation, even though the necessary optimality condition is not satisfied, the amount of finite element approximation error can be reduced and the refined mesh configuration obtained by subdivision of elements whose error amount is large as shown in Fig. 4.9. However, since the numbers of elements and nodes are increased by refinement, some additional justification is needed to consider the h-adaptation method.

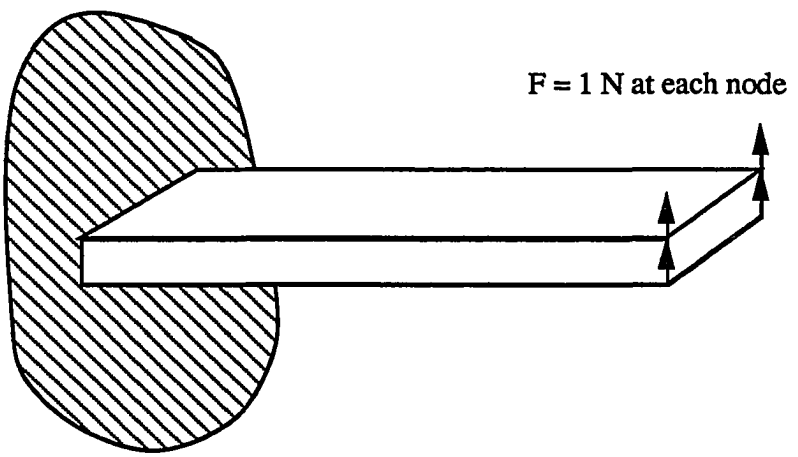

Young's Modulus	:	2.08 E11 Pa
Poisson's Ratio	:	0.3
Density	:	7800 kg/m3
Dimension	:	0.5b x 0.25h x 5.0L (m)

Fig. 4.7 Undeformed Shape and Properties of Beam

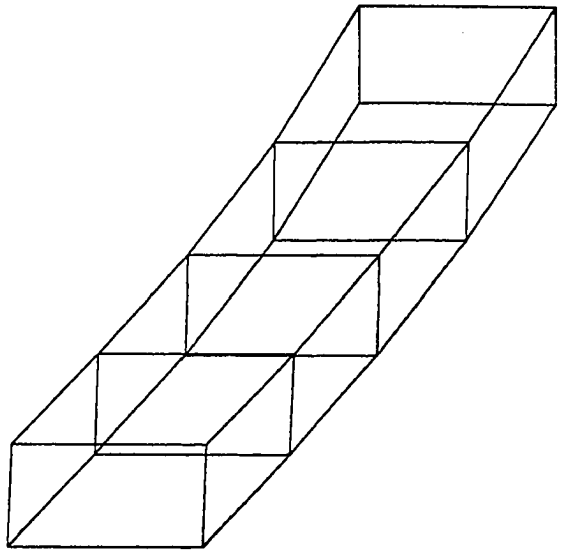

(a)Deformed Shape at Time Step 3 with Regular Mesh of 4 Elements

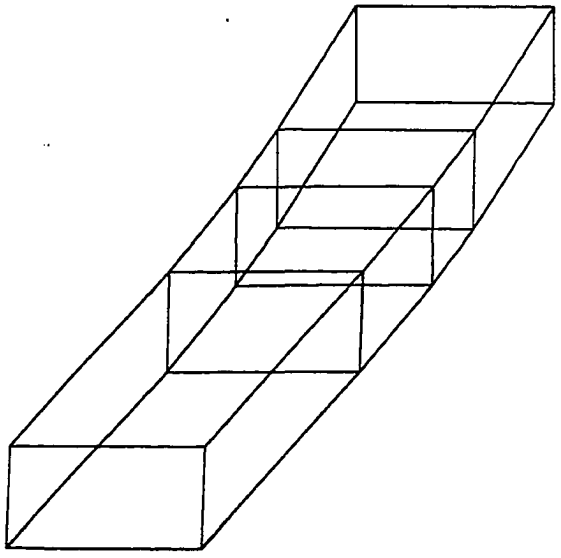

(b)Deformed Shape with Mesh Adaptation by r-Method

Fig. 4.8 Response of Cantilever Beam using r-Method (4 Elements)

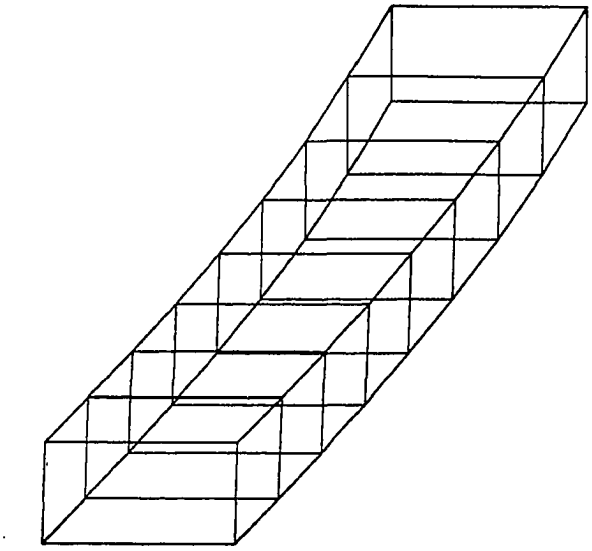

(a)Deformed Shape at Time Step 3 with Regular Mesh of 8 Elements

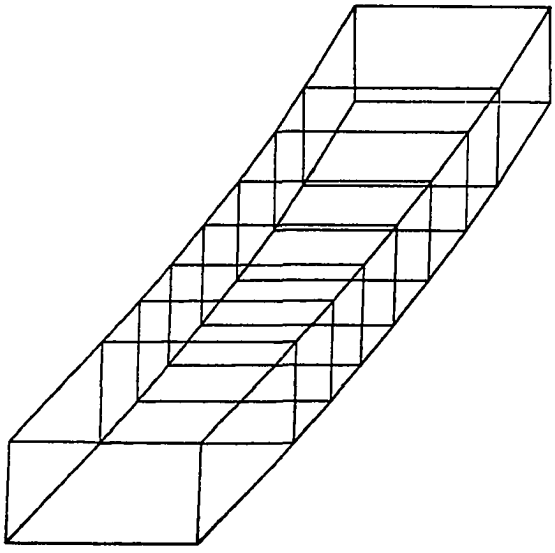

(b)Deformed Shape with Mesh Adaptation by r-Method

Fig. 4.9 Response of Cantilever Beam using r-Method (8 Elements)

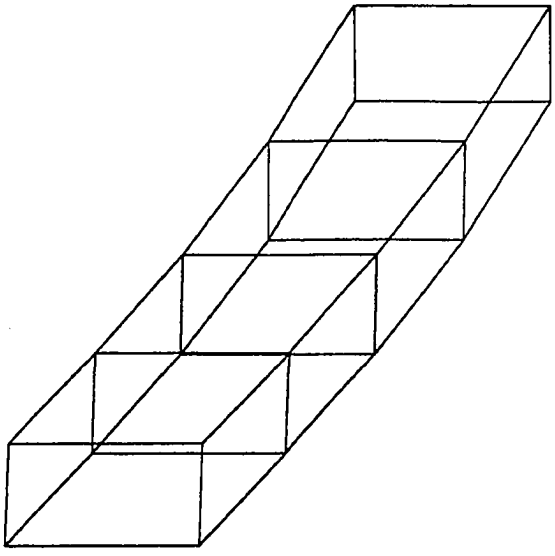

(a)Deformed Shape at Time Step 3 with Regular Mesh

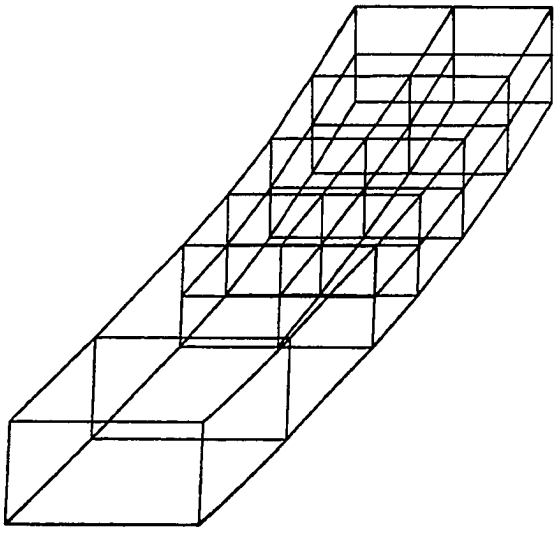

(b)Deformed Shape with Mesh Adaptation by h-Method

Fig. 4.10 Response of Cantilever Beam using h-Method (4 Elements)

Table 4.1. Error Distribution of Beam
(4 Elements)

Unit: m

Elem No.	Time Step 1		Time Step 3	
	Initial Mesh	r-adaptation	Initial Mesh	r-adaptation
1	0.7726E-02	0.2244E-02	0.1670E+00	0.4515E-01
2	0.1553E-01	0.5036E-02	0.3357E+00	0.1089E+00
3	0.3871E-02	0.5152E-02	0.8367E-01	0.1179E+00
4	0.7191E-02	0.2464E-02	0.1554E-01	0.5327E-01

Table 4.2. Error Distribution of Beam
(8 Elements)

Unit: m

	Time Step 1		Time Step 3	
	Initial Mesh	r-Adaptation	Initial Mesh	r-Adaptation
1	0.1211E-02	0.7869E-03	0.2619E-01	0.1701E-01
2	0.3036E-02	0.2078E-02	0.6562E-00	0.4492E-01
3	0.1616E-02	0.6603E-03	0.3494E-01	0.1427E-01
4	0.1197E-02	0.7843E-03	0.2588E-01	0.1696E-01
5	0.7143E-03	0.4184E-03	0.1544E-01	0.9045E-02
6	0.3750E-03	0.2369E-03	0.8106E-02	0.5121E-02
7	0.1544E-03	0.4831E-03	0.3339E-02	0.1044E-01
8	0.2260E-03	0.1278E-03	0.4885E-03	0.2763E-02

As seen in Fig. 4.11, the h-adaptation method provides better solutions than the r-adaptation method. The r-adaptation method can not provide better solutions for this kind vibration problem even though the optimum mesh may not be achieved as the h-method.

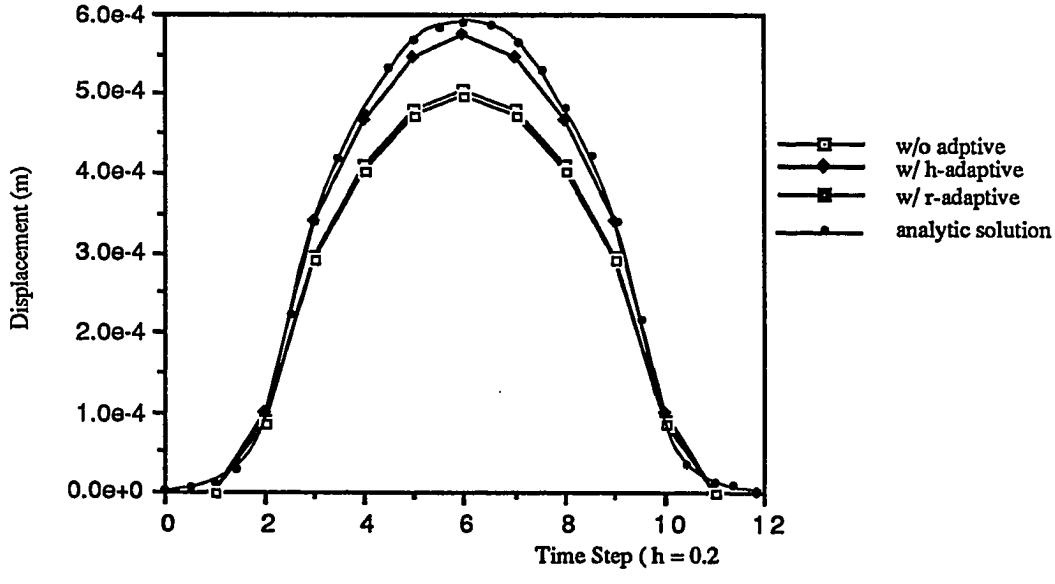

Fig. 4.11 Response of Beam at Each Time Step According to Methods at Free End

CHAPTER V

VARIABLE TIME STEPPING ALGORITHM FOR IMPLICIT TIME INTEGRATION

5.1 Introduction

There have been several time integration schemes developed to solve dynamic problems[59,60,66,77]. These schemes have been verified and found to be quite successful in many different types of problems in the area of dynamics. Previous authors have suggested that integration schemes must be examined for accuracy and stability performance on each individual dynamic problem.

A number of implicit integration methods are in common use for structural dynamics problems, and have been reviewed, both analytically[50, 54, 66, 69, 71], and by numerical experiment[52, 68, 73, 74, 75]. The implicit algorithms are unconditionally stable. The evidence indicates that these algorithms can use quite large time steps, and will provide reasonable accuracy in the solution, when the determination of lower modes are of prime concern. It is seen that the implicit algorithm has been one of the most effective time integration methods for the transient analysis of linear structural dynamics. A substantial saving of computational effort can be attained by using an unconditionally stable algorithm because a large time step can be used.

Most numerical experiments show a steady and rapidly increasing growth of error as the time step increases. Accuracy requirements suggest that it is important to control the error in the time matching scheme. In the practical and professional environments, it has become evident that there is a great need for an algorithm that can calculate the optimum time step in an automatic fashion during the solution process. The requirements for such an algorithm should be: significant error control, computational efficiency, and convenience of implementation. Many researchers have addressed this problem, but it is recognized in the literature that no satisfactory general approach is available. Strategies implemented in many structural-response codes are mostly empirical or are dedicated to particular situations.

It is a difficult task to assess what the error will be for large systems for which the solution consists of *a priori* unknown combinations of modal response. Moreover, the characteristics of the total responses may change with time, thus, the optimal time step may change during the solution process. Such variations in response are very common for transient and nonlinear problems. The situation is even more complicated when an unconditionally stable algorithm is used.

There have been several variable-step integration procedures proposed for both explicit methods by Krogh[62], Brayton *et al.*[63], Shampine[53], Zadunaisky[64], Park[48], and implicit methods by Wilkinson[65], Hibbit *et al.*[70], Key[68]. The four strategies proposed in the above citations are based on the local truncation error, the residual terms, Richardson's extrapolation method and the deviation from linearity.

The use of the local truncation error is a well-known technique. Several different approaches to error estimation have been reported in the literature. Gear and Tu[67] used an error measure based on truncation error using a predictor-corrector pair applied to a variable multi-step method. Similar expression can be found in Shampine[53], in which the remainder is used to define the error estimation and was used with Euler method. Close

examination of the error estimation defined by a predictor-corrector pair leads to the fact that the apparent frequency can be defined and has been used to adjust time step in explicit method such as central difference scheme. Another approach other than to measure the error can be found in Park[48]. In this case, the highest apparent frequency was used to control the step size in a central difference method. In most implicit methods, for example in Hilber[57], it was attempted to measure the error committed in each time step using a Taylor's series expansion to verify the accuracy of his α-method. However, the use of the local truncation error using a predict-correct pair has been commonly used and is considered to be a very reliable measure to control step size changes. Although this appears to be the case for high accuracy requirements, i. e., the relative local error is less than 10^{-5}, its applicability to oscillatory problems such as structural dynamic problems has not been firmly established. Moreover, in most typical structural dynamic analysis, lower accuracy is often satisfactory if this keeps the analysis cost low. Thus, by improving the traditional truncation error based stepsize change technique, a cost-effective method is presented which will provide a reliable solution.

The method described in this work has many similarities to the technique of step selection developed previously and shown in the literature. The method is primarily based on a local error control technique using a truncation error measure. In order to enhance effectiveness of the traditional algorithm, several improved techniques are introduced for adjusting time step size for solving multi-degree-of-freedom systems.

As a first attempt, a measure of the error committed in each time step during the process of time integration is newly defined. Since the use of truncation error using a predictor-corrector pair cannot reflect the real characteristics of error development in each time step for each individual problem in conjunction with an integration scheme used. The definition of error measure should be appropriate for the specific time integration method, for example, Newmark-β method. In addition, we have assumed a precisely defined twice

differentiable forcing function for obtaining a measure of the truncation error for the forced response system. In practice, forcing functions consist of experimentally observed loads at discrete time intervals, therefore the computation of the required derivatives is not always possible. To resolve such difficulties and to reduce unnecessary computation even when the force can be approximately determined at every time step, a new approach is presented.

The new approach is made to fully implement time step control to the multi-degree-freedom system. Since the previous development is made on a decoupled equation based on modal decomposition, a parameter to control error or to select step size is obtained by superposing several properties up to several modes. If the order of matrices is large, the computer time required to solve all eigenvalues and eigenvectors is enormous. It is tedious to extract only several lower modes of the system, even though these several modes seem to represent dominant structural dynamic characteristics. Thus, "the current frequency", which is derived from the Rayleigh Quotient, is introduced in evaluating the evolution matrix for time integration. Employment of this "current frequency" provides very accurate measure of the truncation error and saves the computation time for evaluating error at each time step.

The success of the method is dependent upon the efficient implementation of the above algorithm to a main solver. These concepts and other practical aspects will be presented in this work through solving typical dynamic problems.

5.2 Time Integration of a Dynamic System

5.2.1 Equation of Structural Dynamics

Consider the matrix equation of structural dynamics:

$$[M]\{\ddot{u}\} + [C]\{\dot{u}\} + [K]\{u\} = \{F\}, \tag{5.1}$$

with initial conditions

$$\{u(0)\}=\{d\},\ \{\dot{u}(0)\}=\{v\},$$

where [M] is the mass matrix, [C] is the damping matrix, [K] is the stiffness matrix, {u} is the displacement vector, and {F} is the external force vector, and {d} and {v} are the given initial data.

Applying the modal decomposition procedure to (5.1) yields the corresponding SDOF equations which, if we suppress the modal index *l*, appear as:

$$\ddot{u} + 2\xi\omega\,\dot{u} + \omega^2 u = F, \tag{5.2.a}$$

$$u(0)=d, \text{ and } \dot{u}(0)=v. \tag{5.2.b}$$

5.2.2 Temporal Discretization

An approximate solution of (5.1) can be obtained using the Newmark-β time integration algorithm. In the Newmark-β method, a Taylor series expansion of displacements and velocities is used to construct linear relationships.

Consider the following family of one-step difference methods to obtain approximate solutions of the initial-value problem:

$$u^{n+1}=u^n + \Delta t\ \dot{u}^n + \frac{\Delta t^2}{2}[(1-\beta)\ddot{u}^n + \beta\ \ddot{u}^{n+1}] + R_n, \tag{5.3.a}$$

$$\dot{u}^{n+1}= \dot{u}^n + \Delta t\,(1-\gamma)\ddot{u}^n + \Delta t\ \gamma\ \ddot{u}^{n+1} + R_n', \tag{5.3.b}$$

$$\ddot{u}^{n+1} = \frac{\Delta u}{\beta \Delta t^2} - \frac{\dot{u}^n}{\beta \Delta t} - \frac{1}{\beta}\left(\frac{1}{2}-\beta\right)\ddot{u}^n, \tag{5.3.c}$$

where $\Delta u = u^{n+1} - u^n$ with initial conditions

$u(0)=u_0$,

$\dot{u}(0)=\dot{u}_0$,

$\ddot{u}(0)=(F_0 - 2\xi\omega\dot{u}_0 - \omega^2 u_0)$.

Here, Δt is the time step size, n is the time step number, u^n, $\dot{u}^n$, and, $\ddot{u}^n$ are the approximations to $u(t_n)$, $\dot{u}(t_n)$, and $\ddot{u}(t_n)$, respectively, in which $F_n = F(t_n)$,and β and γ are the free parameters of integration which govern the accuracy and stability of the algorithm. If $\beta=\frac{1}{4}$ and $\gamma=\frac{1}{2}$ the Newmark-β method is obtained. If $\beta=\frac{1}{6}$ and $\gamma=\frac{1}{2}$ the Wilson-θ method is obtained.

The remainder terms are given by

$$R_n = -(\beta - \tfrac{1}{6})h^3u^{(3)}(\tau) + O(h^4u^{(4)}), \tag{5.4.a}$$

$$R_n' = -(\gamma - \tfrac{1}{2})h^2u^{(3)}(\tau) + O(h^3u^{(4)}), \tag{5.4.b}$$

and the maximal accuracy is obtained when $\gamma=\frac{1}{2}$ and $\beta=\frac{1}{6}$. These remainder term will be further discussed in the section 5.3.2. It can be verified that this choice corresponds to a linear interpolation of acceleration over the time interval.

For transient dynamic problems, Eq. (5.1) may be written in time difference form as follows:

$$[M]\{\ddot{u}^{n+1}\} + [K]\{\Delta u^{n+1}\} = \{P(x^n)\}^{n+1} - \{F(x^n)\}, \tag{5.5}$$

where

$\{P(x^n)\}$: external Load,

$\{F(x^n)\}$: internal Load,

u^{n+1} : displacement = $x^{n+1} - x^n$, and

$\ddot{u}^{n+1}$: acceleration at time n+1.

Substituting Eq.(5.3) to Eq. (5.5) to yields:

$$[K^*]\{\Delta u^{n+1}\} = \{P(x^n)\}^{n+1} - \{F^*(x^n)\}, \tag{5.6}$$

where

$[K^*] = [K] + [M] / \beta \Delta t^2$, and

$$\{F^*\} = \{F\} - [M]\left(\frac{\dot{u}^n}{\beta \Delta t} + \frac{1}{\beta}\left(\frac{1}{2} - \beta\right)\ddot{u}^n\right).$$

From the Eq.(5.4) to (5.6), we can express the implicit time integration scheme in terms of y^n, and y^{n+1} as follows:

$$[A_1]\{y^{n+1}\} = [A_2]\{y^n\} + \{H^n\} \tag{5.7}$$

where

$$[A_1] = \begin{bmatrix} 1+\Delta t^2 \beta\omega^2 & 2\Delta t^2 \beta\xi\omega^2 \\ \Delta t\, \gamma\omega^2 & 1+2\Delta t\, \gamma\xi\omega \end{bmatrix},$$

$$[A_2] = \begin{bmatrix} 1-\frac{\Delta t^2}{2}(1-2\beta)\omega^2 & \Delta t\,(1-\Delta t(1-2\beta)\xi\omega) \\ -\Delta t\,(1-\gamma)\omega^2 & 1-2\Delta t\,(1-\gamma)\xi\omega \end{bmatrix},$$

$$\{H^n\} = \begin{Bmatrix} \frac{\Delta t^2}{2}\{(1-2\beta)F^n+2\beta F^{n+1}\} \\ \Delta t\{(1-\gamma)F^n+\gamma F^{n+1}\} \end{Bmatrix}, \text{ and}$$

$$\{y^{n+1}\} = \begin{Bmatrix} u^{n+1} \\ \dot{u}^{n+1} \end{Bmatrix}.$$

Also, Eq.(5.7) can be written as follows:

$$\{y^{n+1}\} = [A]\,\{y^n\} + \{L^n\}, \tag{5.8}$$

where

$$[A] = [A_1]^{-1}[A_2]$$

$$= \frac{1}{J}\begin{bmatrix} 1+2\Delta t\,\gamma\xi\omega & -2\Delta t^2\beta\xi\omega^2 \\ -\Delta t\,\gamma\omega^2 & 1+\Delta t^2\beta\omega^2 \end{bmatrix}\begin{bmatrix} 1-\frac{\Delta t^2}{2}(1-2\beta)\omega^2 & \Delta t\,(1-\Delta t(1-2\beta)\xi\omega) \\ -\Delta t\,(1-\gamma)\omega^2 & 1-2\Delta t\,(1-\gamma)\xi\omega \end{bmatrix},$$

$$\{L_n\} = [A_1]^{-1}\begin{Bmatrix} \frac{\Delta t^2}{2}\{(1-2\beta)F^n+2\beta F^{n+1}\} \\ \Delta t\{(1-\gamma)F^n+\gamma F^{n+1}\} \end{Bmatrix}$$

$$= [A_1]^{-1}\begin{bmatrix} \frac{\Delta t^2}{2}(1-2\beta) & \frac{\Delta t^2}{2}2\beta \\ \Delta t(1-\gamma) & \Delta t\gamma \end{bmatrix}\begin{Bmatrix} F^n \\ F^{n+1} \end{Bmatrix},$$

and $J = (1+\Delta t^2\beta\omega^2)(1+2\Delta t\,\gamma\xi\omega)-(2\Delta t^2\beta\xi\omega)(\Delta t\,\gamma\omega^2)$.

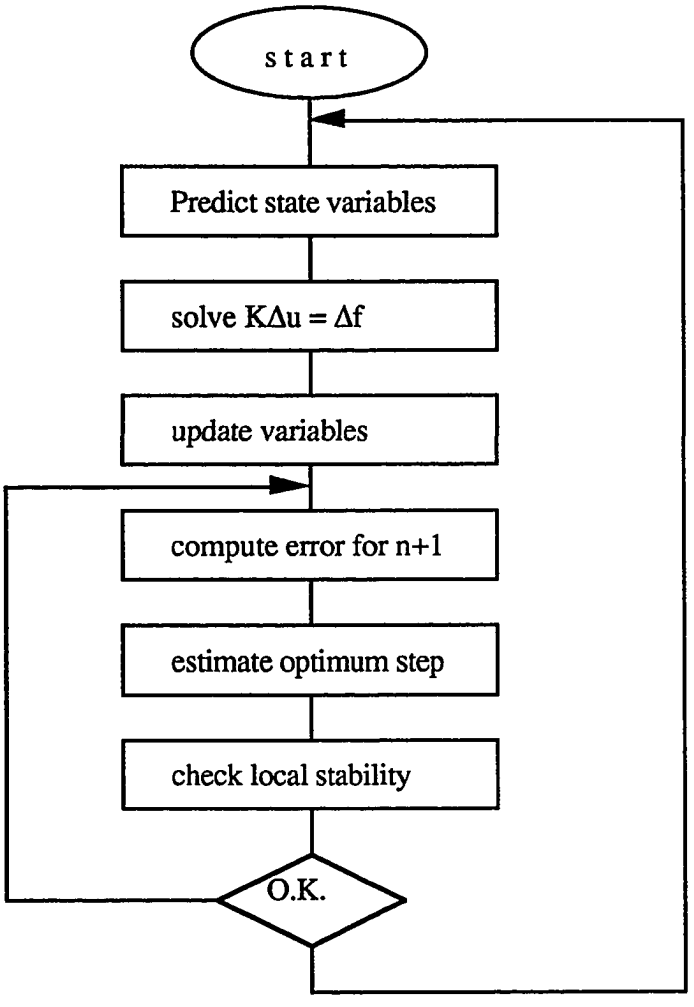

Fig. 5.1 Schematic Procedure of Direct Time Integration with Newmark-β method

From Eq.(5.8), if we assume there is no damping coefficient, the amplification matrix [A] can be written as follows:

$$[A] = [A_1]^{-1}[A_2]$$

$$= \frac{1}{J_{A1}}\begin{bmatrix} 1 & 0 \\ -\Delta t\,\gamma\omega^2 & 1+\Delta t^2\beta\omega^2 \end{bmatrix}\begin{bmatrix} 1-\frac{\Delta t^2}{2}(1-2\beta)\omega^2 & \Delta t \\ \Delta t\,(1-\gamma)\omega^2 & 1 \end{bmatrix}$$

$$= \frac{1}{J_{A1}}\begin{bmatrix} 1-\frac{\Delta t^2}{2}(1-2\beta)\omega^2 & \Delta t \\ -\Delta t\,\omega^2+\frac{\Delta t^3}{2}(\gamma-2\beta)\omega^4 & 1+\Delta t^2(\beta-\gamma)\omega^2 \end{bmatrix}$$

$$= \frac{1}{J_{A1}}\begin{bmatrix} A_{11}^{o} & A_{12}^{o} \\ A_{21}^{o} & A_{22}^{o} \end{bmatrix}, \tag{5.9}$$

where $J_{A1}=1+\Delta t^2\beta\omega^2$. Here, it is noted that the matrix $[A]^{-1}$ has the following properties:

$$[A]^{-1} = \frac{1}{\det|A|}\begin{bmatrix} A_{22} & -A_{12} \\ -A_{21} & A_{11} \end{bmatrix}$$

$$= \frac{1}{J_A}\begin{bmatrix} A_{22} & -A_{12} \\ -A_{21} & A_{22} \end{bmatrix}$$

$$= \frac{J_{A1}^2}{J_A}\begin{bmatrix} A_{22}^{o} & -A_{12}^{o} \\ -A_{21}^{o} & A_{11}^{o} \end{bmatrix}$$

$$= \frac{1}{J_A^{o}}\begin{bmatrix} A_{22}^{o} & -A_{12}^{o} \\ -A_{21}^{o} & A_{11}^{o} \end{bmatrix}, \tag{5.10}$$

where J_A^{o} denotes J_{A1}^2/J_A and J_A is $1+h^2\omega^2(\beta-\gamma+\frac{1}{2})$.

5.2.3 Difference Equation

The Newmark-β method can be written in terms of the following equations:

$$\mathbf{z}^{n+1} = f(t_{n+1}, y_{n+1}), \tag{5.11.a}$$

$$\mathbf{f} = \begin{Bmatrix} \dot{u} \\ \{\, F(t) - 2\xi\omega\,\dot{u} - \omega^2 u \,\} \end{Bmatrix}, \tag{5.11.b}$$

$$u^{n+1}=u^n+\Delta t\, z^n+\frac{\Delta t^2}{2}[(1-2\beta)\dot{z}^n+2\beta\ \dot{z}^{n+1}], \text{ and} \tag{5.11.c}$$

$$\dot{u}^{n+1}=\dot{u}^n+\Delta t\,[(1-\gamma)\dot{z}^n+\gamma\,\dot{z}^{n+1}]\,. \tag{5.11.d}$$

Also, we have the complementary relationship about z:

$$z^{n+1}=z^n+\Delta t\,[(1-\gamma)\dot{z}^n+\gamma\,\dot{z}^{n+1}]. \tag{5.11.e}$$

Here, $\mathbf{y}^{n+1}$ and z^{n+1} are the approximation of $\mathbf{y}(t_{n+1})$ and $\dot{\mathbf{y}}(t_{n+1})$. Thus, from Eq.(5.11.a) to Eq.(5.11.e), we obtain following equation:

$$\begin{Bmatrix} u^{n+1} \\ \dot{u}^{n+1} \end{Bmatrix} = \begin{Bmatrix} u^n \\ \dot{u}^n \end{Bmatrix} + \begin{bmatrix} \frac{\Delta t}{2} & \frac{\Delta t^2}{2}(\gamma-2\beta) \\ 0 & \Delta t\,(1-\gamma) \end{bmatrix} \begin{Bmatrix} z^n \\ \dot{z}^n \end{Bmatrix} + \begin{bmatrix} \frac{\Delta t}{2} & \frac{\Delta t^2}{2}(2\beta-\gamma) \\ 0 & \Delta t\,\gamma \end{bmatrix} \begin{Bmatrix} z^{n+1} \\ \dot{z}^{n+1} \end{Bmatrix},$$

or

$$\mathbf{y}^{n+1} = \mathbf{y}^n + \Delta t\,\Phi^n\,, \tag{5.12}$$

where

$$\Phi^n = (\mathbf{C}_a z^n + \mathbf{C}_b z^{n+1})\,,$$

and

$$\mathbf{C}_a = \begin{bmatrix} \frac{1}{2} & \frac{\Delta t}{2}(\gamma-2\beta) \\ 0 & (1-\gamma) \end{bmatrix}, \qquad \mathbf{C}_b = \begin{bmatrix} \frac{1}{2} & \frac{\Delta t}{2}(2\beta-\gamma) \\ 0 & \gamma \end{bmatrix}.$$

If $\beta=\frac{1}{2}$ and $\gamma=\frac{1}{4}$, the equation stated above can be written as follows:

$$\mathbf{y}^{n+1} = \mathbf{y}^n + \frac{1}{2}\Delta t \ (\mathbf{z}^n + \mathbf{z}^{n+1}), \tag{5.13}$$

which is the well-known trapezoidal rule.

5.3 Computational Aspects of the Newmark-β Method

5.3.1 Source of Error and Local Error

Let $\mathbf{u}(t^n)$ denotes the solution of Eq.(5.1) obtainable with exact computations. The computational error $\mathbf{e}_n$ is defined as the residual:

$$\mathbf{e}_n = \mathbf{u}(t^n) - \mathbf{u}^n, \tag{5.14}$$

where $\mathbf{u}^n$ is the computed solution. The computational errors results from the propagation and accumulation of local errors committed at each time step. Consequently, an analysis of Eq.(5.18) must begin with the study of local errors. Also, identification and analysis of computational errors resulting from mathematical approximations of algorithms should be emphasized.

Local error may be studied by ignoring the processes of propagation and accumulation. These errors can be classified into inherent error, truncation error, and round-off error. Mathematical models of engineering problems including structural dynamics or any physical problem inevitably contain some inherent errors. These errors result from incomplete understanding of natural phenomena, the stochastic or random nature of many processes, and uncertainties in experimental measurements. Often, a model includes only the most pertinent features of the physical process and is deliberately stripped of superfluous.

Even if an error-free mathematical model could be developed, it could not, in general, be solved on computer. A digital computer can perform only a limited number of simple arithmetic operations on finite, rational numbers. Thus, rounding error can be developed by the use of finite precision arithmetic.

The errors introduced in approximating the solution of a mathematical problem by a numerical method is usually termed the truncation error, or solution error, of the method. In the next section, however, truncation error will be explained in more detail.

5.3.2 Local Truncation Error

To solve the initial value problem of Eq.(5.1) consider a general linear multi-step method. The general linear multi-step method may be written in the form:

$$\sum_{j=0}^{k} \alpha_j u_{n+j} = \Delta t \sum_{j=0}^{k} \beta_j f_{n+j} , \tag{5.15}$$

where α_j and β_j are constant and h is the step size; we assume that $\alpha_k \neq 0$ and that not both α_o and β_o are zero. Since (5.15) can be multipled on both sides by the same constant without altering the relationship, the coefficient α_j and β_j are arbitrary to the extent of a constant multiplier.

From Eq.(5.15), we can derive any linear multistep methods of given specification. For Newmark-β method, which is the most reliable one step implicit method, both α_j and β_j can be determined.

$$u^{n+1} + \alpha_o u^n = \Delta t(\beta_1 f_{n+1} + \beta_2 f_n) \tag{5.16}$$

we write down the associated approximate relationship:

$$u(t_n + \Delta t) = u^n + \Delta t[\, \beta_1 u^{(1)}(t_n+\Delta t\,)+\beta_2\, u^{(1)}(t_n)\,], \tag{5.17}$$

and choose α_o, β_1, β_2, so as to make the approximation as accurate as possible. The following expansions are used:

$$u(t_n + h) = u(t_n) + \Delta t\, u^{(1)}(t_n\,)+ \frac{\Delta t^2}{2!}u^{(2)}(t_n) + \ldots.$$

$$u^{(1)}(t_n + h) = u^{(1)}(t_n)+ \Delta t\, u^{(2)}(t_n\,)+ \frac{\Delta t^2}{2!}u^{(3)}(t_n) + \ldots.$$

Substituting in Eq. (5.16) and collecting the terms on the left hand side gives:

$$C_o u(t_n) + C_1\, \Delta t\, u^{(1)}(t_n)+ C_2\Delta t^2 u^{(2)}(t_n\,)+ C_3\Delta t^3 u^{(3)}(t_n) + \ldots. \simeq\ 0, \tag{5.18}$$

where

$$C_o = 1+ \alpha\ ,\ \ C_1 = 1 - \beta_1 - \beta_2\,,\ C_2 = \frac{1}{2} - \beta_1\,,\ \ C_3 = \frac{1}{6} - \frac{1}{2}\beta_1\ \ .$$

Thus, from the above relationship, its local truncation error can be defined by:

$$\tau_u = (\frac{1}{6} - \frac{1}{2}\beta_1)\Delta t^3 u^{(3)}(\zeta)\ ,\ t_n < \zeta < t_n +\Delta t. \tag{5.19}$$

The local truncation error term defined in Eq.(5.19) is intentionally called the "remainder" of the variable approximation method itself which is previously mentioned in Eq.(5.14). The local truncation error introduced in the process of the Newmark-β method is further discussed in next section.

5.3.3 Contribution of Truncation Error to Global Error in the Newmark-β Method

From Eq.(5.13), Newmark-β method may be rewritten as follows:

$$\mathbf{y}(t^{n+1}) = \mathbf{y}(t^n\,) + \Delta t\, \Phi^n +\tau^n\,, \tag{5.20}$$

where t^n is the trucation error term.

It is a well known the hypothesis that $\| \tau^n \| < \tau \Delta t^3$, for all $t_n \in [0,\alpha]$, where τ is a positive constant.

Let $E_n = y(t_n) - y^n$, then we have following relationship:

$$E^{n+1} = E^n + \Delta t [\underline{\Phi}^n - \Phi^n] + \tau^n, \tag{5.21}$$

where $\Phi^n = [\Phi_1^n, \Phi_2^n]^T$ and $\underline{\Phi}^n = \Phi(t_n)$.

Suppose Φ to be continuous in t and y, we then have:

$$| \underline{\Phi}^n - \Phi^n | \leq L | \underline{y}^n - y^n |,$$

where

$$L = \begin{bmatrix} L_{11} & L_{12} \\ L_{21} & L_{22} \end{bmatrix}, \tag{5.22}$$

or

$$L_{11} = |C_{a11}| L_1 + |C_{a12}| L_2 + |C_{b11}| L_1 L_2 \Delta t + |C_{b12}| L_2 (1 + L_2 \Delta t),$$

$$L_{12} = |C_{a12}| L_2 + |C_{b11}| L_1 (1 + L_2 \Delta t) + |C_{b12}| L_2 (1 + L_1 \Delta t + L_2 \Delta t),$$

$$L_{21} = |C_{a21}| L_1 + |C_{a22}| L_2 + |C_{b21}| L_2 L_1 \Delta t + |C_{b22}| L_2 (1 + L_2 \Delta t),$$

$$L_{22} = |C_{a22}| L_2 + |C_{b21}| L_1 (1 + L_2 \Delta t) + |C_{b22}| L_2 (1 + L_1 + L_2 \Delta t).$$

See Appendix 1 for additional detail. Using the relationship of Eq.(5.22), we have

$$| E^{n+1} | \leq | E^n | + \Delta t L | \underline{y}^n - y^n | + | \tau^n |,$$

or

$$|\mathbf{E}^{n+1}| \leq |\mathbf{E}^{n}| + \Delta t\,\mathbf{L}\,|\mathbf{E}^{n}| + |\boldsymbol{\tau}^{n}|$$

$$\leq [\mathbf{I} + \Delta t\,\mathbf{L}]\,|\mathbf{E}^{n}| + |\boldsymbol{\tau}^{n}|$$

$$\leq |[\mathbf{I} + \Delta t\,\mathbf{L}]^{n}\,\mathbf{E}_0| + |\Sigma\,|[\mathbf{I} + \Delta t\,\mathbf{L}]^{m}|\,|\boldsymbol{\tau}_{n-m-1}|$$

$$\leq |[\mathbf{I} + \Delta t\,\mathbf{L}]^{n}\,\mathbf{E}_0| + C.\,|\Sigma\,\boldsymbol{\tau}_{n-m-1}|$$

$$\leq |[\mathbf{I} + \Delta t\,\mathbf{L}]^{n}\,\mathbf{E}_0| + C.\,n.\,\max|\boldsymbol{\tau}_{n-m-1}|$$

$$\leq |[\mathbf{I} + \Delta t\,\mathbf{L}]^{n}\,\mathbf{E}_0| + C.\,n.\,t_n.\,\Delta t^{k}. \qquad (5.23)$$

In dynamic problems, the local errors committed at t_n are propagated to solution $u(t_n)$ by the feedback effect of historical terms as seen in Eq.(5.23). A description of the propagation and accumulation process in terms of "error influence coefficients" is presented in [54].

5.4 Truncation Error Measure of the Newmark-β Method

To evaluate truncation error, a characteristic equation of the integration algorithm may be provided. A characteristic equation can be obtained if we have a time difference equation. Here, as a first step of evaluating the truncation error, we will derive a time difference equation from Eq.(5.8) by eliminating velocities and accelerations. If we use Eq.(5.8) again:

$$\{y^{n+1}\} = [A^{n}]\,\{y^{n}\} + \{L^{n}\}. \qquad (5.24)$$

By using Eq. (5.24) repeatedly for time step n, we have

$$\{y^n\} = [A^{n-1}]\ \{ y^{n-1} \} + \{L^{n-1}\} \tag{5.25}$$

Defining matrix [A'] from the nature of matrix [A] in eq. (5.24) as follows:

$$[A'] = \begin{bmatrix} A_{22} & -A_{12} \\ -A_{21} & A_{11} \end{bmatrix} = J_A [A]^{-1}$$

where J_A is the determinant of [A].

Resultant properties can be determined as follows:

$$[A'][A] = \begin{bmatrix} A_{22} & -A_{12} \\ -A_{21} & A_{11} \end{bmatrix} \begin{bmatrix} A_{11} & A_{12} \\ A_{21} & A_{22} \end{bmatrix} = J_A[A]^{-1}[A]$$

$$= \begin{bmatrix} A_{11}A_{22} - A_{12}A_{21} & 0 \\ 0 & A_{11}A_{22} - A_{12}A_{21} \end{bmatrix}$$

and

$$[A'] + [A] = \begin{bmatrix} A_{11} + A_{22} & 0 \\ 0 & A_{11} + A_{22} \end{bmatrix}$$

As we can see, both resulting matrices are diagonalized.

Premultiplying Eq. (5.25) by $[A^{n'}]$, we have

$$[A^{n'}]\{y^n\} = [A^{n'}][A^{n-1}]\ \{ y^{n-1} \} + [A^{n'}]\{L^{n-1}\}. \tag{5.26}$$

Substituting Eq.(5.25) to Eq.(5.24), we have

$$\{y^{n+1}\} - ([A^{n'}] + [A^n])\{ y^n \} + [A^{n'}][A^{n-1}]\{y^{n-1}\} - \{L^n\} + [A^{n'}]\{L^{n-1}\} = 0. \tag{5.27}$$

Eq. (5.27) is called two-step time difference equation of the Newmark-β method. If $[A^n]$ has the same property as $[A^{n-1}]$, the difference equation can be decomposed into two independent equations for displacement and velocities as follows:

$$u^{n+1} - A_1^d u^n + A_2^d u^{n-1} - L_1^n + A_{22}^n L_1^{n-1} - A_{12}^n L_2^{n-1} = 0, \tag{5.28.a}$$

$$v^{n+1} - A_1^v v^n + A_2^v v^{n-1} - L_2^n - A_{21}^n L_1^{n-1} - A_{11}^n L_2^{n-1} = 0, \qquad (5.28.b)$$

where v denotes $\dot{u}$, and

$$A_1^d = (A_{11}^n + A_{22}^{n'}),\ A_1^v = (A_{11}^{n'} + A_{22}^n),$$

$$A_2^d = (A_{11}^n A_{22}^{n'} - A_{12}^n A_{21}^{n'}),\ A_2^v = (A_{11}^{n'} A_{22}^n - A_{12}^{n'} A_{21}^n).$$

The error committed in each time step by replacing the differential equation Eq.(5.7) by the difference equations Eq. (5.28.a) and (5.28.b) are called local the truncation errors for displacement and velocity, respectively.

5.4.1 Evaluation of Truncation Error

There are ways to evaluate the truncation error committed in each time step. From Eq.(5.27) and (5.28), the local truncation errors for the velocity and the displacement are defined by:

$$(\Delta t)^2 \tau_d^n = u^{n+1} - A_1^d u^n + A_2^d u^{n-1} - L_1^n + A_{22}^n L_1^{n-1} - A_{12}^n L_2^{n-1} \qquad (5.29.a)$$

$$(\Delta t)\, \tau_v^n = v^{n+1} - A_1^v v^n + A_2^d v^{n-1} - L_2^n - A_{21}^n L_1^{n-1} + A_{11}^n L^{n-1} \qquad (5.29.b)$$

To rewrite the last three terms of Eq.(5.29), the following properties are defined:

$$E_1 = -D_{12}, \quad E_2 = A_{22}D_{12} - A_{12}D_{22}, \quad E_3 = A_{22}D_{11} - A_{12}D_2,$$

$$E_4 = -D_{22}, \quad E_5 = A_{11}D_{22} - A_{21}D_{12} - D21, \quad E_6 = A_{11}D_{21} - A_{21}D_{11}.$$

Eq. (5.27) can be represented as follows;

$$(\Delta t)^2\tau_d^n = d^{n+1} - A_1^d d^n + A_2^d d^{n-1} + E_1F^{n+1} + E_2F^n + E_3F^{n-1} \quad (5.30.a)$$

$$(\Delta t)\,\tau_v^n = v^{n+1} - A_1^v v^n + A_2^v v^{n-1} + E_4F^{n+1} + E_5F^n + E_6F^{n-1} \quad (5.30.b)$$

By the first method, which was shown in Hilber[51], the truncation error can be expressed using Taylor's series. Assuming u(t) to be continuously differentiable up to any required order, all terms in Eq.(5.30) can be expanded into a finite Taylor series at t. Also, in Eq.(5.30), it is assumed that the time step size is not changed from the (n)th step to the (n+1)th step so that $[A^n] = [A^{n-1}]$. Then, $A_1 = A_1^d = A_1^v$, $A_2 = A_2^d = A_2^v$. Using the differential equation of motion, the truncation errors for the displacement and velocity can be expressed as[see Appendix 1]:

$$\begin{aligned}\tau_d &= [\Omega^{-2}T_0 - T_2 + \Omega^2 T_4]\omega^2 u + [\Omega^{-1}T_1 - \Omega T_3]\omega\dot{u} \\ &+ [\,(T_2 - \Omega^2 T_4)F + T_3(\frac{\Omega}{\omega})\dot{F} + T_4(\frac{\Omega}{\omega})^2\ddot{F}\,] \\ &+ [\,Q_0(\frac{\Omega}{\omega})^{-1}F + Q_1(\frac{\Omega}{\omega})\dot{F} + Q_2(\frac{\Omega}{\omega})^2\ddot{F}\,] + O(\Delta t^3),\end{aligned} \quad (5.31)$$

and

$$\begin{aligned}\tau_v &= [-T_1 + \Omega^2 T_3]\omega^2 u + [\Omega^{-1}T_0 - \Omega T_2]\omega\dot{u} \\ &+ [\,T_1F + T_2(\frac{\Omega}{\omega})\dot{F} + T_3(\frac{\Omega}{\omega})^2\ddot{F}\,] \\ &+ [\,R_0(\frac{\Omega}{\omega})^{-1}F + R_1(\frac{\Omega}{\omega})\dot{F} + R_2(\frac{\Omega}{\omega})^2\ddot{F}\,] + O(\Delta t^3),\end{aligned} \quad (5.32)$$

where

$$T_0 = 1 - A_1 + A_2\ ,\ T_i = (\,1 + (-1)^i A_2\,)/\,i!\ ,$$

$$Q_0 = E_1 + E_2 + E_3 , \quad Q_i = (B_1 + (-1)^i B_3) / i! ,$$

$$R_0 = B_4 + B_5 + B_6 , R_i = (B_4 + (-1)^i B_6) / i!,$$

and the circular sampling frequency $\Omega = \omega \Delta t$. Also, u and F denote u^n and F^n, respectively.

5.4.2 New Improved Definition of Truncation Error

The computation method of the truncation error using Taylor's series is easily applicable to the homogeneous equation of free vibration, however difficulties arise when trying to extend this method to the forced vibration case. For the forced response system, we have assumed a precisely defined forcing function with continuous first and second time derivatives. In practice, forcing functions consist of experimentally observed loads at discrete time intervals, therefore the computation of the required derivatives is not always possible. To resolve such difficulties and reduce unnecessary computation even when it is possible to determine force at every time step, a new approach is presented. This new method to evaluate truncation error, is relatively simple when it is compared to the initial one. Practically, the truncation errors for displacements and velocities committed in each time step, can be evaluated by using the remainder terms defined in Eq. (5.5).

Using the difference equation(5.24) including the remainder terms, after elimination of acceleration terms, the numerical solution of the system can be recast in the form of the matrix equation:

$$\{y^{n+1}\} = [A^n] \{ y^n \} + \{ L^n \} + [A_1^n]^{-1} \{ R^n \}. \qquad (5.33)$$

Now we define truncation of the system as:

$$\{S^n\} = [A_1^n]^{-1}\{R^n\},$$

or

$$\begin{Bmatrix} S_d \\ S_v \end{Bmatrix} = \frac{1}{J}\begin{bmatrix} 1+2\Delta t\,\gamma\xi\omega & -2\Delta t^2\beta\xi\omega^2 \\ -\Delta t\,\gamma\omega^2 & 1+\Delta t^2\beta\omega^2 \end{bmatrix}\begin{Bmatrix} (\beta-\frac{1}{6})\Delta t^3 u^{(3)}(\zeta) \\ (\gamma-\frac{1}{2})\Delta t^2 u^{(3)}(\zeta) \end{Bmatrix}, \tag{5.34}$$

where

$$J=1+\Delta t^2\beta\omega^2.$$

If there is no force term, then, Eq. (5.31) will be represented as following form:

$$\{y^{n+1}\} = [A^n]\{y^n\} + \{S^n\}. \tag{5.35}$$

Using a method similar to that used in obtaining the two-step difference equation of Eq.(5.27) and (5.28), following equation can be obtained:

$$\{y^{n+1}\} - ([A'^n]+[A^n])\{y^n\} + [A'^n][A^{n-1}]\{y^{n-1}\} - \{S^n\} + [A'^n]\{S^{n-1}\} = 0. \tag{5.36}$$

From the relationship between the displacement in the two-step method and the terms consisting of the remainder as seen in Eq.(5.36), the truncation error for displacement and velocity can be defined. Thus, we define the truncation error as follows:

$$\begin{aligned} \{\tau^n\} &= \{S^n\} - [A'^n]\{S^{n-1}\} \\ &= [A_1^n]^{-1}\{R^n\} - [A'^n][A_1^{n-1}]^{-1}\{R^{n-1}\} \\ &= [A_1^n]^{-1}\{R^n\} - [D]\{R^{n-1}\}. \end{aligned} \tag{5.37}$$

In Eq.(5.37), since the term of $[D]=[A'^n][A_1^{n-1}]^{-1} = J_A\,[A^n]^{-1}[A_1^{n-1}]^{-1}$, in which J_A is the determinant of [A], and $[A^n]^{-1} = ([A_1^n]^{-1}[A_2^n])^{-1} = [A_2^n]^{-1}[A_1^n]$, the [D] matrix can be rewritten as follows:

$$[D] \quad = J_A\,[A_2^n]^{-1}[A_1^n][A_1^{n-1}]^{-1}.$$

If we assume that $[A_1^n]$ is equal to $[A_1^{n-1}]$, then:

$$[D] \quad = J_A\,[A_2]^{-1}$$

$$= \frac{J_A}{J_{A2}}\begin{bmatrix} 1 & -\Delta t \\ -\Delta t\,(1-\gamma) & 1-\frac{\Delta t^2}{2}(1-2\beta)\omega^2 \end{bmatrix},$$

where $J_{A2} = 1+\frac{\Delta t^2\,\omega^2}{2}(2\beta-2\gamma+1)$.

The advantage of the second method is that is simpler and more compact in view of the expression used to compute the truncation error than the one expressed in Eq. (5.31) and (5.32). This expression can be easily applied to evaluating the truncation error committed in each time step in a forced response system as well as in a free response system that is to be solved. Also, for the case of a variable step algorithm, the second method is more advantageous in evaluating truncation error committed through the transition time frame from a stage of a fixed time step to a stage of a time step other than that used in the previous time step.

From Eq.(5.37), when the system is undamped and the free parameters $\beta$and γ are selected as $\frac{1}{4}$ and $\frac{1}{2}$ respectively, the expression for the truncation error for the displacement is simplified in following form:

$$\tau_d^{\,n} = \frac{1}{J_A}(R_d^n - R_d^{n-1})$$

$$= \frac{1}{J_A}\left(\frac{h^3}{12}\,u_n^{(3)} - \frac{h^3}{12}\,u_{n-1}^{(3)}\right) \qquad (5.38)$$

where R_d is the remainder term as defined in Eq.(5.4) and J_A is the determinant of the matrix A.

5.4.2 Current Mode and Current Frequency

In the previous section, an investigation of evaluating the truncation error measure has been presented only for the single-degree-of-freedom system, which is analogous to the uncoupled equations obtained by conventional mode decomposition. In order to extend this evaluation technique to the multi-degree-of-freedom system, further investigation of the characteristics of the structural dynamics of multi-degree of freedom system is required.

As seen in Eq.(5.37), for every time step, we need to evaluate the amplification matrix [A], and other related properties which include the modal frequency at each decoupled equation. The modal frequencies and vectors are obtained after the eigenvalue analysis of the structural problem is solved. If the order of the matrices is large, the computer time required to solve all eigenvalues and vectors are enormous. The analysis of the eigenvalue problem may be the most time consuming phase in most cases of structural dynamic problems including the direct time integration procedure. It is even tedious to extract the lower modes of the system which dominates the response in most structural dynamic analyses. Thus, there should be a measure of frequency, which is sufficiently accurate to approximate at each integration time step.

The Rayleigh quotient is a well-known method for computing eigenvalues when the corresponding eigenvectors are known [47,78]. The method is particularly useful in eigenvalue computation by means of vector iterations. A similar type of expression may also be used for finding a current, characteristic frequency in step-by-step dynamic response analysis. This is given by:

$$\omega_k^2 = \frac{\Delta u_k{}^t K_k \ \Delta u_k}{\Delta u_k{}^t \ M \ \Delta u_k}, \tag{5.39}$$

K_k is the tangent stiffness for step k. The mass matrix is normally constant. ω_k is the current, characteristic angular frequency. This frequency is generally not any particular eigenfrequency, but it reflects rather the incremental response from all eigenmodes. This may be seen from writing the incremental solution vector as

$$\Delta u_k = \sum_{i=0}^{m} \Delta Y_{ik} \Phi_i \, . \tag{5.40}$$

$Y_i(t)$ is the response function for eigenvector Φ_i, and m is the total number of eigenvectors. Then, because of the orthogonality properties of the eigenvectors,

$$\omega_k^2 = \frac{\sum_{i=0}^{m} \Delta Y_{ik}^2 \Phi_i^t K_k \Phi_i}{\sum_{i=0}^{m} \Delta Y_{ik}^2 \Phi_i^t M \Phi_i} = \frac{\sum_{i=0}^{m} \Delta Y_{ik}^2 K_{ik}}{\sum_{i=0}^{m} \Delta Y_{ik}^2 M_i} \, . \tag{5.41}$$

K_i and M_i are the generalized stiffness and mass for eigenvectors *i*. Thus, Eq.(5.56) shows the modal composition of the current frequency.

A corresponding measure for a current, characteristic period may be found

$$T_k = \frac{2\pi}{| \omega_k^2 |^{1/2}} \, . \tag{5.42}$$

It is worth noting that the current period changes with time for a stationary response as well as for a nonstationary response of multi-degree-of-freedom systems. T_k is tied to the current stiffness and response.

5.5. Automatic Time Step Selection

In the preceding section, we have discussed the essence of a direct time integration and how the truncation error can be measured. Those studies are carried out based on a decoupled equation system. However, when we extend these idea to the multi-degree-of-freedom system and, other large scale system with finite elements, some additional considerations are required to obtain reasonably accurate solutions, where the exact solution is generally not obtained. Thus, we will discuss in detail about strategies of time step size selection, and its implementation to the practical structural problems.

As marked before, the truncation error has been most widely used for an error measure to adjust the time step size. However, it still remains an expensive method since time step adjustment based on the truncation error is appropriate for high accuracy requirements. Also, the computation of error bound resulted in substantial additional cost. In typical structural dynamic analysis, much lower accuracy is often satisfactory due to analysis cost. Thus, it is desirable to have a cost-effective and reliable algorithm which provides reasonably accurate solution.

There are several major factors that affect the efficiency of a variable step integration procedure: the basic integration formula which dictates stability and accuracy for a fixed time step integration; the step-size control strategy to satisfy a specified error bound at the same time to avoid instability. In practice, it is often desirable to select the step size to be as large as possible, consistent with a specified local error. This can be accomplished with an adaptation of the difference formula to a variable step integration procedure.

5.5.1 Norm of Truncation Error Measure

Since we have considered the truncation error as an error measure for each component i , a proper local error measurement at each time step for the integration procedure is required to evaluate system-wise errors. A detailed component-by-component calculation of $\mathbf{e}(t_n)$ is seldom useful(or even possible). All that is needed for practical applications is a rough estimate of relative error $\| \mathbf{e} \| / \| u \|$, or $\| \mathbf{e} \| / h$, given the local level of accuracy required and some problem-identification parameters.

In most explicit algorithms, it is reasonable to take the maximum among them, viz...

$$\varepsilon^{n+1} = \max \left\{ \left| \frac{\tau_1}{u_1} \right| , \left| \frac{\tau_2}{u_2} \right| , \ldots \left| \frac{\tau_N}{u_N} \right| \right\} .$$

However, it is noted that error norms of l-type

$$\left\| \frac{\tau_1}{h} \right\|_p = \left\{ \left| \frac{\tau_1}{h} \right|^p + \left| \frac{\tau_2}{h} \right|^p + \ldots + \left| \frac{\tau_N}{h} \right|^p \right\}^{1/p} , \qquad (5.43)$$

have been proved to be suitable for implicit formulas, where h denotes the time step. In this case the relative error norm is defined by:

$$\varepsilon^{n+1} = \left\| \frac{\tau_1}{h} \right\| . \qquad (5.44)$$

Let us define:

$$\varepsilon_k^{n+1} = \frac{u_k^{(3)}}{h} ,$$

then we have

$$\varepsilon^{n+1} = \frac{h^3}{12} \left\| \frac{u_k^{(3)}}{h} \right\|_p . \qquad (5.45)$$

For a fixed error bound ε_{max}, Eq. (5.61) allows us to define:

$$h_{max} = \left(\frac{12\varepsilon^{n+1}}{\varepsilon_{max}} \right)^{1/3}. \tag{5.46}$$

Another measure, we can define other than Eq.(5.45), is an energy norm of truncation error. As done to obtain the current frequency, we define the energy norm as follow:

$$E_\tau = \tau_v^T M \tau_v + \tau_d^T K \tau_d . \tag{5.47}$$

The energy norm defined by Eq.(5.47) is not actually involved in the time adjusting algorithm, but is used as an indicator of the algorithm's performance.

In adjusting the time step, as a practical matter, it is too ambitious to use Eq.(5.46) since we do not want to have many rejections, and aiming at equality with the maximum local error permissible will cause frequent overshoot. The drawback of expression Eq.(5.46) is that it implies, as a rule, that the step length will be changed every time. As discussed earlier, this is not desirable, in particular when solving a linear problem. Too frequent and too dramatic changes of the time step may also tend to destabilize the algorithm and possibly distort the energy balance. It is therefore desirable to introduce a type of smoothing or breaking mechanism.

Let the current time step ratio ζ be defined by:

$$\zeta = \log(\tau / \varepsilon_{max} h_{n-1}). \tag{5.48}$$

The actual setting of new time step is now determined by:

$$h_n = f (\zeta) h_{n-1}, \tag{5.49}$$

where $f(\zeta)$ is a tuning function that determines the sensitivity of the time stepping algorithm.

Fig. 5.2 shows some examples of such tuning functions. In the first case $f(\zeta)$ is simply proportional to the step-ratio ζ, which means that the new time step is given by Eq. (5.49). This implies that the step length will be adjusted for every time step. Such a tuning function should only be used in nonlinear analysis in which the stiffness is recomputed for every time step. Second tuning function is a simple step function which either doubles or divides the step in half. Using this tuning function the step length is not changed unless a major change in the response has taken place. After adjusting new time step based on the procedure as stated above, the new time step is examined to meet the local error tolerance. If the estimated local error based on the new time step does meet the test, we accept the solution and continue the computation. Arguing as previously, following strategy for automatic time selection can be suggested.

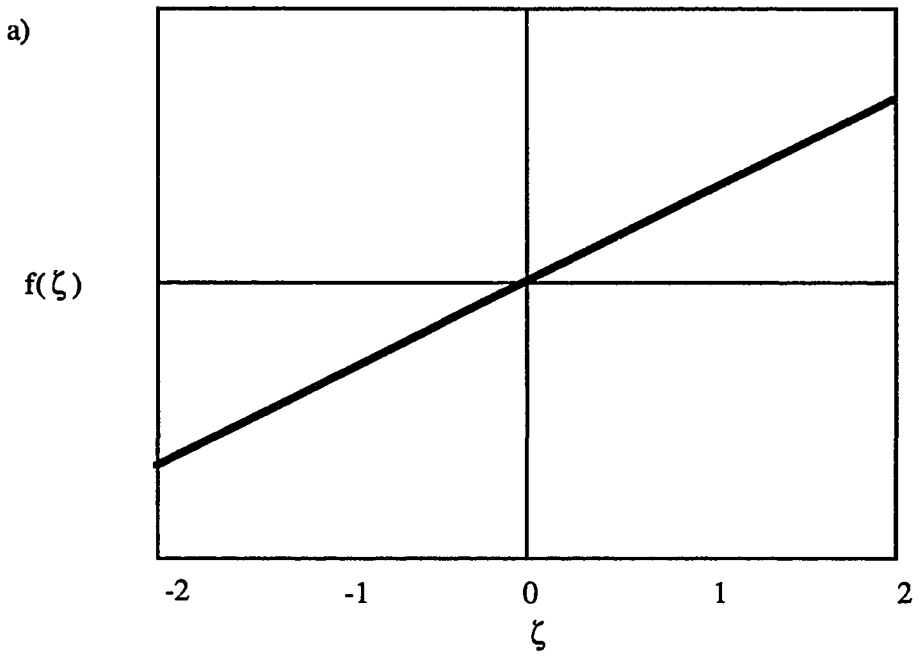

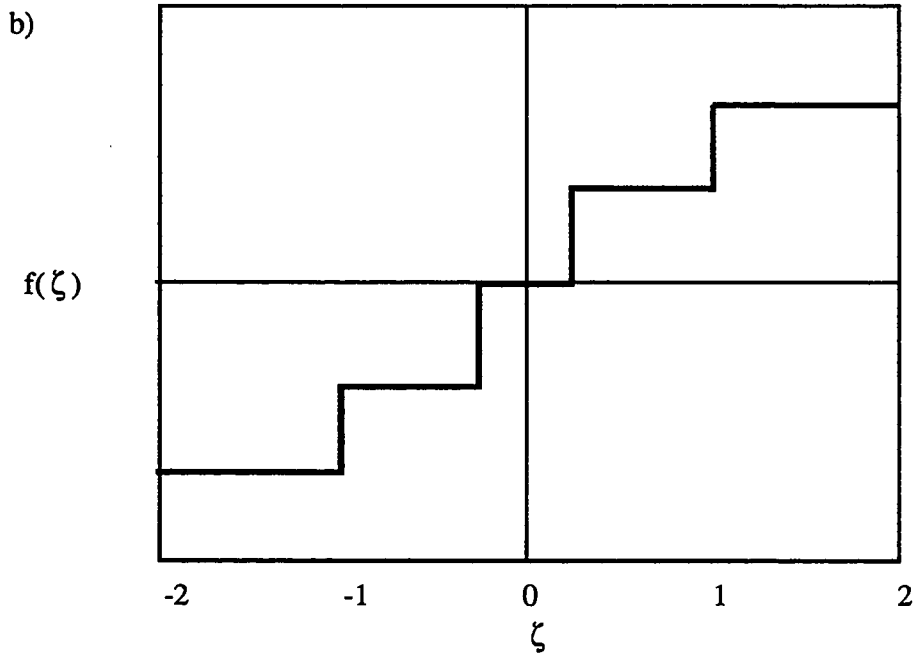

Fig. 5.2 Time Step Tuning Functions

5.5.2 Automatic Time Selection Strategies

Rule 1. If |est| > ε, reject solution and recompute it with a new step size. If |est| $\leq \varepsilon_{max}$, accept the solution and use a new step size for the next step. In either case use the expression as shown in Eq.(5.49) for obtaining a new step size.

Some limits on the step size h are necessary. An algorithm may reduce its time step to be very small near a point where the solution has some kind of discontinuity. In most cases, the code successfully continues the integration and does not consume too much time. For this reason, we have counted function evaluation in this algorithm to provide a measure of computational effort, rather than to request user to supply a minimum and maximum time step size. In this algorithm, a maximum and minimum step size are determined by a initial step size supplied by user. Also, the actual minimum and maximum, or an average time step is evaluated while the integration is proceeding.

Rule 2. The step size is not permitted to be larger than a maximum step size. Some limits on the change in step size are of practical importance. A very large change can mean that the approximation valid for "small" h is breaking down. Another important consideration is that of "chattering" in the step size.

Rule 3. The step size is not permitted to increase by more than a factor of 4 or decrease by more than a factor of 1/5.

In summary, a desired local accuracy ε per unit change in time and initial step size is required. This algorithm estimates the local accuracy and tries to use a step as large as is compatible with the error requirement.

5.5.3 Effect of Step Change on Local Stability

The most typical, and therefore most important, case in structural dynamics is "underdamping". We will establish appropriate measure which fully characterize the accuracy of the variable time integration algorithm. To carry out this development, we shall begin with some considerations of variable step algorithm for the discrete case.

From Eq.(5.24) and Eq.(5.25),

$$\{y^{n+1}\} = [A]^n \{ y^n \} + \{ L^n \} ,$$

and

$$\{y^n\} = [A]^{n-1} \{ y^{n-1} \} + \{ L^{n-1} \} ,$$

for time step at n+1 and n.

The appropriate eigenvalue problem is obtained by taking

$$\{y^{n+1}\} = \lambda\{ y^n \} ,$$

which is substituted into Eq.(5.38) without considering the force term to yield:

$$([A] - \lambda[I])\{y^n\} = 0 . \qquad (5.50)$$

Equation (5.50) has a nontrivial solution only if:

$$\det | [A] - \lambda[I] | = 0 ,$$

and another eigenvalue problem for the Newmark-β method in the following form:

$$(\lambda^2 - \lambda ([A^n']+[A^n])+ [A^n'][A^{n-1}]) \{y^{n-1}\} = 0 , \qquad (5.51)$$

which is called an quadratic eigenvalue problem.

However, in the case of variable time step algorithms above, the solution is no longer valid since the step size, h^n, from t_n is different from h^{n-1}. Now, we use:

$$\{y^n\} = \lambda^n \{ y^{n-1} \} ,$$

and

$$\{y^{n+1}\} = \lambda^{n+1} \{ y^n \} = \lambda^{n+1} \lambda^n \{ y^{n-1} \} . \tag{5.52}$$

Substituting Eq.(5.52) into Eq.(5.27), one finds the following eigenvalue problem of variable time step algorithm for the Newmark-β method:

$$(\lambda^{n+1}\lambda^n - \lambda^n ([A^{n'}]+[A^n] + [A^{n'}][A^{n-1}]) \{y^{n-1}\} = 0. \tag{5.53}$$

In most cases of underdamped systems, the solution of the eigenvalue problem of (5.53) has the following form:

$$\begin{aligned} \lambda_{1,2} &= \exp (-\xi \underline{\Omega} \pm i \underline{\Omega}_d) \\ &= e^{-\xi \underline{\Omega}} (\cos \underline{\Omega}_d \pm i \sin \underline{\Omega}_d), \end{aligned} \tag{5.54}$$

where $\underline{\Omega} = \underline{\omega} \Delta t$ and $\underline{\Omega}_d = (1- \xi^2)^{1/2} \underline{\Omega}$, and

$$\begin{aligned} \xi &= \frac{\log e^{-\xi \underline{\Omega}}}{\underline{\Omega}} \\ &= \frac{\log e^{-\xi \underline{\Omega}}}{\underline{\omega} \Delta t}, \text{ and} \end{aligned} \tag{5.55}$$

$$\underline{\Omega}_d = \arg (\lambda_{1,2}).$$

Local stability in the present situation is concerned with the rate of growth or decay of powers of the amplification matrix. To prove the convergence theorem, we will need to show that:

$$\| A \| \leq \text{const., for any n.} \tag{5.56}$$

It turns out that this requirement is guaranteed if the following conditions are satisfied:

(i) $\rho(A) \leq 1$, and

(ii) Eigenvalues of A of multiplicity grater than one, are strictly less than one in modulus.

To compute the spectral density, ρ, the eigenvalues solved from Eq.(5.55) can used as:

$$\rho(A) = \max(\lambda_1 , \lambda_2). \tag{5.57}$$

A matrix A satisfying (i) and (ii) is said to be *spectrally stable*.

The effects of step change on local stability can now be evaluated from Eq.(5.57) by requiring that:

$$|\lambda| \leq 1.0 \tag{5.58}$$

in order for Eq.(5.54) to give bounded solution.

Based on the rules and procedures stated above, we can summarize the algorithm for adjusting the time step-size as shown in Fig.5.3.

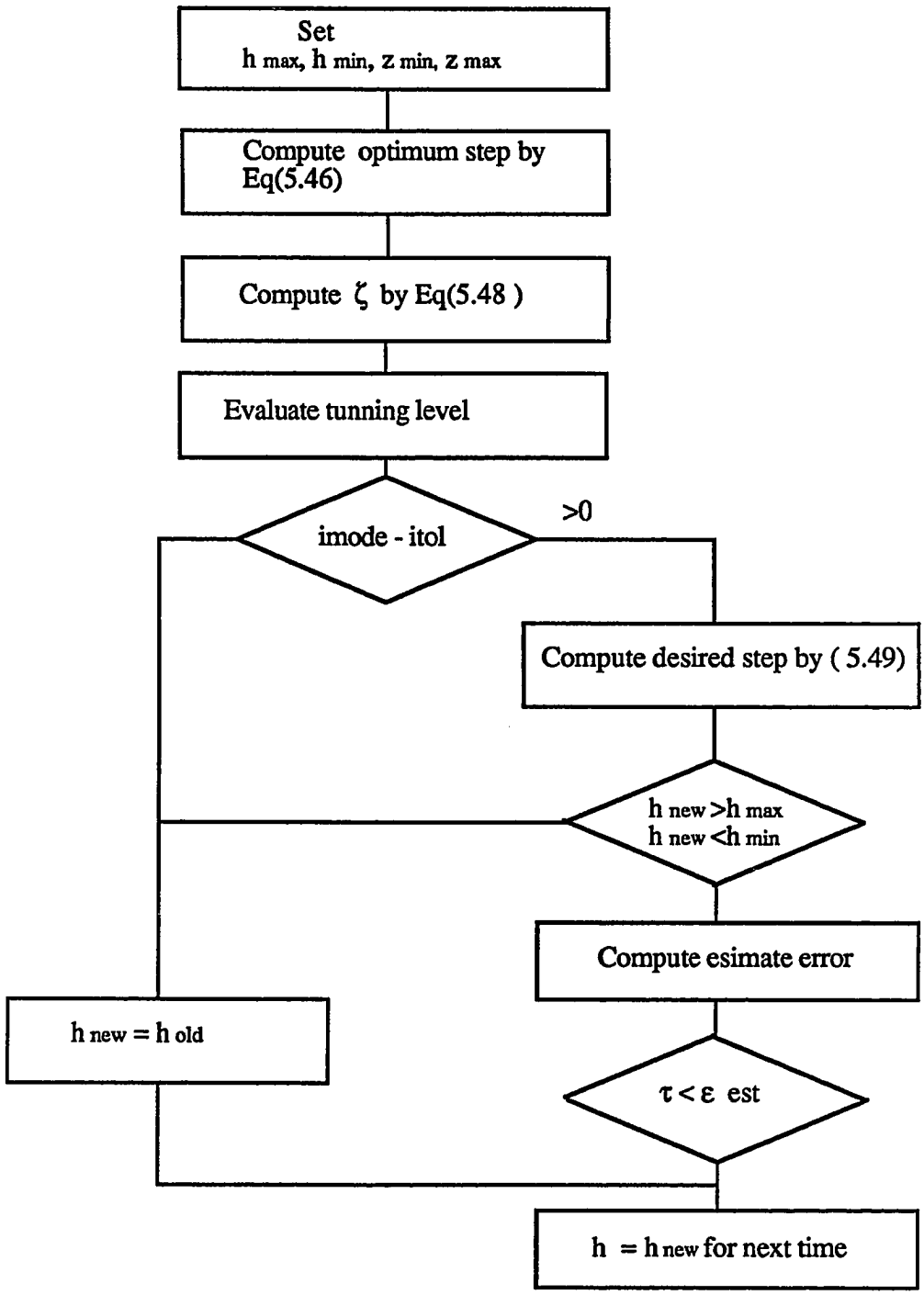

Fig. 5.3 Variable Time Adjusting Process

5.6. Numerical Examples

5.6.1 Example 1(Simple Spring-Mass System)

The numerical study consists of a single-degree-of-freedom system. The system is modeled with non-zero damping subjected to an initial non-zero displacement and velocity excitation.

The study of this single-degree-of freedom system lies mainly in observing the truncation error computed using the method developed in this work with the one obtained from Taylor's expansion. A second objective is to investigate how the time-step adjusting algorithm is working with different tolerance descriptions to the truncation error.

The system is solved with the computer program T1D using the automatic time stepping algorithm outlined in previous section. For the first test purpose, the system is solved with time step size of 0.001 seconds under the initial condition described below. In this case, the variations of the indicator of truncation error are obtained. For the second test purpose, investigations are carried out for values of different tolerance of maximum allowable local error, ε_{max} and initial time step h_o equal to 0.001. The values of maximum allowable truncation error are 0.5E-3, 0.1E-3, and 0.5E-4, respectively. The step length h_{max} is set to equal to 5 times of initial time step.

The pertinent system parameters corresponding to the equations (5.1)-(5.2) are

M=1kg, C=0,

$K = M\omega^2 = (100\pi)^2$ kg/sec^2, and

$d_0=0$, $v_0=\pi$, $F(t)=0$, $t > 0$.

Parameter values for the integration algorithms are

$\gamma=\frac{1}{2}$, $\beta=\frac{1}{4}$.

For the first test objective, the problem is solved with no time-step adjustment applied. The solution is compared with the exact solution. The solution error at each time, i.e., the total truncation error, is shown in Fig. 5.4. Computed truncation errors obtained using two methods are both identical as seen in Fig. 5.5. In this figure, it is seen that amplitude of truncation error using the error indicator defined is a half of the conventional form of error indicator defined using Taylor's expansion technique since the amount of error using Taylor's expansion is actually computed over a two time-step interval. However, the error indicator seems to be well defined and can be used for the error analysis of the time integration algorithm.

In the second test case, computations are carried out for three different maximum allowable truncation errors. The response for the case of fixed time step is shown in Fig. 5.6. Variation of the time step is shown in Fig.5.7. The initial step-length was set to 0.001 and is equivalent of 20% of the fundamental period. Fig.5.7 shows that the time-step changes rapidly over the whole time history even though the system is linear and the loading condition is linear and constant. This proves that the algorithm is sensitive to the change of displacement and velocity of system response since the algorithm is based on the truncation error which is combination of displacement and velocity. In this example, it is recognized that the local truncation error is controlled as time step changes. In the first test case with tolerance of 0.0005, the average time step size 0.45E-3, which is 45% of the initial step length(9% of fundamental period). In this case, it is observed that the maximum amount of local truncation error is reduced to 4% of the one with fixed time step size of 0.001 as shown in Fig. 5.8.

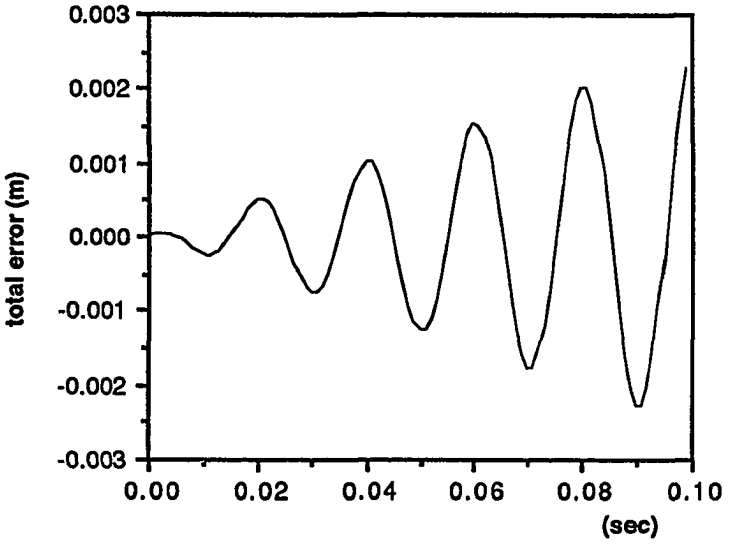

Fig. 5.4 Variation of Total Error with Fixed Step Size h=0.001

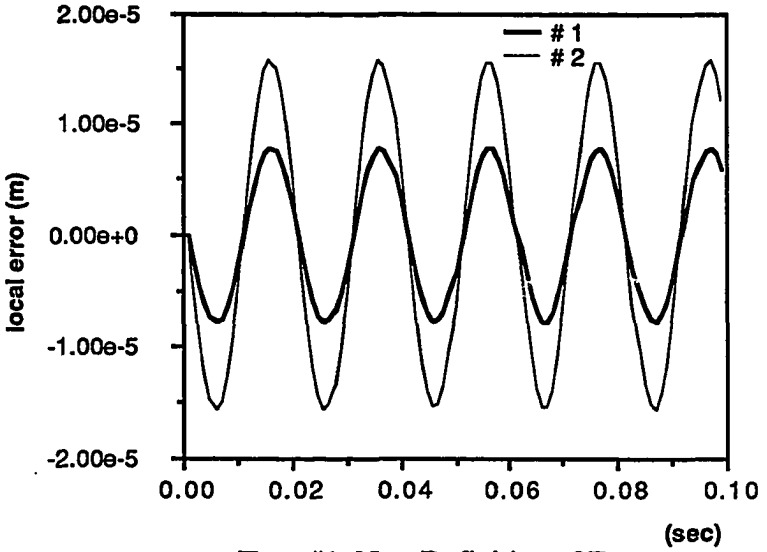

Type #1: New Definition of Error
Type #2: Defined by Taylor's Series

Fig. 5.5 Comparison of Truncation Error Based on Its Definition

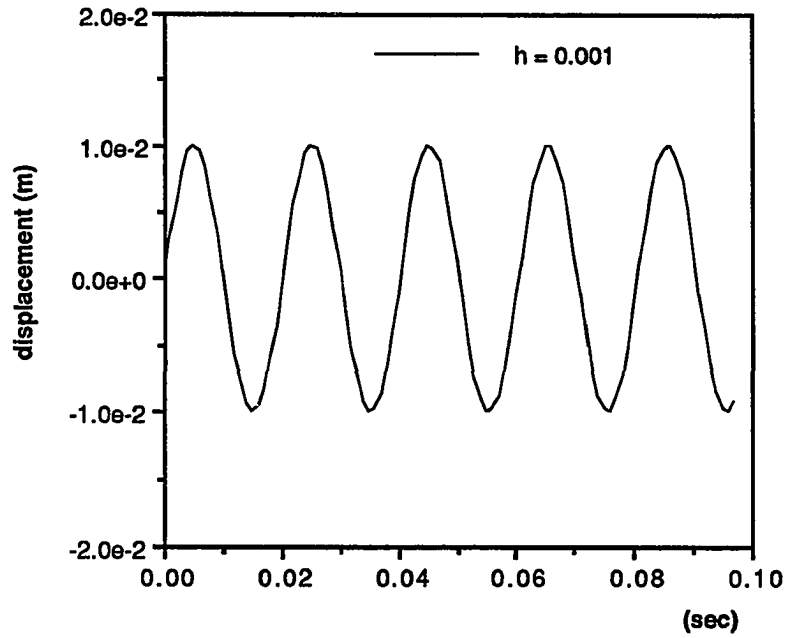

Fig. 5.6 Time Response of Single Degree of Freedom System(Exmaple 1)

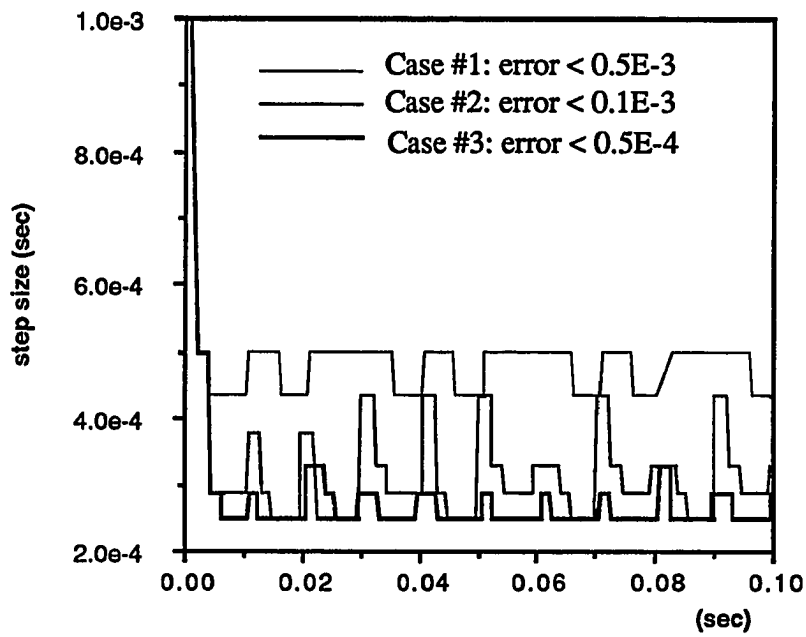

Fig. 5.7 Variation of Time Step Size for Solving Time Response of Example 1

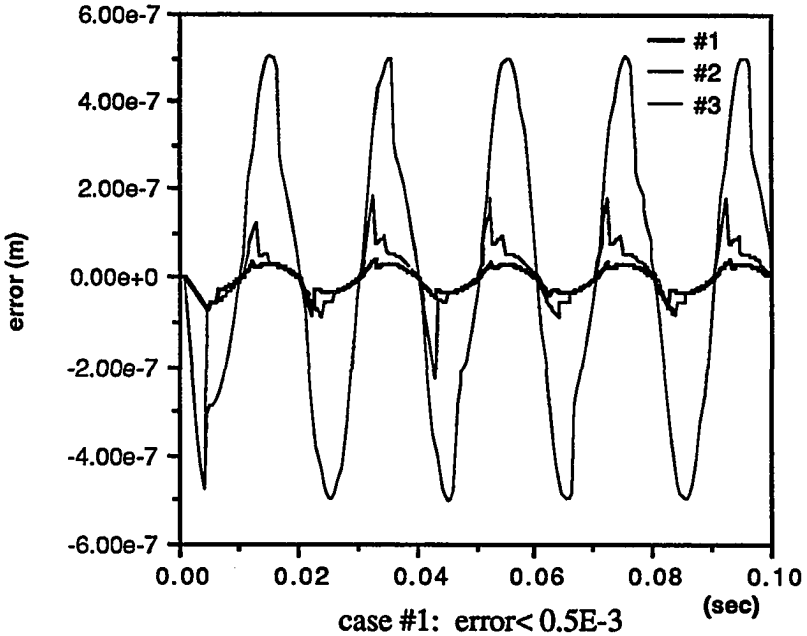

case #1: error< 0.5E-3
case #2: error< 0.1E-3
case #3: error< 0.5E-4

Fig. 5.8 Variation of Truncation Error (Example 1)

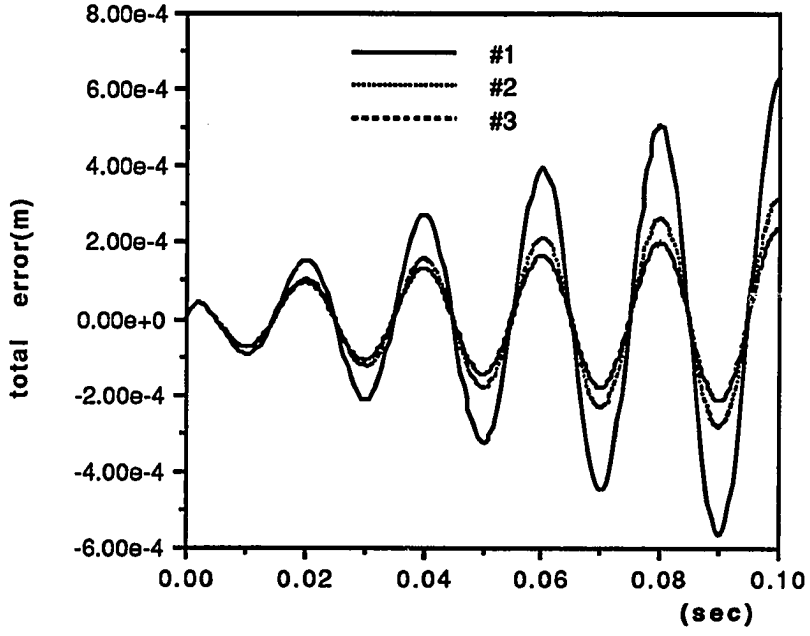

Fig. 5.9 Comparison of Total Error(Example 1)

Fig. 5.9 shows that time step adjusting algorithm also reduces the total global error. The total error, which is measured after 0.1 seconds elapsed, reduced to 6.0E-4 and is of 24% of the one with the fixed time step. It is noted that time adjusting algorithm can not influence the total amount of global error directly, however the error propagation contributed by the truncation error can be controlled.

5.6.2 Example 2 (Spring-Mass System of two-degree-of freedom)

The previous model of a single-degree-freedom system has been investigated mainly to examine the accuracy and the effectiveness of the algorithm. It is important to extend the algorithm to more than one-degree-of-freedom systems for the purpose of further implementation of the algorithm to a finite element analysis. Prior to implementing the algorithm into the finite element method for practical purposes, a simple two-degree-of-freedom system can be selected for observing the characteristic of the algorithm and its the parameter involved when a multi-degree-of-freedom system is solved.

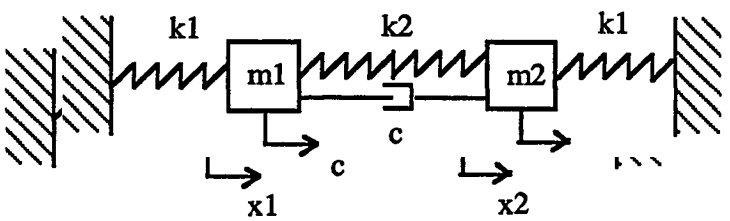

$M_1=M_2=1\text{kg}$, $C=0$

$K_1 = M\omega^2 = (100\pi)^2\ \text{kg/sec}^2$, $K_2 = \frac{1}{2}K_1$

Fig. 5.10 Example of Two Degree of Freedom System

The system is selected as shown in Fig.5.10. This two-degree-of-freedom system consists of two masses, and three springs and one damper. The system is solved and tested under several excitation conditions.

Three test cases are carried out for values of different maximum error tolerance ε_{max} and initial time step h_0 equal to 0.001. The step length h_{max} is set to be equal to 5 times the initial time step the same as in the previous case.

The system parameters are:

$d_1(0)=0,\ v_1(0)=0,\ d_2(0)=0,\ v_2(0)=0,$

$F_1(t)=F_o \sin\omega_e t,\ F_2(t)=\frac{F_o}{2}\sin\omega_e t,\ t > 0,$

and parameter values for the integration algorithms are:

$$\gamma=\frac{1}{2},\ \beta=\frac{1}{4}\ .$$

The exact solution of the above system can be obtained through the mode superposition technique. The system equation is given as follows:

$$[M]\{\ddot{u}\}+[K]\{u\}=\{F\}, \tag{5e.1}$$

where

$$[M]=\begin{bmatrix} m_1 & 0 \\ 0 & m_2 \end{bmatrix},$$

$$[K]=\begin{bmatrix} k_1+k_2 & -k_2 \\ -k_2 & k_1+k_2 \end{bmatrix}.$$

After solving the eigenvalue problem for this system, both eigenvalues and eigenvectors are obtained as:

$$[\Phi]=\begin{bmatrix} 1 & 1 \\ 1 & -1 \end{bmatrix} \quad \text{and,} \quad [\Lambda]=\begin{bmatrix} \lambda_1 & 0 \\ 0 & \lambda_2 \end{bmatrix}. \tag{5e.2}$$

where $\lambda_1 = \frac{k}{m}$ and $\lambda_2 = \frac{2k}{m}$, respectively. Then, substituting $\{u\} = [\Phi]\{q\}$ into Eq.(5e.1), and premultiplying by $[\Phi]^T$, we obtain:

$$[\Phi]^T[M][\Phi]\{q\} + [\Phi]^T[K][\Phi]\{q\} = [\Phi]^T\{F\}. \quad (5e.3)$$

From the orthogonality condition of eigenvectors, we obtain decoupled equation of Eq.(5e.2) in terms of:

$$\{\ddot{q}\} + [\Lambda]\{q\} = [\Phi]^T\{F\}.$$

After solving the above equation and using the relationship of $\{u\} = [\Phi]\{q\}$, we obtain the exact solution, under initial conditions of $u_1=u_2=0$ and $\ddot{u}_1=\ddot{u}_2=0$, as follows:

$$u_1 = (A_1 + A_2)\sin\omega_e t + \alpha_1 \sin\omega_1 t + \alpha_2 \sin\omega_1 t + \beta_1 \cos\omega_1 t + \beta_2 \cos\omega_2 t,$$

and

$$u_2 = (A_1 - A_2)\sin\omega_e t + \alpha_1 \sin\omega_1 t - \alpha_2 \sin\omega_1 t + \beta_1 \cos\omega_1 t - \beta_2 \cos\omega_2 t, \quad (5e.4)$$

where

$$A_1 = \frac{0.25 f_0}{\omega_1^2 - \omega_e^2},$$

$$A_2 = \frac{0.75 f_0}{\omega_2^2 - \omega_e^2},$$

$$\alpha_1 = -\frac{\omega_e}{\omega_1}, \alpha_2 = -\frac{\omega_e}{\omega_2} \text{ and } \beta_1=\beta_2=0.$$

The time history of displacement of at the first node is shown in Fig. 5.11. The responses are identical for the two cases. The variation of total error is shown in Fig. 5.12. The variation of the time step are shown in Fig. 5.13. In the second test case, the average

step-length is 1.6E-4 second which is of 32% of the initial step size. In this case, the average of energy norm of truncation error reduced to 2 % of the one with fixed time step as seen in Fig. 5.15.

The energy norm of the truncation error defined by Eq.(5.47) itself may not provide anything but it does give some indication for adjusting time step since the expression of energy norm is an function of time step. However, the current frequency or the energy norm of the truncation error can give indication of the accuracy and predict the dynamic system characteristics as well. Fig. 5.14 shows the variation of current frequency, which represents the instaneous characteristic frequency of the system. Since system has two natural frequencies, 314 rad/sec and 444 rad/sec, respectively, and its corresponding modes of vibration, the current frequencies during integration are between these natural frequencies. As shown in Fig. 5.14, the current frequencies computed with time adjustment process are shown to be more accurate in the response region of first mode of 314 rad/sec than the frequencies computed without step adjustment process.

However, stability problems may arise in the step adjustment process due to abrupt change in time step size. In some test cases of the problem, such an instability is experienced. In Fig. 5.16, the variations of damped frequency are obtained and are shown for two different cases. In the first case under an allowable error of 0.005, the adjustment algorithm allowed the time step size to change frequently as seen in Fig. 5.13 while such a rapid change under an allowable error of 0.0005 is not shown during the time elapsed except at the initial stage. As a result, it is shown that the numerically damped current frequency possess some periodic noise, which contributes observed error, in the case of 0.005 error bound as seen in Fig. 5.16. Also, it is shown that magnitudes of spectral radius, a more accurate definition for stability measure, exceed stability limit, which should not be more than one for stable condition. Thus, in such case, more careful treatment is needed to avoid the instability.

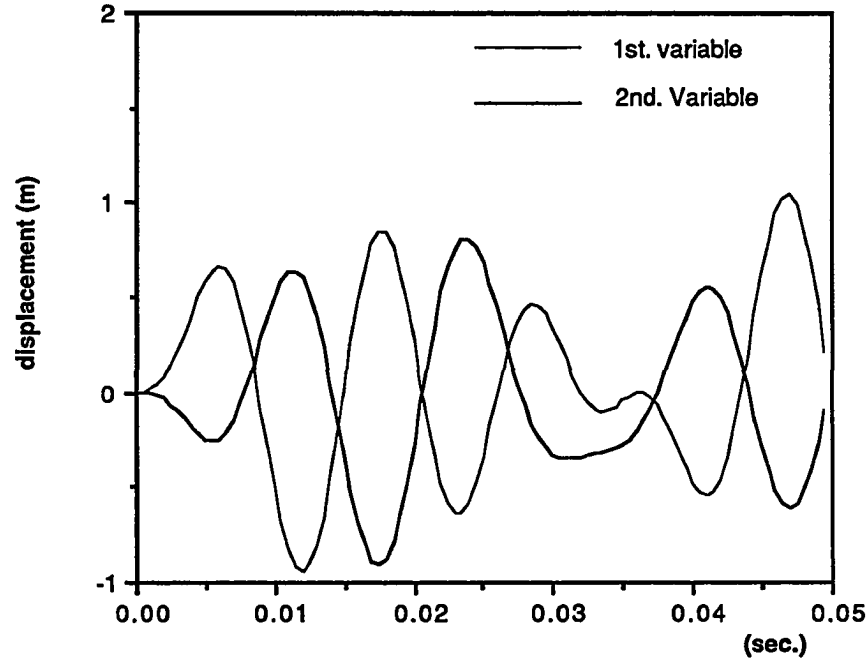

Fig. 5.11 Time Response of Two Degree of Freedom System of Example 2

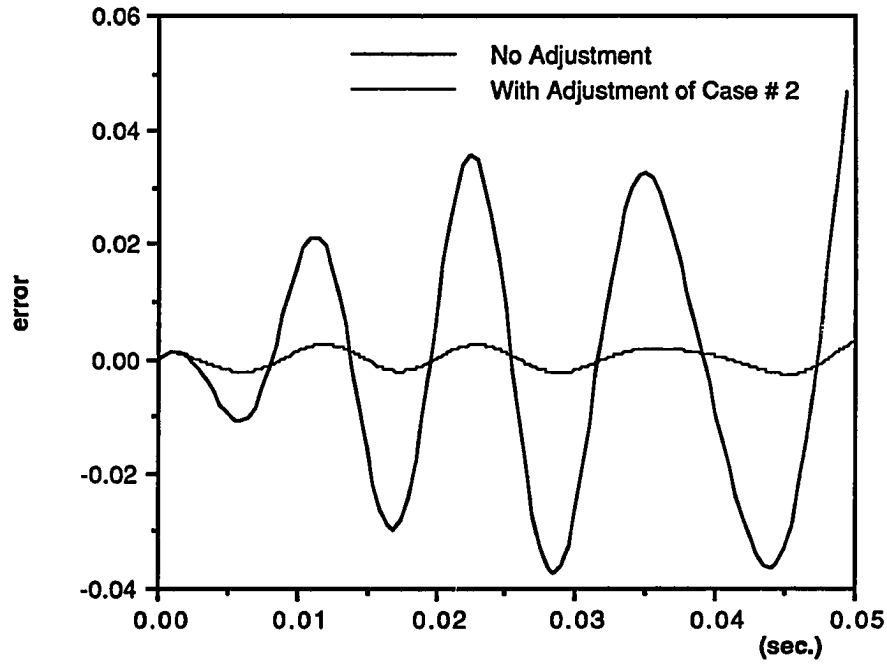

Fig.5.12 Variation of Total Error in Response of Two Degree of Freedom System of Example 2

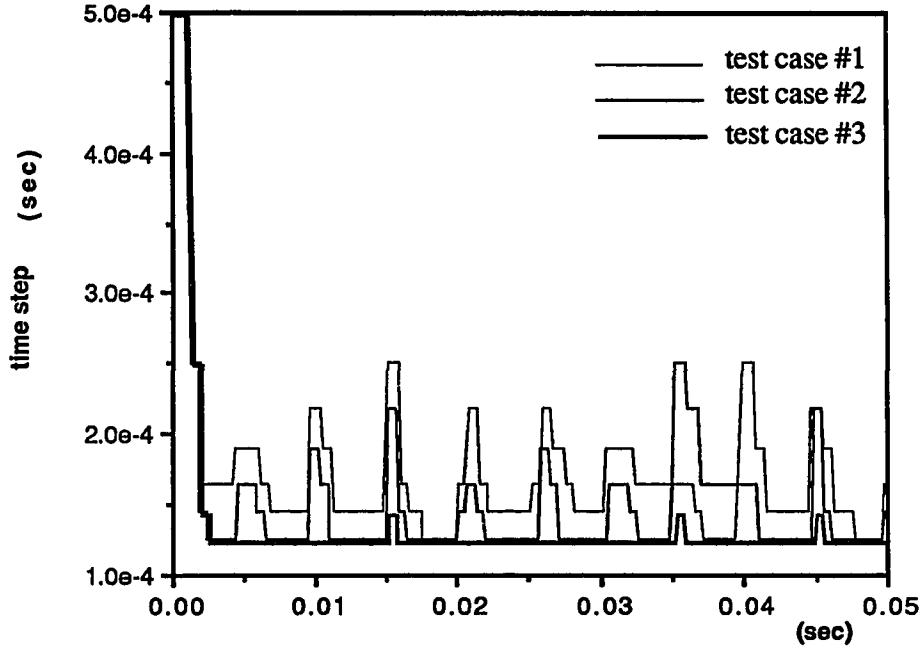

Fig. 5.13 Variation of Time Step in Solving Time Response of Two Degree of Freedom System of Example 2

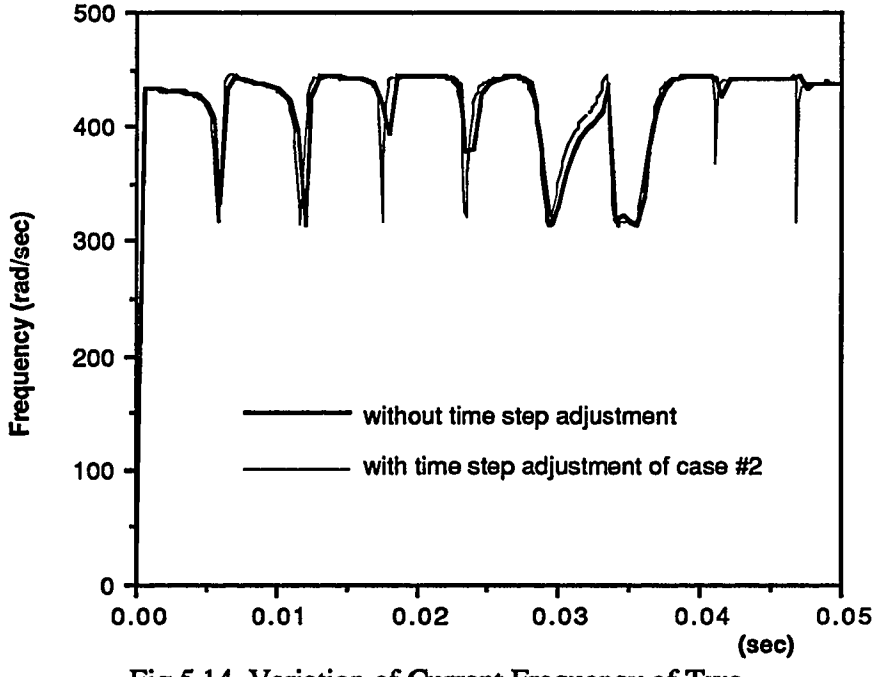

Fig.5.14 Variation of Current Frequency of Two Degree of Freedom System of Example 2

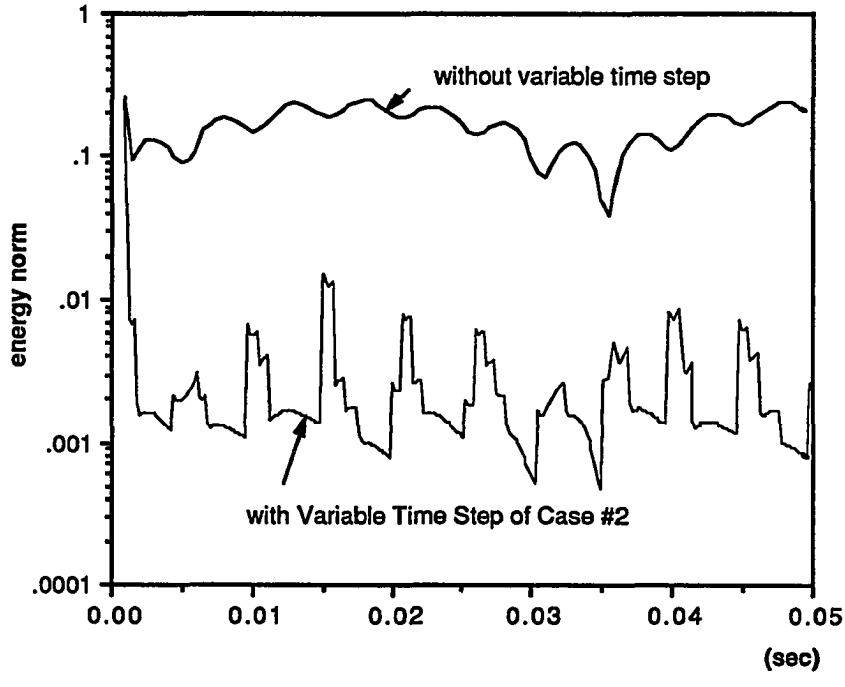

Fig. 5.15 Variation of Energy Norm of Truncation Error Two Degree of Freedom System of Example 2

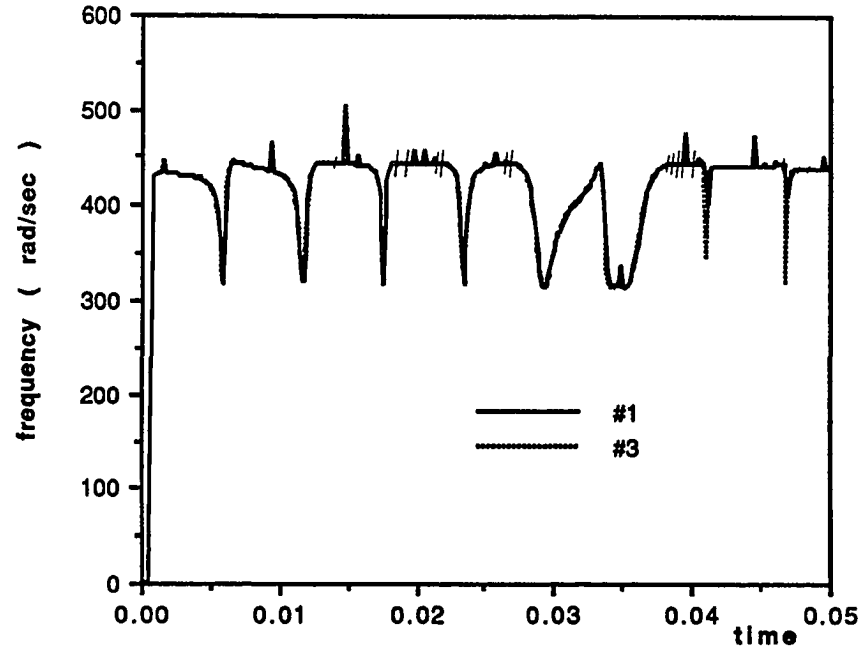

Fig.5.16 Variation of Damped Frequency of Two Degree of Freedom System of Example 2

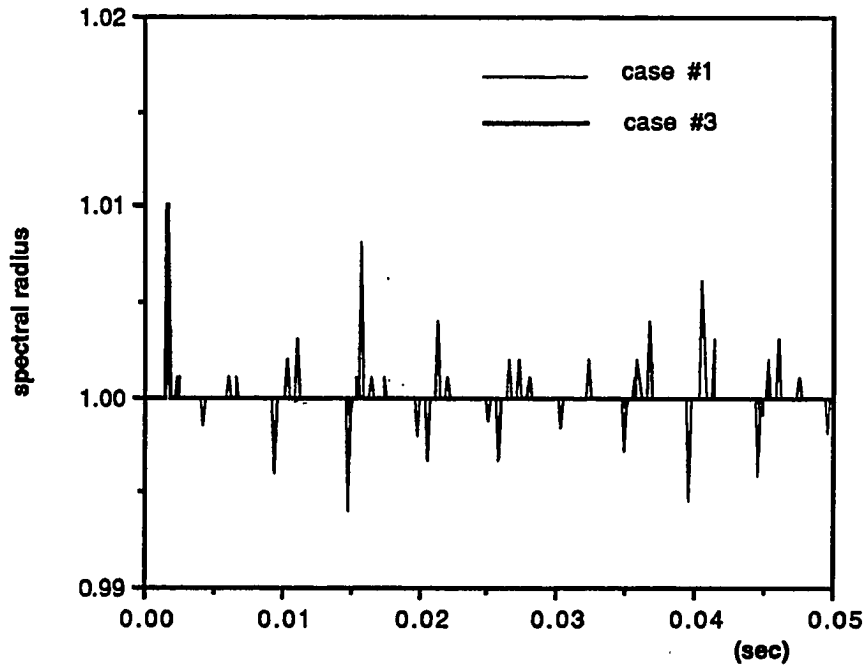

Fig. 5.17 Variation of Spectral Radius for Newmark -beta Method with Step Adjusting Algorithm for solving Example 2

5.6.3 Example 3 (Simply Supported Beam modeled with 3-D HEXA8 Finite Elements)

Based on the previous two examples, which are investigated mainly for examining the accuracy and the effectiveness of the algorithm, the algorithm is implemented to analyze the finite element model.

A simply supported beam is modeled by eight equally spaced 8-node 3-D finite elements over the half of its length. The beam is excited in the transverse motion with a harmonic point load acting at the mid point. The period of fundamental mode is 1 second. The harmonic forcing function starts with zero intensity. Damping is introduced proportional to the mass and the stiffness with proportional factors adapted to 10 percent of the critical value of the first and third modes of vibration. The beam is excited with load frequency equal to the third eigenfrequency. By treating this beam as an Euler beam, eigenfrequencies of the system can be found follows:

$\omega_1 = 6.29$ rad/sec and $\omega_3 = 56.66$ rad/sec

The pertinent system parameters corresponding to the system are:

$E = 2.1E11\ N/m^2$, $\rho = 70$ kg/m, $\nu = 0.3$, $L = 24m$, $I = 4.48E\text{-}5\ m^4$,

$P_o = 450$ N,

and parameter values for the integration algorithms are

$\gamma = \frac{1}{2}, \beta = \frac{1}{4}$.

The system is solved and tested under several analysis conditions. Test conditions are given for the maximum allowable norm of truncation error, 1.0E-4, 5.0E-5, 1.0E-5, and 5.0E-6, respectively.

Four test cases are carried out for values of initial time step h_0 equal to 0.001. The maximum and minimum step length , h_{max} and h_{min} are set to equal to 5 times and 0.2 of initial time step, respectively, same as previous model.

When it can be assumed that damping is proportional, we can write:

$$\phi_i{}^T C \phi_j = 2 \omega_i \xi_i \delta_{ij}, \tag{5.59}$$

where ξ_i is a modal damping parameter and δ_{ij} is the Kronecker delta.

Damping effects can readily be taken into account in mode superposition analysis provided that Eq.(5.59) is satisfied. However, assuming that it would be numerically more effective to use a direct step-by-step time integration scheme and that realistic damping ratios are known. In that case, it is necessary to evaluate the matrix C explicitly, which yields the established damping ratios ξ_i , when C is substituted into Eq.(5.59). If p=2, Rayleigh damping can be assumed, which is of the form:

$$C = \alpha K + \beta M, \tag{5.60}$$

where α and β are constants to be determined from the two given damping ratios that correspond to unequal frequencies of vibration.

As we assumed that damping is introduced proportional to the mass and stiffness with factors adapted to 10 percent of critical of the first and third vibrations for this example of multiple degree of freedom system. The system has natural frequencies of 12.5 and 56.6 rad/sec for the first mode and the third mode, respectively. Establish the constants α and β for Rayleigh damping in order that a direct time integration can be carried out.

Using the relation in Eq.(5.59) we obtain using (5.60):

$$\phi_i{}^T (\alpha K + \beta M) \phi_j = 2 \omega_i \xi_i \delta_{ij},$$

$$\alpha + \beta \omega_i^2 = 2 \omega_i \xi_i \delta_{ij} .$$

Using this relation for ω_1, ξ_1 and ω_3, ξ_3 , we obtain two equations for α and β :

$$\alpha + \beta \omega_i^2 = 2 \omega_1 \xi_1 , \text{ and}$$

$$\alpha + \beta \omega_3^2 = 2 \omega_3 \xi_3 .$$

The solution is α= 1.123, and β = 0.00318. Thus the damping matrix to be used is

$$C = 1.123\ K + 0.00318\ M.$$

The time history of displacement is shown in Fig. 5.18. The responses are identical for the four different test cases. Variations of the time step for each test cases are shown in Fig.5.19.

Fig. 5.20 shows the variation of current frequency, which represents the instaneous characteristic frequency of the system at each time step. Since system has infinitely many natural frequencies, starting from 6.29 rad/sec for the first modes, and its corresponding modes of vibration, the current frequencies along the time frame also are in the range of these natural frequencies. However, Fig. 5.20 shows that the range of the current frequencies are finite distributed because of the excitation frequency being equal to the third eigenfrequency. As shown in Fig.5.20, the current frequencies computed with the time adjustment process are shown to be more accurate in the response region of first mode of 6.29 rad/sec than the frequencies computed without the time step adjustment process.

In Fig. 5.20, it is shown that the enegy norm of the local truncation error may be controlled effectively. The energy norm of the truncation error for each test cases are confined in some range of tolerance which is given and controlled within the program.

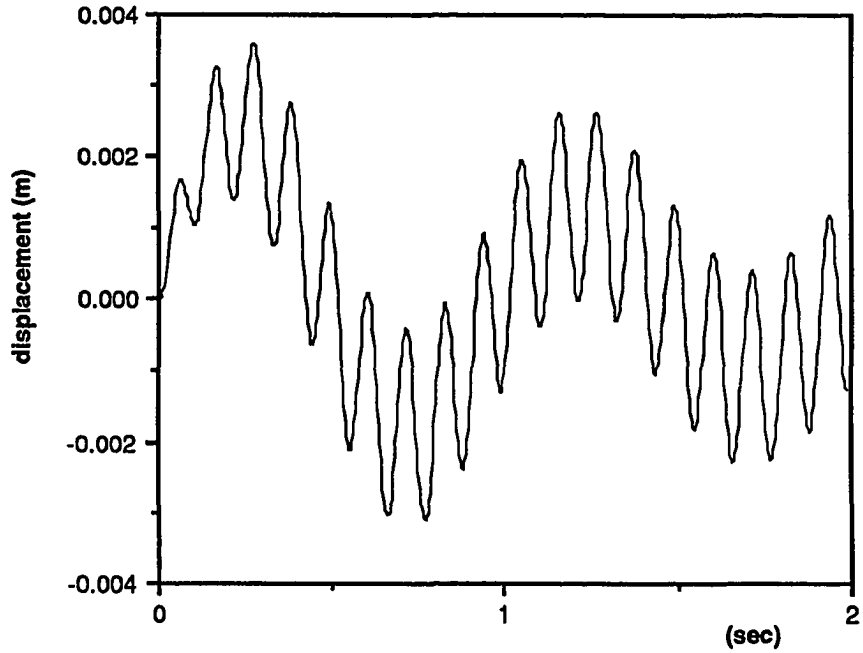

Fig.5.18 Time Response of Simply Supported Beam of Example 3

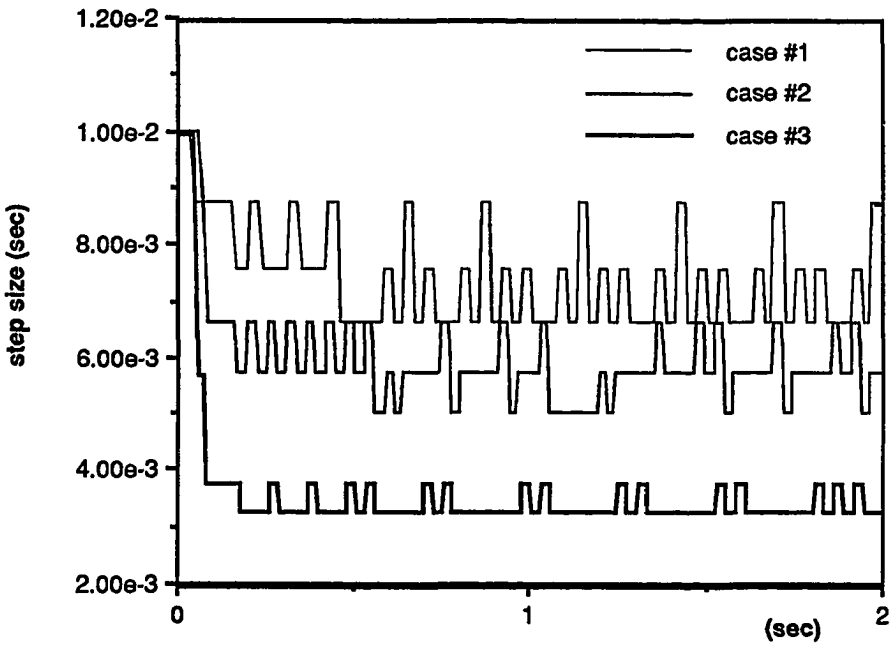

fig.5.19 Variation of Time Step Size for Solving Time Response of Simply Supported Beam of Example 3

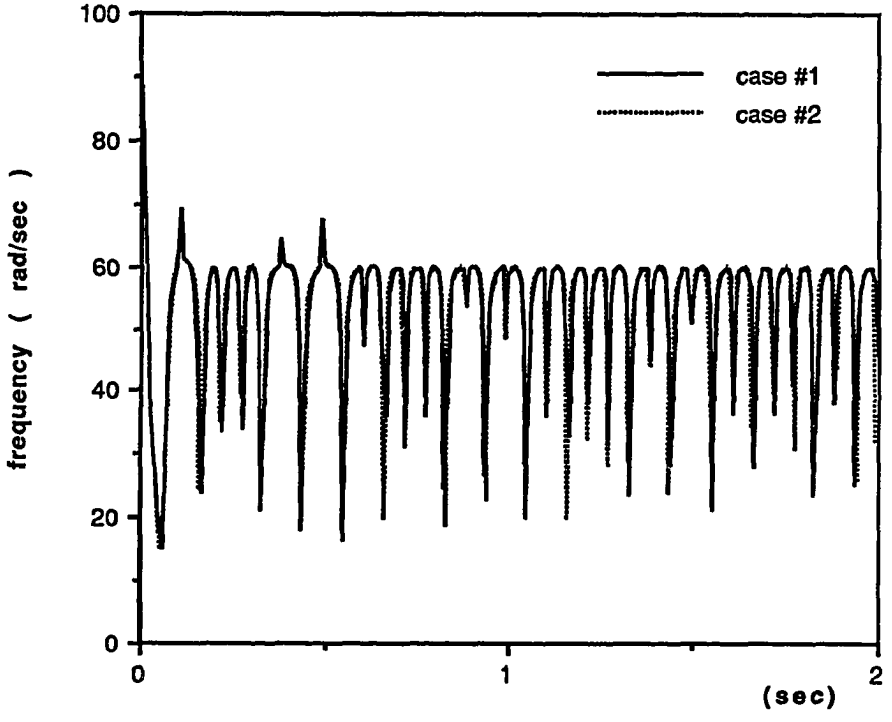

Fig. 5.20 Variation of Current Frequency of Simply Supported Beam(Example 3)

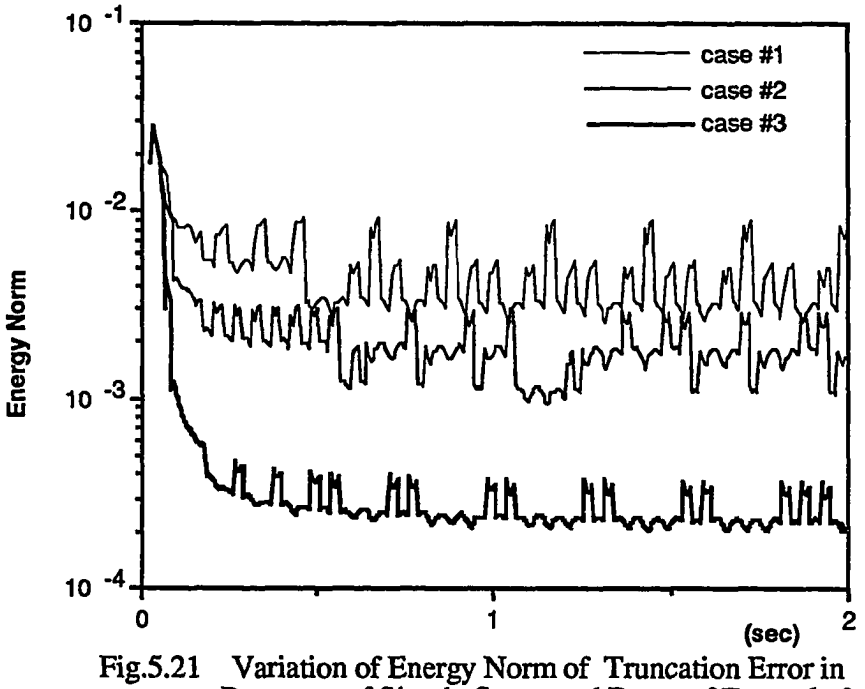

Fig.5.21 Variation of Energy Norm of Truncation Error in Response of Simply Supported Beam of Example 3

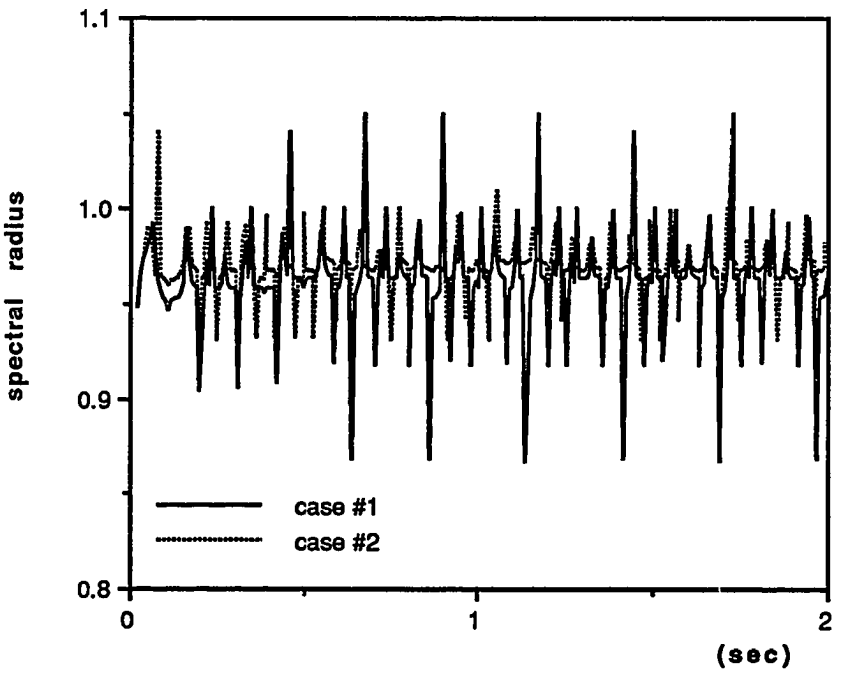

Fig. 5.22 Variation of Spectral Radius for Newmark-beta Method with Step Adjusting Algorithm for Solving Example 3

As in previous problem, even with dampings, some stability problems were encountered. In Fig. 5.22, it is shown that magnitudes of the spectral radius are ranged between 0.85 and 1.05, exceed the stability limit at some time, which should not be more than one for stability.

5.7 Conclusion

In most applications of implicit methods to problems of structural dynamics, past research indicates that quite large time steps can be used and will provide reasonable accuracy in the solution when the solution of lower modes are of prime concern. However, since most of the numerical studies show a steady and rapidly increasing growth of error as the time step increases, the accuracy requirements suggest that it is important to consider the control of error in the time matching schemes, as well as the appropriate selection of the method of control of the time step size. Thus, an algorithm is needed which can calculate optimum time step in a automatic fashion during the solution process.

The basis for such algorithm should be error control, computational efficiency, and convenience of implementation. There are two major factors that effect the efficiency of a variable step integration procedure: the basic integration formula which dictates stability and accuracy for fixed time step integration and the step-size control strategy used to satisfy a specified error bound and at the same time to avoid instability.

The method which is described in this paper has many similarities with the technique of step selection previously developed which are shown in the literature. To control error, the truncation error is the first candidate as a measure. However, a cost-

effective method is required in order to provide a relatively cheap and reliable solution, such as improving the effectiveness of traditional stepsize change technique using the truncation error measure.

As a first attempt, the measure for evaluating the truncation error committed during the process of time integration in each time step is newly defined. To evaluate the truncation error, we have assumed a precisely defined twice differentiable forcing function for evaluating the truncation error for the forced response system. In practice, forcing functions consist of experimentally observed loads at discrete time intervals, therefore the computation of the required derivatives is not always possible. To resolve such difficulties and reduce unnecessary computation even when it is possible to determine force and its derivations at every time step, a new approach is presented in this chapter.

The second attempt is made to implement this method to the multi-degree-freedom system. Since the previous development is made on a single decoupled equation based on modal decomposition, such properties must be considered systemwise using mode superposition. It is tedious to extract several lower modes from the system, in which these lower modes seem to dominate the structural response. Thus, an approximate measure of frequency is needed to represent the system reasonably in the range of interesting frequencies. The current frequency, which derived from Rayleigh Quotient, is introduced in evaluating the evolution matrix for time integration. Employment of this current frequency provides very accurate measure for the truncation error, and saves the computation time required to evaluate the error at each time step.

In all examples solved, it is shown that the local truncation error might be effectively controlled. The truncation error norms for each example were confined and controlled within some range of a given tolerance. Also, it is recognized that substantial time saving was attained by using the variable time stepping algorithm developed.

In the example of two-degree-of-freedom system, which has two natural frequencies, 314 rad/sec and 444 rad/sec respectively, the current frequencies along the time frame ranged between these natural frequencies. The current frequencies computed with time adjustment process are shown to be more accurate in the response region of the first mode of 314 rad/sec than the frequencies computed without the time step adjustment process.

In the beam problem, it is shown that the current frequency which represents the instaneous characteristic frequency of the system ranged between 6.29 Hz and 60 Hz. This revealed that the current frequencies computed with time adjustment process are more accurate in the response region of the first mode of 6.29 rad/sec than the frequencies computed without the time step adjustment process.

It is shown that the numerically damped current frequency possess some noise frequency, what is sometime called error. Also, it is shown that the magnitudes of the spectral radius, a more accurate definition for stability measure, exceed the stability limit, which should not be more than one for stability.

In the examples solved, some stability problems were experienced with the time stepping algorithm, even inclusion of damping. It is shown that magnitudes of the spectral radius sometime exceed the stability limit, which should not be more than one for stability.

CHAPTER VI

EXPERIMENTAL MODAL ANALYSIS OF DIESEL ENGINE CYLINDER BLOCK

6.1 Introduction

An experimental modal analysis of a diesel engine cylinder block was performed. This analysis was conducted in order to obtain the dynamic characteristics of the cylinder block structure of the Daewoo-M.A.N. D0846HM diesel engine.

The objective of the experimental modal analysis, or modal testing, was to determine the modal parameters, which consist of the modal frequencies, the modal damping, and the mode shapes. Modal analysis requires a thorough integration of three components, the theoretical basis of vibration, the accurate measurement of vibration, and realistic and detailed data analysis. This chapter is concerned with these major parts of the experimental modal analysis.

Modal analysis consists of a sequence of steps to obtain the modal parameters. The first step is to obtain the frequency response function, or transfer function. There are various types of frequency transfer functions derivable from data. These are receptance, mobility, and inertance[See Appendix 2]. The second step is to extract modal parameters from the measured frequency response function, and to derive the analytical function from

the extracted parameters. The third step is to perform curve fitting which compares the analytical curve with the measured frequency response function curve. If agreement is good, then the extracted parameters can be used to derive the mode shapes. The last step is to derive mode shapes, usually by means of circle fitting (Nyquist plot). Further analysis may be performed to obtain a mathematical model. This is derived from the modal parameters, and from which the structural response can be predicted under an arbitrary excitation. This is the procedure of modal testing. Alternatively, the mathematical model can be achieved directly by the FEM.

The most crucial portion of the modal analysis in this work was to accurately identify and discriminate between the rigid body motions and the structural modes. Since modal analysis has been well established over the last two decades, this chapter will deal with experimental issues rather than theoretical ones.

The computer aided testing system, GR2515 from GENRAD Corp., specially designed for modal analysis, has been used for the experiment. This system was programmed to store the exciter and the response signals and to produce the frequency response function. This system software yields the Bode diagram, and the Nyquist plot.

To obtain a measurable input of mechanical force energy, excitation(see Appendix 2 for details) of the structure was provided by an input hammer. Plastic impact tips gave the best frequency response in the frequency interval of interest(e.g., frequency ranges 0-1000 Hz). These were mounted in the end of the hammer head. The force transducer was mounted between the impact tip and the hammer head to measure the impact force as a function of time. An accelerometer has been used throughout the experiment to measure the structural response.

6.2 The Experimental Set-Up of the Cylinder Block

The block was tested on various types of supports, which can be mathematically defined as boundary conditions. Through the tests, under various configurations of supports, it was found that the actual support conditions can greatly influence the response of the experimental measurement as shown in Fig.6.2b. Therefore, the experiment should be arranged to be minimally influenced by the supports. This can be achieved by adopting boundary conditions like, grounded support, simple support, or free-free support. This support definition should be incorporated into the the finite element model. Consequently, a simply supported boundary condition was adopted. Practically, in case of the complicated support, the frequency response function shows a number of peaks, and the peaks are spaced closely.

As shown in Fig. 6.2a and 6.2b, the spurious modes, and the modes of no interests, can be eliminated by modifying the supports. Eventually, well-separated frequency response functions (FRF) can be obtained as shown in Fig. 6.2b.

It is noted that if there is no restriction in choosing the boundary condition, the free-free support is desirable since a better and easier analysis is realized. This may be achieved by suspending the object by cables or by laying it on sufficiently soft sponge-like material. In any method of support, the rigid body motions usually appear on the FRF plot in the low frequency region, and these motions must be identified through the analysis.

6.3. Location of Points for Measuring Response and Excitation

There are two methods to locate points for measuring the response and the excitation. In the first method, the response is measured in one direction at one point, while the excitation is applied at each point in all directions in turn. In the second method, the structure is excited at one point while the responses is measured at various points. Theoretically, these two methods produce identical results. In the experiment, the first method was used. The measurements were taken at 132 points in all directions. The measuring locations are shown in Fig.6.3.

Most of the measurement points were located on the surface of the engine block. In general, the response can be measured in all three directions at each point. However, at some points, for example, on the side wall, the response could not be measured because geometrical complications made it difficult to apply the impact force in y-direction. Even though no measurement can be made in some directions at some points, the global motion motion can still be determined sufficiently.

When a point for measuring and/or excitation is located at the node of a certain mode, that mode will not appear on the frequency response function(FRF). This means the amplitude for that mode will be very small and will not show on the Bode plot of FRF. But this FRF will show all other peaks except the peak mentioned above. Fig. 6.5a and 6.5b are the examples of this. For this reason, more than one FRF should be analyzed when extracting modal parameters. For the analysis, it is desirable to obtain a point mobility or point inertance for FRF. Point mobility is one where the response coordinate and the excitation coordinate are identical. An advantage is that the point mobility is expected to have the highest valued residuals[see Appendix 2 for deatails]. Conversely, the

transfer mobility is one where the response coordinate and the excitation coordinate are different, and will have the lowest valued residuals.

The location of the points for measuring the response should be carefully chosen to avoid missing modes of interests, for example, the several lowest modes which have greatest physical meaning. By means of the experiment, it was found that the response must not be measured at the midpoint or at a quarter wave length since these points are nodes of the second and the third modes. In other words, the measuring point should be located away from the midpoint of the testing structure. For instance, when the structure is nearly symmetric, and the response is measured at the midpoint, the even-numbered modes, such as 2nd, 4th, and 6th mode etc., will not appear on the FRF as shown in Fig 6.5a,and 6.5b.

In addition, there is a method to evaluate the measured FRF curve. It is useful to check the FRF plot quickly for point inertance and transfer inertance. In case of point inertance, the FRF curve should show antiresonance with zero amplitude between two resonances as shown in Fig. 6.5a, 6.5b. The reason is that their sum of response magnitude is zero since they are of equal magnitude but opposite sign at the point where two resonances cross. In the case of the transfer inertance, as shown in Fig. 6.4a and 6.4b, the FRF curve should show a round curve with some amplitude between two resonances. The reason is that the sum is twice, since they have same sign at the point where two resonances cross.

6.4 Parameter Extraction

The natural frequencies can be easily be correlated with the peaks on the FRF plot. However, another technique is needed to determine the damping factors and mode shapes

from the FRF. It is noted that even if the peaks are easily recognizable, it is not easy to distinguish which are the natural frequencies of the structure, since any boundary condition might produce rigid body motions on the FRF plot. Thus, some method must be provided to determine the natural frequencies from measured frequencies on the FRF plot, by identifying rigid body motions through the mode shape analysis.

The resonance frequencies and damping factors can be extracted with the aid of the GR2515 in which there are three available functions, such as the search peak(SDOF), the complex exponential method (time domain, MDOF), and the polynomial method (MDOF). In this experiment, both the search peak and the complex exponential method were used to extract the modal parameters.

6.4.1 Mode Shape Extraction Using the Circle Fitting Method

The major objective of circle fitting is to derive the mode shapes. The circle plot, or Nyquist plot, gives information concerning mode shapes, or displacements. Then it is obvious that if the amplitudes at all response coordinates are obtained, the mode shapes can easily be drawn as shown in Fig.6.8. To derive the mode shapes, both the response at resonance and the circle fitting methods were used. However, it is known that the circle fitting method is more accurate than the response at resonance[87,91].

As previously discussed, the FRF contains all the information about the amplitude, and phase at each increment of frequency in real and imaginary domain. It is well known that in the vicinity of a resonance, the plot of real vs imaginary, with respect to the damping factor describes an the exact circle. Therefore, if the appropriate parameter is chosen for the type of damping model, an exact circle is produced.

In order to verify the extracted parameters obtained from curve fitting, the circle fitting method was used. If the extracted parameters were not good, the circle fitting gave a

distorted circle as shown in Fig. 6.7. When the extracted parameters were good, the circle fitting method gave an almost exact circle as shown in Fig. 6.8 .

In the preceding section, we have discussed the resonance frequency and the damping factor for one FRF. Usually, only two or three transfer functions are required to derive the modal parameters because they are global. However, in the case of deriving the mode shapes, all of the transfer functions, in this case 132, must be analyzed to obtain all the modal constants which produce the mode shape for each resonant frequency. In other words, if five peaks are chosen for modal analysis in a frequency region, we have to analyze 132 x 5 = 660 transfer functions. Initially the curve fitting method was used to quickly determine the modal parameters then circle fitting was performed in order to get the refined modal constants, i.e., mode shapes.

6.4.2 Modal Constant

The modal constant is the most important parameter for determining mode shape. In this section, more detail concerning mode shape determination is discussed.

The modal constant can be written as:

$$ {}_rA_{jk} = {}_r\Phi_j \, {}_r\Phi_k \, . \qquad (6.1) $$

where Φ are eigenvectors and r denotes r-th mode, j and k denote an arbitrary measurement coordinate.

Equation (6.1) represents the modal constant for r-th mode and the transfer inertance(j,k). For point inertance, the equation can be written in the form of:

$$ {}_rA_{kk} = {}_r\Phi_k \, {}_r\Phi_k \, . \qquad (6.2) $$

As a result of extracting the modal parameters, the modal constant, ${}_rA_{jk}$, can be obtained by circle fitting. Since we know ${}_r\Phi_k$ from Eq. (6.2) for the point inertance, the eigenvector can determined as ${}_r\Phi_j = {}_r\Phi_k/{}_rA_{jk}$. Thus, any eigenvector can be derived in terms as follows:

$$ {}_r\Phi_m = {}_r\Phi_k/{}_rA_{mk}. \tag{6.3} $$

In this procedure, the mode shape can be determined by deriving the eigenvector matrix[Φ]. Also, the modal constant can be used to establish the accuracy of the mathematical model as mentioned in the introduction. For that reason the point inertance has an important role, both mathematically and experimentally.

6.5 Identification of Rigid Body Motion

As shown in Fig. 6.9a, 6.9b and 6.9c, and Fig. 6.10a and 6.10b, it was found that there are five resonances in the frequency region of 0-1000 Hz. From THE FRF plot, rigid body motion should be identified and excluded in order to determine the real structural mode shapes of the engine block. As mentioned before, the rigid body motions are antifacts of the support conditions.

Fig.6.10a represents the rotational motion about z-axis and it might be a rigid body motion. However, since Fig.6.10b shows quite complicated motion, a careful investigation is required to identify it. Even though it was eventually found that it is the second rigid body mode, several things must be considered. As shown in Fig. 5a, there are five resonances on the FRF plot. The point inertance, denoted by the sign '2X+ 2X+', can be seen in the right bottom corner on the plot. The first one is the response coordinate and the second one is the excitation coordinate. In the same manner, measurement is taken at

'11X+', midpoint of the longitudinal length of the engine block, where the excitation and response coordinates are located. As shown in Fig.6.5b the FRF plot contains only three peaks. The other two peaks have disappeared.

As mentioned before, in the case of point mobility,(11X+, 11X+) it should pass through the center node of the 2nd mode,4th mode etc., and then such modes should not appear on the FRF plot. For convenience, each peak is numbered as shown in Fig. 5a. The peak of #1 is easily defined as rigid body motion (see Fig.6.10a), therefore, it is obvious that peak #2 or #3 might be the fundamental mode, but in observing the Fig. 5b, peak #2 and #4 have disappeared, so we might deduce that peak #2 is not a fundamental mode because in such coordinate(11X+, 11X+) the even number mode like the second and 4th modes must disappear. Eventually, we identify peak #1 as the fundamental mode and the second mode to be peak #4. It is assumed at this point that peak #5 might be the third mode. This was proved through mode shape analysis.

Thus, if the fundamental mode is #3 peak, it is concluded that #2 peak is a rigid body motion. Now a question arises in viewing Fig. 6.10b. It shows a very complicated picture from which it is difficult to identify rigid body motion. But it seems that the problem comes from the closely spaced peaks(#2 and #3). In such a case it is quite difficult to get the precise modal parameters, which means that it is difficult to have good curve fitting as shown in Fig. 6.6b. The figure shows some disagreement between the measured curve and the analytic curve, consequently deviation of the parameters produces slightly distorted modal constants. This results in a complicated picture, but generally it represents rotational motion about y-axis.

In addition, there are three more reasons why #2 peak is considered as rigid body motion. The first is that the damping factor is too high(0.030) comparing with the structural damping(0.005) as shown in the conclusion section. The second is that the antiresonance

between #2 and #3 peaks does not approach zero as shown by Fig.6.5a. If they reflect the structural mode, the two components at cross point must have same the magnitude, but with opposite signs. These sum must be zero, a conclusion based on theorem for an undamped or lightly damped system. The third is that #2 peak is located in the low frequency region, type of rigid body motion should be.

6.6 Conclusion

In this experiment, five modes have been obtained in the frequency region up to 1000Hz. These modes consist of the fundamental, the second, and the third mode, and two rigid body modes. The natural frequencies and modal damping were obtained by means of curve fitting for both the search peak and the complex exponential methods, and the mode shapes were obtained by means of the circle fitting method.

Through the experiment, it was found that there are two rigid body motions which meet at 63 Hz, rotation in z-axis and 159Hz, rotation in y-axis. Theoretically, the frequencies of rigid body motions are much lower than the natural frequencies of the structure. The rigid body motion can be changed as the support configulation changes. The value of the rigid body motion itself does not have significance since our basic interest lies in the structural dynamic behavior of the block.

However, the rigid body motion should be minimized and further experimental plans developed to eliminate these motions.

Table 6.1 Structural Modes

Mode No.	Frequency (Hz)	Damping Factor(%)	Remark
1	199.67	0.00588	1. Bending Mode
2	430.0	0.00775	Torsional Mode
3	573.5	0.00351	2. Bending Mode

Table 6.2 Rigid Body Modes

Mode No.	Frequency (Hz)	Damping Factor(%)	Remark
1	63.7	0.017	rotation about z-axis
2	159.2	0.031	rotation about y-axis

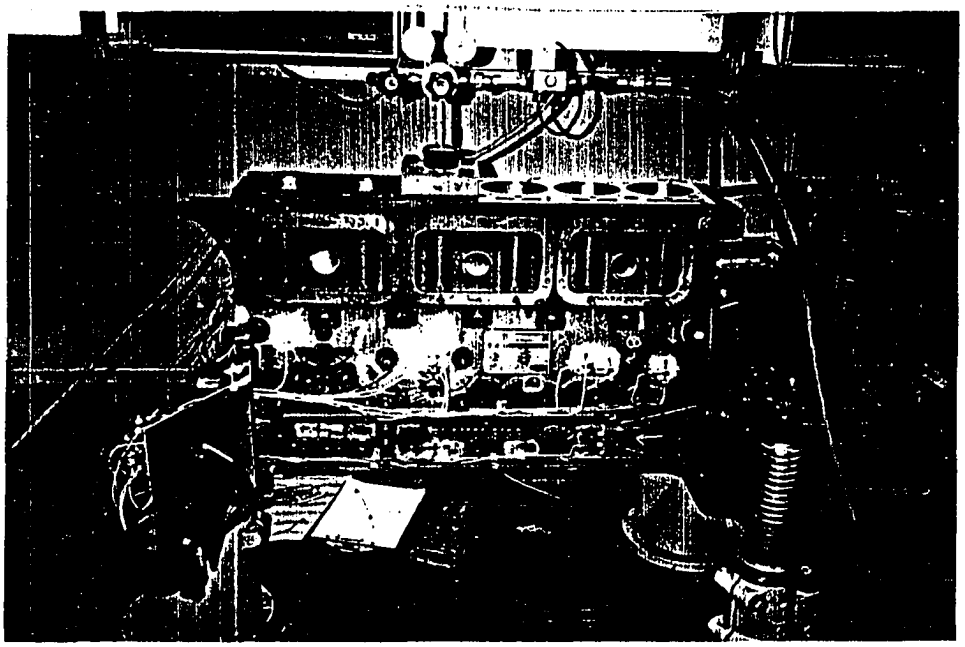

(a) Initial Set-up with Four Supporting Pillar Assembly (2"dia.x 17"length).

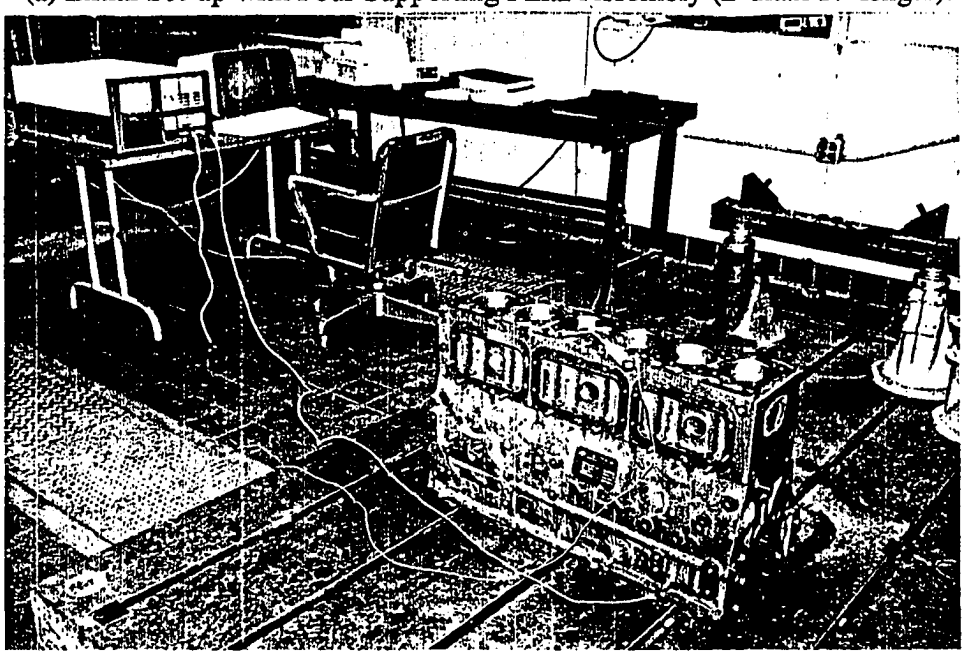

(b) Modified Set-up with Supports Using Four Steel Balls(1/4"dia.), Attached to Each Bottom Corner of Cylinder Block.

Fig. 6.1 Experimental Set-Up of Diesel Engine Cylinder Block

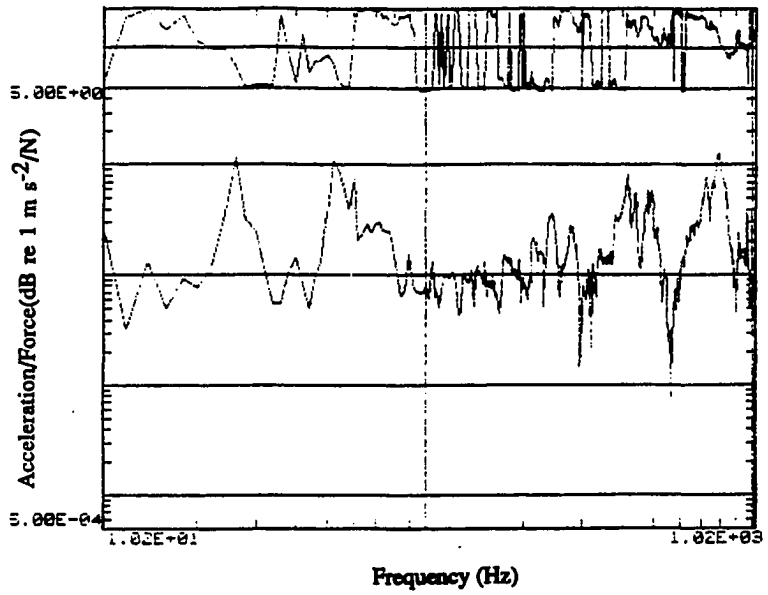

(a) FRF Plot Measured at the Transfer Inertance (8X+ 2X+) for the Engine Block as Initially Set-Up.

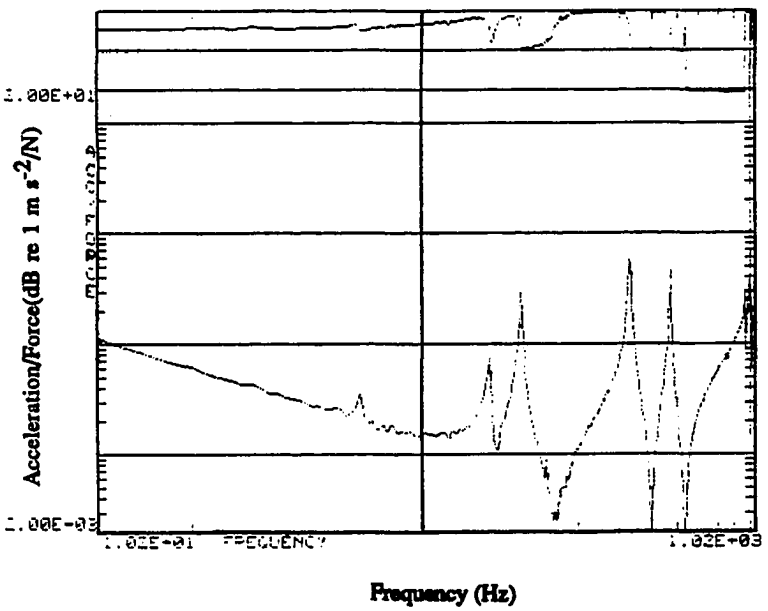

(b) FRF Plot Measured at the Point Inertance (2X+ 2X+) for the Engine Block of Modified Set-Up.

Fig. 6.2 Comparison of Frequency Response according to Cylinder Block Support Configuration

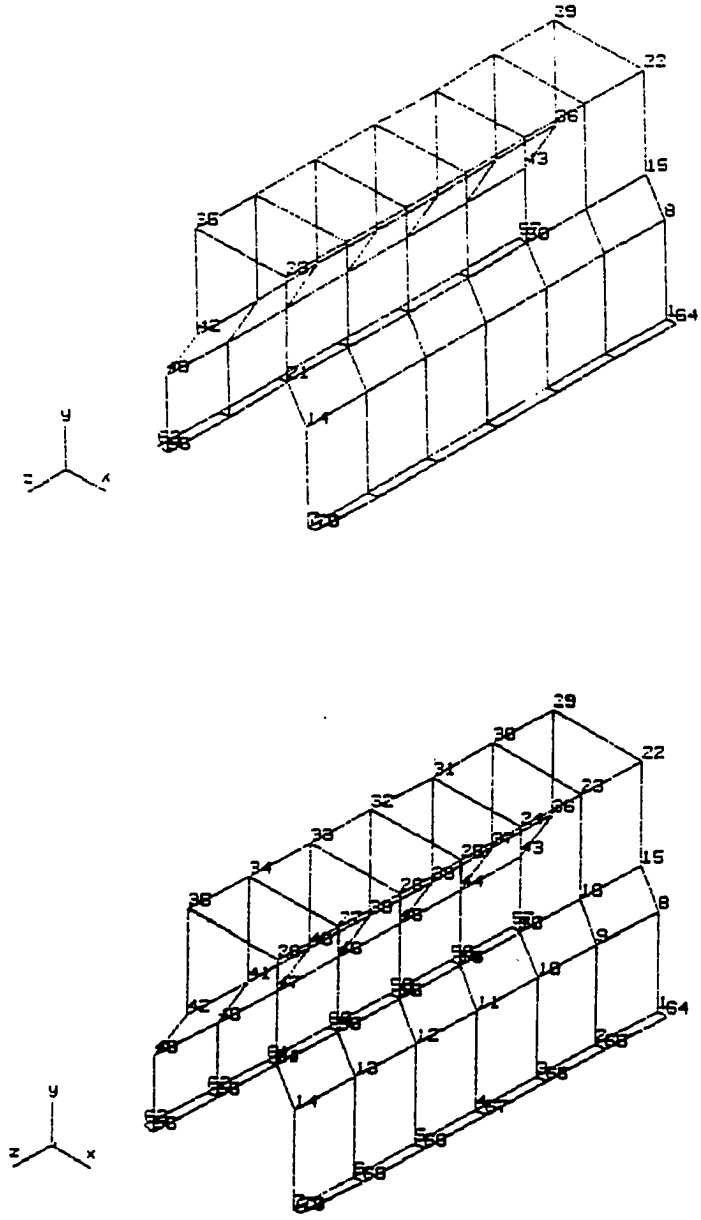

70 Nodes and 132 Measurement Points in all Directions

Fig. 6.3 Measuring Point Mesh of the Cylinder Block

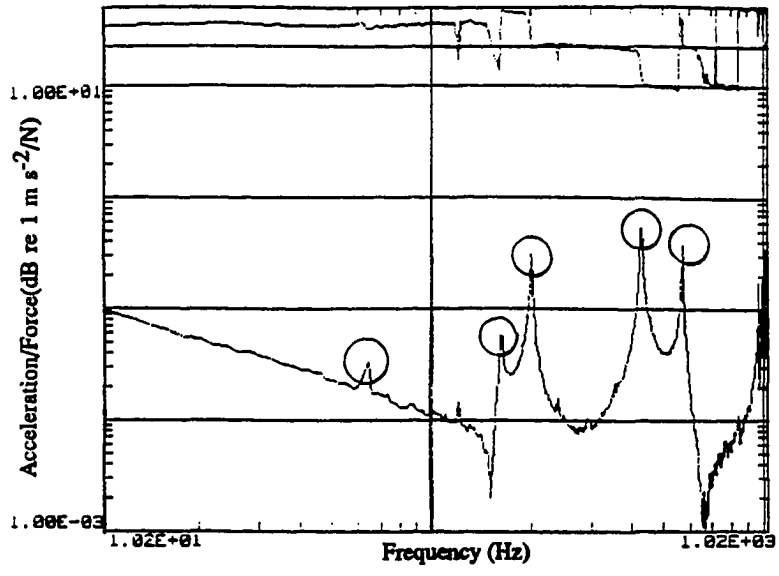

(a) FRF Plot with All Peaks for the Transfer Inertance(2X+ 6X+)

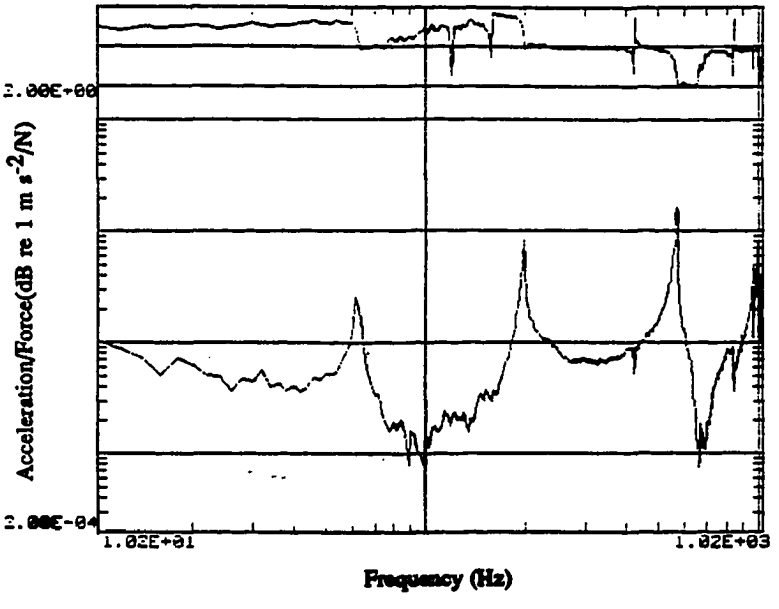

(b) FRF for the Transfer Inertance(2X- 11X-), Showing only Three Peaks with Two Peaks Missed due to theResponse Coordinate (11X-), Positioned in Center of the Structure.

Fig. 6.4 Different Frequency Response Results According to Measuring Location

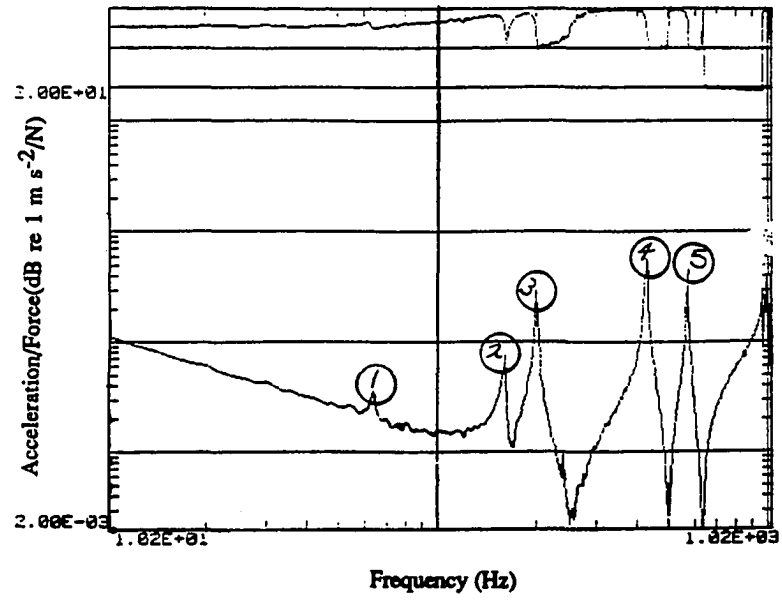

(a) FRF Plot for the Point Inertance(2X+ 2X+), Showing All Five Peaks

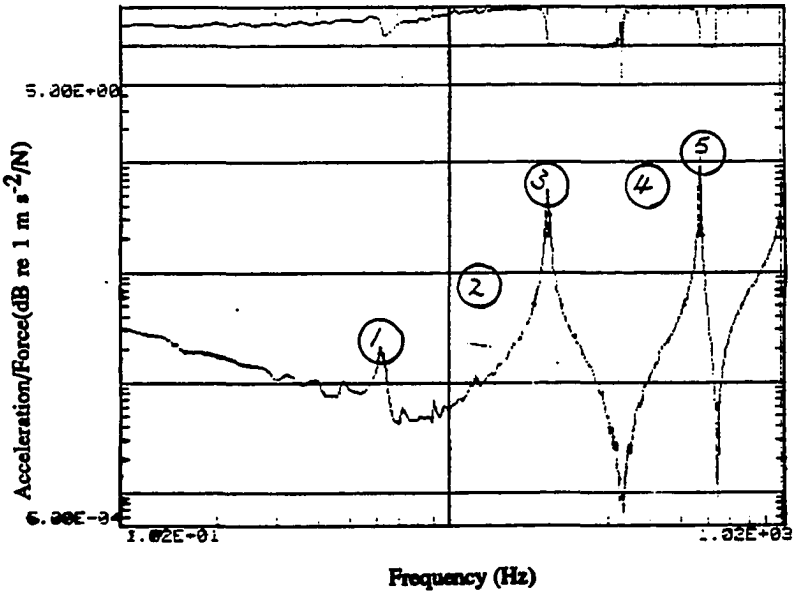

(b) FRF Plot for Point Inertance (11X+ 11X+), Showing Three Peaks with Missing Two Peaks due to the Coordinate (11X+), Positioned in the Middle of the Structure.

Fig. 6.5 Different Frequency Response Results According to Position for Point Inertance

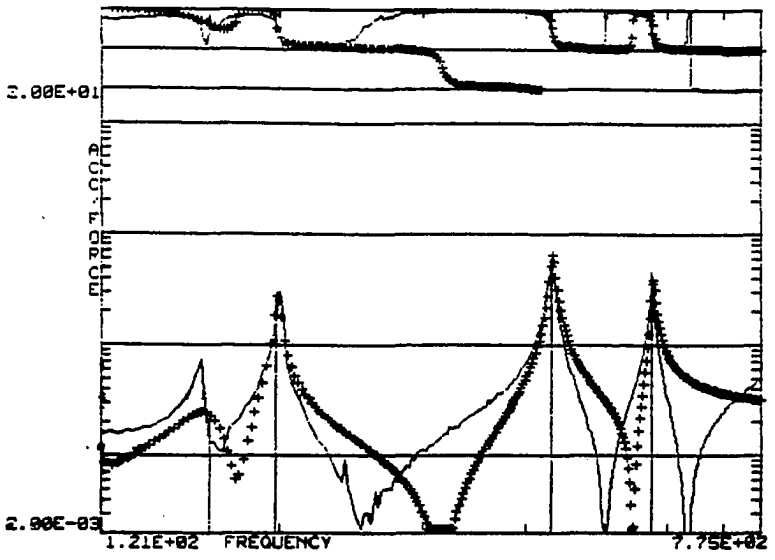

(a) The Curve Fitted Frequency Response Using Complex Exponential Method Without Adding Residuals.

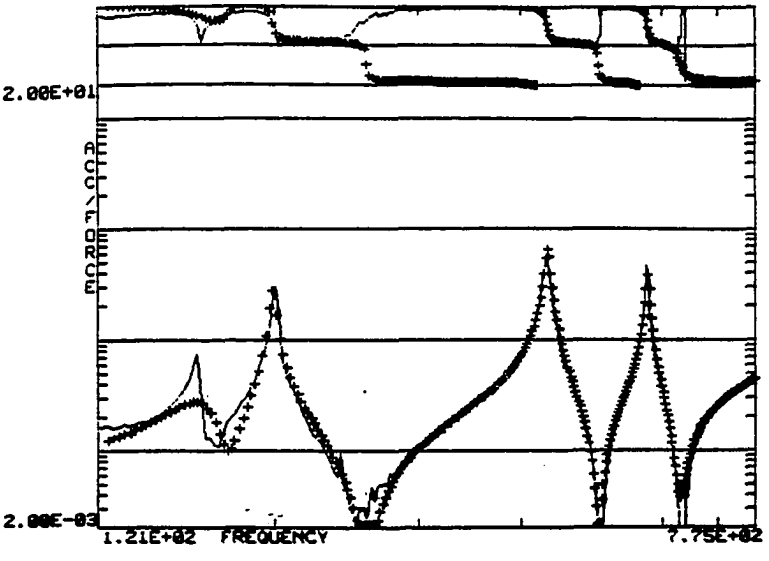

(b) The Curve Fitted Frequency Response Using Complex Exponential Method After Adding Residuals.

Fig. 6.6 Analytic Frequency Response Plot with Residual Effects

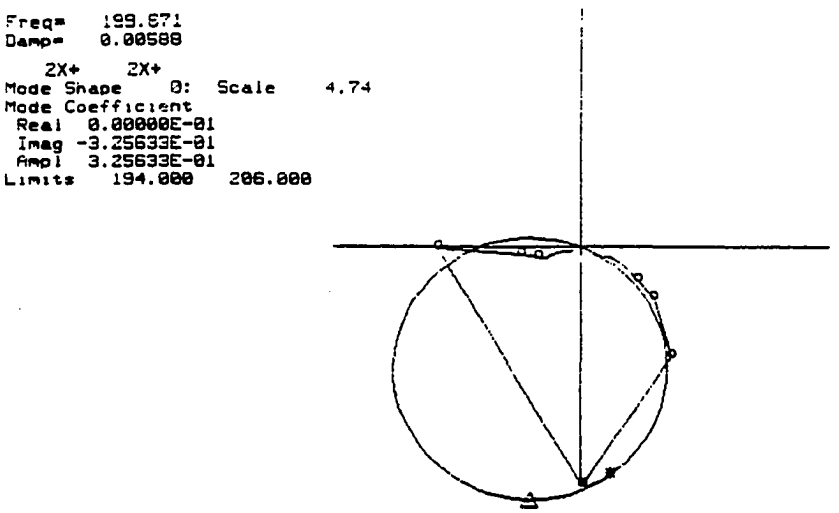

Fig. 6.7 Nyquist Plot for 2X+ 2X+ Coordinates, Frequency 199.67Hz, Damping Coefficient 0.00588, in which a Minimum of Six Points Are Needed to Plot.

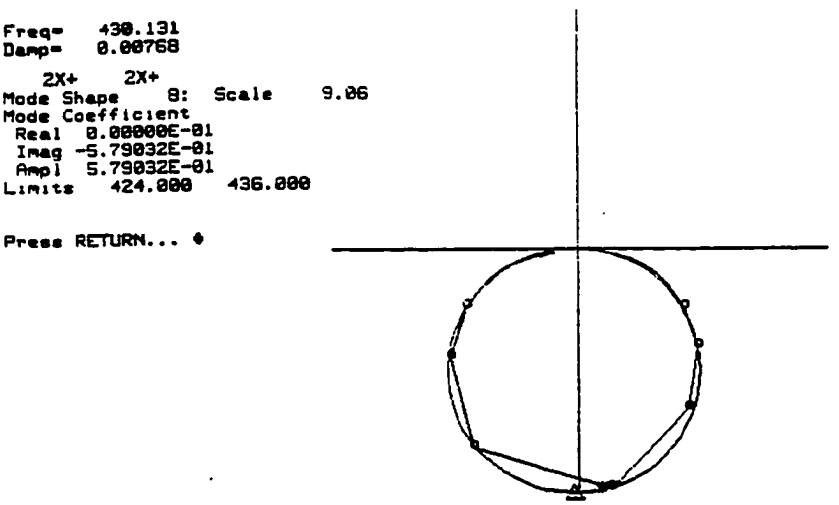

Fig. 6.8 Nyquist Plot for 2X+ 2X+ Coordinates, Natural Frequency 430 Hz, Damping Coefficient 0.00768, Showing the Exact Circle.

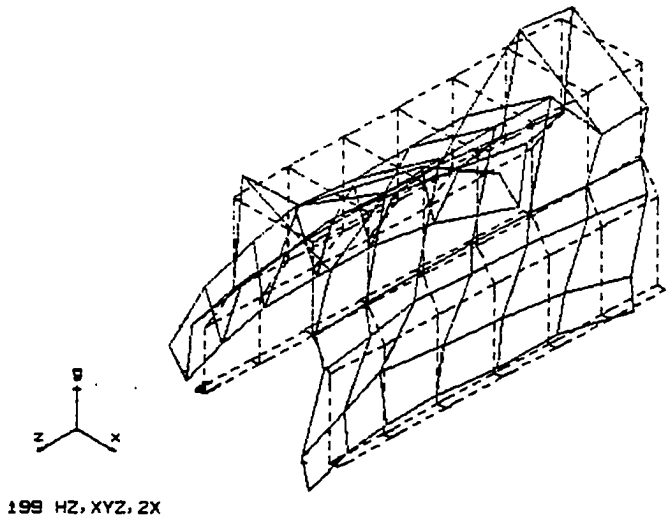

(a) Fundamental Mode Shape at a Frequency of 199.67 Hz

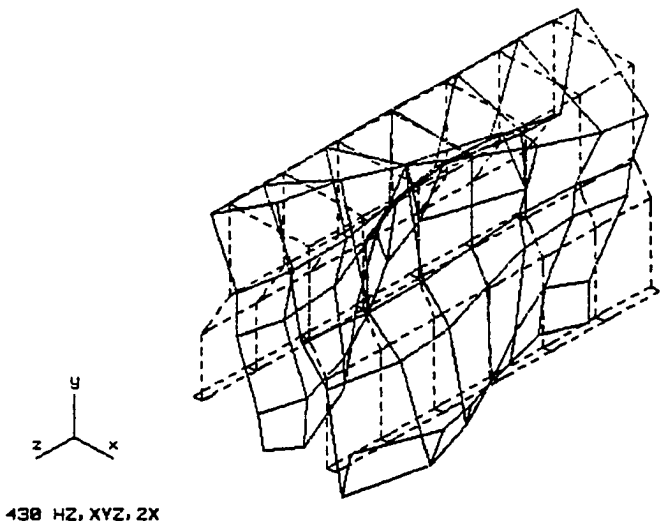

(b) The Second Mode Shape at a Frequency of 430 Hz.

Fig. 6.9 Mode Shapes of Cylinder Block From Modal Testing

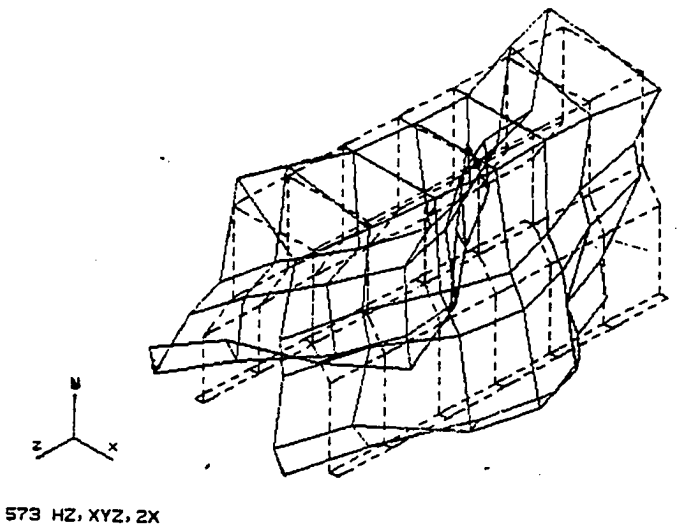

(c) The Third Mode Shape at a Frequency of 573.5 Hz

Fig. 6.9 Mode Shapes of Cylinder Block From Modal Testing(Continued)

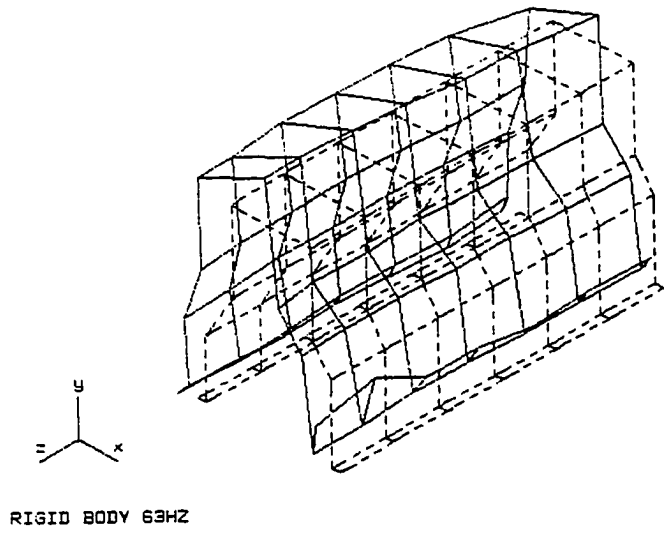

(a) The First Rigid Body Motion , Rotation about z-axis at a Frequency of 63.7 Hz.

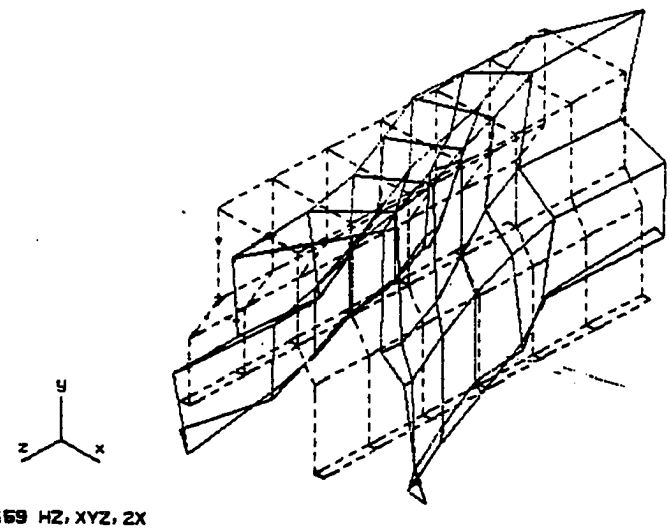

(b) The Second Rigid Body Motion, Rotation about y-axis at a Frequency of 159 Hz.

Fig. 6.10 Rigid Body Motions of Cylinder Block from Modal Testing

CHAPTER VII

CONCLUDING REMARKS

Analytical and experimental investigations of a diesel engine cylinder block have been performed. As market needs change, it is increasingly necessary for the engine industry to reduce analysis costs in the process of designing an engine, and to integrate various analysis procedures. To reduce the time and the cost for analysis and simulation of a particular design, a simpler finite element modeling technique using only 8 node solid elements for both dynamic and static analyses has been developed. Based on this integrated modeling technique of finite elements, eigenvalues are calculated and compared with the experimental data obtained from modal testing of an actual engine cylinder block.

In chapter 2, in order to improve the computational efficiency as well as accuracy for bending dominated problems, the newly developed directional reduced integration (DRI) technique is extended to dynamic problems and applied to formulate element stiffness matrices. For problems in which out-of-plane motion is of prime importance, like cylinder block vibration, 8-node elements have not provided an accurate solution of the eigenvalue problem due to their over-estimation of bending stiffness. Results using this new formulation are compared with results obtained using traditional beam and plate elements.

In chapter 3, results are given for finite element modelling and analysis performed on a diesel engine cylinder block. According to the eigenvalue analysis for the engine block, the

directional reduced integration method with hourglass control provides fairly good agreement with the experimental data obtained from modal testing. Furthermore, dynamic characteristics of the cylinder block are discussed based on the computational results. A significant time saving may be realized by using the simplest element to generate a finite element model. However, in finite element approximation, there is still some unacceptable error. The error may be developed either during the finite element formulation in the space or during the numerical integration process when a direct time integration is used to solve dynamic problems.

In chapter 4, an adaptive finite element method is introduced to reduce finite element approximation error in the space. Since a large structure like engine block was solved, a practical consideration for the adaptive method is employed in order to enhance the capability of the adaptive method in a design analysis process of large structure. An additional investigation was made on the mesh refinement process, especially the h-method, in conjunction with an space index mesh generation.

In chapter 5, to minimize error due to time integration, a variable time stepping algorithm is introduced based on local truncation error control. In order to improve the accuracy and to reduce the possibility of instability that might occur during the time step changing process, the definition of truncation error measure was modified. Also, the current frequency, which is derived from the Rayleigh Quotient, is introduced in evaluating the evolution matrix for computing error for multi-degree-of-freedom systems. Employment of the current frequency provides very accurate measure of the truncation error and saves the computation time required for evaluating error at each time step.

In chapter 6, the experimental modal testing for the correlation study is presented. In the experiment, the lowest five modes have been obtained in the frequency region of 0Hz to 1000Hz. These modes consist of the fundamental three modes and two rigid body modes.

The natural frequencies and modal damping were obtained by means of curve fitting for both the search peak and the complex exponential methods, and the mode shapes were obtained by means of the circle fitting method. It was found that there are two rigid body motions which meet at 63 Hz, rotation about the z-axis and 159Hz, rotation about the y-axis. The observed frequencies of rigid body motion from modal testing might be influenced by Coulomb friction introduced by the support configurations. Since the frequencies of the rigid body motions should be much lower than these frequencies, future experiments on the cylinder block should be designed to eliminate or reduce these rigid body motions.

The current study of engine block structural analysis should be extended to running engine conditions. A future study should include stress analysis. Also, since the engine will be analyzed under an environment of the integrated computer aided engineering techniques which have been described in chapter 4 and 5, the objectives for our study as stated in the introduction may be achieved.

In the adaptive finite element method, which was briefly described in chapter 4, several techniques should be further developed for analyzing very large three dimensional structures. As studied before, especially in the h-adaptive method, there were some difficulties for generating adaptive grids for 3 dimensional general structures. Also, it is recommended that some algorithm such as QUADTREE and OCTREE, which are the hierarchical data structures, can be used for generating meshes more effectively in conjunction with the space index node and element coordinates which were introduced in chapter 4.

A local stability problem arises when the variable time stepping algorithm is used. Such a stability problem should be improved through a stabilization process. There has been no firmly established algorithm available, however further investigation on the stabilization process is desired to minimize the possibilities of instability.

APPENDICES

APPENDIX 1

REMARKS ON NEWMARK-β METHOD

A1.1 Differential Equation Form of Newmark-β Method

The mathematical theory of ordinary differential equation is with the first order system of ordinary differential equations:

$$\dot{\mathbf{y}} = \mathbf{f}(t, \mathbf{y}). \tag{A1.1}$$

The initial-value problem consists of finding a y which satisfies Eq.(A1.1) subject to

$$\mathbf{y}(0)=\mathbf{y}_0, \tag{A1.2}$$

where $\mathbf{y}_0$ is the given initial data.

Eq. (5.1) can be written in first-order form by employing the following definition:

$$\mathbf{y} = \begin{Bmatrix} \mathbf{u} \\ \dot{\mathbf{u}} \end{Bmatrix}, \tag{A1.3}$$

and

$$f(t,y) = \left\{ \begin{array}{c} \dot{u} \\ M^{-1} (F(t) - C \dot{u} - K u) \end{array} \right\}. \qquad \text{(A1.4)}$$

The Newmark-β method can be written in terms of following equations:

$$z^{n+1} = f(t_{n+1}, y_{n+1}), \qquad \text{(A1.5.a)}$$

$$u^{n+1} = u^n + \Delta t\, z^n + \frac{\Delta t^2}{2}[(1 - 2\beta)\dot{z}^n + 2\beta\, \dot{z}^{n+1}], \qquad \text{(A1.5.b)}$$

$$\dot{u}^{n+1} = \dot{u}^n + \Delta t\, [(1 - \gamma)\dot{z}^n + \gamma \dot{z}^{n+1}] . \qquad \text{(A1.5.c)}$$

where $z^{n+1} = \{ z^{n+1},\ \dot{z}^{n+1} \}^T$. Also, we have the complementary relationship about z as following:

$$z^{n+1} = z^n + \Delta t\, [(1 - \gamma)\dot{z}^n + \gamma \dot{z}^{n+1}] . \qquad \text{(A1.5.d)}$$

Here, $\{y^{n+1}\}$ and $\{z^{n+1}\}$ are the approximation of $\{y(t_{n+1})\}$ and $\{\dot{y}(t_{n+1})\}$. Thus, from Eq.(A1.5.a) to Eq.(A1.5.d), we obtain following equation:

$$\left\{ \begin{array}{c} u^{n+1} \\ \dot{u}^{n+1} \end{array} \right\} = \left\{ \begin{array}{c} u^n \\ \dot{u}^n \end{array} \right\} + \left[\begin{array}{cc} \frac{\Delta t}{2} & \frac{\Delta t^2}{2}(\gamma - 2\beta) \\ 0 & \Delta t\,(1-\gamma) \end{array} \right] \left\{ \begin{array}{c} z^n \\ \dot{z}^n \end{array} \right\} + \left[\begin{array}{cc} \frac{\Delta t}{2} & \frac{\Delta t^2}{2}(2\beta - \gamma) \\ 0 & \Delta t\, \gamma \end{array} \right] \left\{ \begin{array}{c} z^{n+1} \\ \dot{z}^{n+1} \end{array} \right\}, \qquad \text{(A1.6.a)}$$

or

$$y^{n+1} = y^n + \Delta t\ (C_a z^n + C_b z^{n+1}) \qquad \text{(A1.6.b)}$$

$$= y^n + \Delta t\ \Phi^n ,$$

where

$$\Phi^n = (C_a z^n + C_b z^{n+1}) ,$$

$$C_a=\begin{bmatrix} \frac{1}{2} & \frac{\Delta t}{2}(\gamma-2\beta) \\ 0 & (1-\gamma) \end{bmatrix},$$

and

$$C_b=\begin{bmatrix} \frac{1}{2} & \frac{\Delta t}{2}(2\beta-\gamma) \\ 0 & \gamma \end{bmatrix}.$$

Assume f(t,y) is a continuous function of t on the interval $[0,\alpha]$, $\alpha > 0$, and that there exists a constant L such that

$$\| f(t,y_1)-f(t,y_2) \| \le L \| y_1 - y_2 \|,$$

for all $t \in [\,0, \alpha\,]$ and all y_1 and y_2. Under these hypothesis, a unique solution of the initial-value problem is known to exist for all $0 < t < \alpha$, and the mapping of y_0 to y(t) is continuous. Furthermore, if f is a k - times differentiable function of its arguments, then y(t) will be $(k+1)$ - times continuous differentiable.

Let us now consider general one-step methods of form :

$$y_0 = y(0),$$

$$y^{n+1} = y^n + \Delta t \ \Phi\,(t^n, y^n, f, \Delta t\,), \ n=1,2...N\,. \qquad \text{(A1.7)}$$

Suppose that Φ to be continuous in t and y, and it is not mentioned about f(t,y) and Δt in Φ, explicitly. For the general procedure we assume that

$$| \Phi(t,u)-\Phi(t,v) | \le L\, | u - v |, \qquad \text{(A1.8)}$$

for all $a \le x \le b$, all $0 \le \Delta t \le h_0$, any continuous function satisfying a Lipschitz condition and, for all u, and v.

Here, we suppose that

$$y^{n+1} = y^n + \Delta t\ \Phi\ (t_n, y^n) + \Delta t\ \tau_n \tag{A1.9}$$

with τ_n "small".

With $u_1=u$ and $u_2=\dot{u}$, Eq. (A1.4) is transformed into the system

$$\begin{Bmatrix} \dot{u}_1 \\ \dot{u}_2 \end{Bmatrix} = \begin{Bmatrix} u_2 \\ (F(t) - 2\xi\omega\ u_2\ - \omega^2 u_1) \end{Bmatrix} \tag{A1.10}$$

with initial conditions.

Clearly, $f_1(t,u_1,u_2) = u_2$ satisfies the Lipschitz condition with $L_1=1$. With $f_2(t,u_1,u_2) = M^{-1}(F(t) - Cu_2 - Ku_1)$, we have

$$\begin{aligned} |\, f_2(t,\underline{u}_1,\underline{u}_2) - f_2(t,u_1,u_2)\,| &\le |M^{-1}(F(t) - C\underline{u}_2 - K\underline{u}_1) - M^{-1}(F(t) - Cu_2 - Ku_1)| \\ &\le L_2|\underline{u}_2 - u_2| + L_2\,|\underline{u}_1 - u_1|, \end{aligned} \tag{A1.11}$$

where $L_2 = \max(\,|\,2\xi\omega\,|\,,\,|\,\omega^2\,|\,)$, and $\underline{u}_i = u_i(t^n)$. Meanwhile, we can define as:

$$f_1^{n+1} = f_1(t_n+h,\ u_1^n + \Delta t\, f_1^n,\ u_2^n + \Delta t\, f_2^n),$$

$$f_2^{n+1} = f_2(t_n+h,\ u_1^n + \Delta t\, f_1^n,\ u_2^n + \Delta t\, f_2^n).$$

Now, we can write

$$\begin{aligned} |\, f_1^{n+1} - \underline{f}_1^{n+1}\,| &= |\, u_2^{n+1} - \underline{u}_2^{n+1}\,| \\ &\le L_1\,|u_2 - \underline{u}_2| + L_1\Delta t\ |\, f_2 - \underline{f}_2| \\ &\le L_1\,|u_2 - \underline{u}_2| + L_1\Delta t\ (\,L_2|u_2 - \underline{u}_2| + L_2\,|u_1 - \underline{u}_1|\,) \\ &\le L_1 L_2 h\,|u_1 - \underline{u}_1| + L_1(1 + L_2\Delta t)\,|u_2 - \underline{u}_2|\,, \end{aligned}$$

$$| f_2^{n+1} - \underline{f}_2^{n+1}| = |(F(t_{n+1}) - 2\xi\omega u_2^{n+1} - \omega^2 u_1^{n+1}) - (\underline{F}(t_{n+1}) - 2\xi\omega \underline{u}_2 - \omega^2 \underline{u}_1^{n+1})|$$

$$\leq L_2 (|u_2 - \underline{u}_2| + \Delta t \; | f_2 - \underline{f}_2 | + |u_1 - \underline{u}_1| + \Delta t \; | f_1 - \underline{f}_1 |)$$

$$\leq L_2 (|u_2 - \underline{u}_2| + \Delta t \; (L_2 |u_2 - \underline{u}_2| + L_2 |u_1 - \underline{u}_1|))$$
$$+ L_2 \; (|u_1 - \underline{u}_1| + \Delta t \; L_1 |u_2 - \underline{u}_2|)$$

$$\leq L_2 (1 + L_2 \Delta t \;) |u_1 - \underline{u}_1| + L_2 (1 + L_1 \Delta t + L_2 \Delta t) |u_2 - \underline{u}_2| \; .$$

Φ^n can be rewritten in following form:

$$\Phi^n = C_a z^n + C_b z^{n+1}$$

$$= C_a z^n + C_b z(t_n + \Delta t \, , \, y_n + \Delta t \; z^n) \; . \qquad \text{(A1.12)}$$

Let $\underline{y}^n = y(t_n)$, $\underline{z}^n = z(t_n)$, and $\underline{\Phi}^n = \Phi(t_n)$, then we can write

$$\Phi^n - \underline{\Phi}^n = C_a (z^n - \underline{z}^n)$$
$$+ \; C_b \{ z(t_n + \Delta t \, , \, y_n + \Delta t \; z^n)) - z(t_n + \Delta t \, , \, \underline{y}_n + \Delta t \; \underline{z}^n) \} \; . \qquad \text{(A1.13)}$$

The continuity of Φ obviously follows from the continuity of f. Since

$$(\Phi - \underline{\Phi})_1 = C_{a11} (f_1^n - \underline{f}_1^n) + C_{a12} (f_2^n - \underline{f}_2^n)$$
$$+ \; C_{b11} (f_1^{n+1} - \underline{f}_1^{n+1}) + C_{b12} \; (f_2^{n+1} - \underline{f}_2^{n+1}) \, , \qquad \text{(A1.14.a)}$$

$$(\Phi - \underline{\Phi})_2 = C_{a21} (f_1^n - \underline{f}_1^n) + C_{a22} (f_2^n - \underline{f}_2^n)$$
$$+ \; C_{b21} (f_1^{n+1} - \underline{f}_1^{n+1}) + C_{b22} (f_2^{n+1} - \underline{f}_2^{n+1}) \, . \qquad \text{(A1.14.b)}$$

Thus, we have

$$|\Phi - \underline{\Phi}|_1 \le \{ |C_{a11}| L_1 + |C_{a12}| L_2 + |C_{b11}| L_1 L_2 h + |C_{b12}| L_2(1 + L_2 h) \} |u_1 - \underline{u}_1| + \{ |C_{a12}| L_2 + |C_{b11}| L_1(1 + L_2 h) + |C_{b12}| L_2(1 + L_1 h + L_2 h) \} |u_2 - \underline{u}_2| ,$$

and

$$|\Phi - \underline{\Phi}|_2 \le \{ |C_{a21}| L_1 + |C_{a22}| L_2 + |C_{b21}| L_2 L_1 h + |C_{b22}| L_2(1 + L_2 h) \} |u_1 - \underline{u}_1| + \{ |C_{a22}| L_2 + |C_{b21}| L_1(1 + L_2 h) + |C_{b22}| L_2(1 + L_1 h + L_2 h) \} |u_2 - \underline{u}_2| .$$

If there is no damping, Eq.(A1.14) become

$$|\Phi - \underline{\Phi}|_1 \le |C_{a11}| L_1 |u_2 - \underline{u}_2| + |C_{b11}| (L_1 |u_2 - \underline{u}_2| + L_1 L_2 h |u_1 - \underline{u}_1|), \quad \text{(A1.15.a)}$$

$$|\Phi - \underline{\Phi}|_2 \le |C_{a22}| L_2 |u_1 - \underline{u}_1| + |C_{b22}| (L_2 |u_1 - \underline{u}_1| + L_1 L_2 h |u_2 - \underline{u}_2|). \quad \text{(A1.15.b)}$$

From the Eq.(A1.15), we can define Lipschitz constant **L** for the error equation of Newmark-β method described in Eq.(A1.5) as follows:

$$\mathbf{L} = \begin{bmatrix} L_{11} & L_{12} \\ L_{21} & L_{22} \end{bmatrix}, \quad \text{(A1.16)}$$

where

$$L_{11} = |C_{a11}| L_1 + |C_{a12}| L_2 + |C_{b11}| L_1 L_2 \Delta t + |C_{b12}| L_2(1 + L_2 \Delta t) ,$$

$$L_{12} = |C_{a12}| L_2 + |C_{b11}| L_1(1 + L_2 \Delta t) + |C_{b12}| L_2(1 + L_1 \Delta t + L_2 \Delta t) ,$$

$$L_{21} = |C_{a21}| L_1 + |C_{a22}| L_2 + |C_{b21}| L_2 L_1 \Delta t + |C_{b22}| L_2(1 + L_2 \Delta t) ,$$

$$L_{22} = |C_{a22}| L_2 + |C_{b21}| L_1(1 + L_2 \Delta t) + |C_{b22}| L_2(1 + L_1 + L_2 \Delta t) .$$

while , for the undamped case, **L** is expressed as follows:

$$L_{11} = |C_{b11}| L_1 L_2 \Delta t$$

$$L_{12} = |C_{a11}| L_1 + |C_{b11}| L_1$$

$$L_{21} = |C_{a22}| L_2 + |C_{b22}| L_2$$

$$L_{22} = |C_{b22}| L_1 L_2 \Delta t \ .$$

For the undamped linear case, the matrix **L** is expressed as following form:

$$\mathbf{L} = \begin{bmatrix} \frac{1}{2}\omega^2 \Delta t & 1 \\ \omega^2 & \frac{1}{2}\omega^2 \Delta t \end{bmatrix}. \qquad \text{(A1.17)}$$

A1.2 Evaluation of Truncation Error using Taylor's Series

The truncation error can be expressed using Taylor's series. It was first shown in Hilber[57]. Even though the truncation error expression for the direct time integration for Newmark family was derived only for the homogeneous case, it is extended to the forced response case in present expression.

Assuming u(t) to be continuously differentiable up to any required order, all terms in Eq.(5.28) can be expanded into finite Taylor series at t. Also, in Eq.(5.28), it is assumed that time step size is not changed from (n)th step to (n+1)th step so that $[A^n] = [A^{n-1}]$. Then, $A_1 = A_1^d = A_1^v$, $A_2 = A_2^d = A_2^v$. Using the differential equation of motion, the first three terms can be expressed:

$$u^{n+1} - A_1u^n + A_2u^{n-1} = \sum_{i=0}^{m} T_i(\Delta t)^{i-2}u^{(i)}(t)$$

$$= T_0(\Delta t)^{-2}u + T_1(\Delta t)^{-1}\dot{u} + T_2\ddot{u} + T_3(\Delta t)u^{(3)} + T_4(\Delta t)^2u^{(4)}$$

$$+ O(\Delta t^3)$$

$$= [\Omega^{-2}T_0 - T_2 + \Omega^2T_4]\omega^2u + [\Omega^{-1}T_1 - \Omega T_3]\omega\dot{u}$$

$$+ [\, T_2F + T_3(\frac{\Omega}{\omega})F + T_4(\frac{\Omega}{\omega})^2(F - \omega^2F)$$

$$+ O(\Delta t^3) \qquad \text{(A1.18)}$$

where $T_0 = 1 - A_1 + A_2$, $T_i = (1 + (-1)^iA_2) / i !$, and the circular sampling frequency $\Omega = \omega \Delta t$. Also, u and F denote u^n and F^n, respectively.

Using derivatives of force terms with respect to time:

$$\dot{F}_n = \frac{F^{n+1} - F^{n-1}}{2\Delta t},$$

$$\ddot{F}_n = \frac{F^{n+1} - 2F^n + F^{n-1}}{\Delta t^2},$$

we will get following expression.

$$u^{n+1} - A_1u^n + A_2u^{n-1} = [\Omega^{-2}T_0 - T_2 + \Omega^2T_4]\omega^2u + [\Omega^{-1}T_1 - \Omega T_3]\omega\dot{u}$$

$$+ [\, T_2 - T_4\Omega^2 - 2T_4]F^n + [\, T_3 - 0.5T_4]F^{n+1}$$

$$+ [\, T_4 - 0.5T_3]F^{n-1} + O(\Delta t^3). \qquad \text{(A1.19)}$$

Similarly, the last three terms of Eq.(5.42) can be expanded using Taylor's series

$$E_1F^{n+1} + E_2F^n + E_3F^{n-1} = \sum_{i=0}^{m} Q_i(\Delta t)^{i-2}F^{(i)}(t), \qquad \text{(A1.20)}$$

where $Q_0 = E_1 + E_2 + E_3$ and $Q_i = (B_1 + (-1)^i B_3) / i !$.

Combining Eq. (A1.19) and (A1.20), we have a truncation error equation for the displacement as follow:

$$\begin{aligned}\tau_d &= [\Omega^{-2}T_0 - T_2 + \Omega^2 T_4]\omega^2 u + [\Omega^{-1}T_1 - \Omega T_3]\omega\dot{u} \\ &+ [(T_2 - \Omega^2 T_4)F + T_3(\frac{\Omega}{\omega})\dot{F} + T_4 (\frac{\Omega}{\omega})^2\ddot{F}] \\ &+ [Q_0(\frac{\Omega}{\omega})^{-1}F + Q_1(\frac{\Omega}{\omega})\dot{F} + Q_2 (\frac{\Omega}{\omega})^2\ddot{F}] + O(\Delta t^3). \qquad \text{(A1.21)}\end{aligned}$$

Also, we can have a truncation error equation for the velocity in similar way as follows:

$$\begin{aligned}\tau_v &= [-T_1 + \Omega^2 T_3]\omega^2 u + [\Omega^{-1}T_0 - \Omega T_2]\omega\dot{u} \\ &+ [T_1F + T_2(\frac{\Omega}{\omega})\dot{F} + T_3 (\frac{\Omega}{\omega})^2\ddot{F}] \\ &+ [R_0(\frac{\Omega}{\omega})^{-1}F + R_1(\frac{\Omega}{\omega})\dot{F} + R_2 (\frac{\Omega}{\omega})^2\ddot{F}] + O(\Delta t^3) , \qquad \text{(A1.22)}\end{aligned}$$

where $R_0 = B_4 + B_5 + B_6$ and $R_i = (B_4 + (-1)^i B_6)$.

APPENDIX 2

GLOSSARY OF MODAL TESTING

A2.1 Basic Properties for Modal Testing

A2.2.1 Auto-Correlation

The term auto-correlation is often defined as follow:

$$R_{xx}(\tau) = E\{x(t)x(t+\tau)\} = \lim \frac{1}{T} \int_0^T x(t)x(t+t)dt \,. \qquad \text{(A2.1)}$$

A cross-correlation function, describing joint properties between two signals x(t) and y(t) is given by

$$R_{xy}(\tau) = E\{x(t)y(t+\tau)\} = \lim \frac{1}{T} \int_0^T x(t)y(t+t)dt \,. \qquad \text{(A2.2)}$$

A2.1.2 Power Spectral Density Function

For continuous signals it is possible to use the power spectral function. For the case of random signal this is the established technique, as the existence of Fourier transform for these is problematical. The function of frequency gives the distribution of the

power of the signal with frequency. Denoting it by $S_{xx}(f)$, we have

$$x^2(t) = \int_{-\infty}^{\infty} S_{xx}(f)\, df \quad . \tag{A2.3}$$

The power spectral density and auto correlation function are related for stationary signals as following:

$$S_{xx}(f) = \int_{-\infty}^{\infty} R_{xx}(\tau)\, \exp(-j\, 2\pi f\tau) d\tau \quad , \tag{A2.4}$$

and

$$S_{xy}(f) = \int_{-\infty}^{\infty} R_{xy}(\tau)\, \exp(-j\, 2\pi f\tau) d\tau \quad . \tag{A2.5}$$

A2.1.3 Transfer Function

In the case of two associated time histories x(t) and y(t), following relationship can be generalized in linear system:

$$y(t) = \int_{-\infty}^{\infty} h(t - t')\, x(t')\, dt' + n(t) \quad , \tag{A2.6}$$

where h(t) is the impulse response function and n(t) is the residuals to compensate some error, introduced during the measuring process.

From Eq. (A2.6), if zero residual is assumed, the transfer function may be written using the power spectral density function as follow:

$$H(f) = S_{xy} \,/\, S_{yy} \quad . \tag{A2.7}$$

A2.1.4 Coherence

Coherence is an indicator of measurement quality. To quantify that part of y designated as residual, we define the coherence function $\gamma^2(f)$. This function can be defined as the ratio as following:

$$\gamma^2(f) = \frac{\text{coherent output power}}{\text{total output power}} = \frac{S_{yy} - S_{nn}}{S_{xy}}$$

$$= \frac{|H|^2 S_{xx}}{S_{yy}}, \qquad \text{(A2.8)}$$

where the coherent power is the one due to the part of y that is linearly related to x. Also, we have the triangular inequality

$$0 \leq \gamma^2(f) \leq 1. \qquad \text{(A2.9)}$$

Therefore, if all measured data are of good quality, the coherence should be unity. This is the condition used in our analysis to confirm that the measurements have been made well. As shown by Fig. A2.4b which corresponds to Fig A2.4a, the coherence plot shows nearly unity except in the the vicinity of the resonances. Theoretically it is expected that a rapid decrease takes place at resonance. The low coherence sometimes comes from noise. Measurements with low coherence should not be accepted in any case. Fig. A2.4b is an example of an acceptable measurement.

A2.2 Measurement

A2.2.1 Excitation

Excitation of the structure provides a measurable input of mechanical force energy, in which excitation sets the structure into vibratory motion. Excitation may be provided by an electric dynamic vibration exacter or an input hammer. These tests were performed

using an impact hammer.

There are two primary impact tips which can be mounted in the end of the hammer head, such as soft tip(rubber or plastic) and hard tip(steel). By performing various calibration tests, it was found that the plastic tip gave a best frequency response function in the frequency interval of interests (e.g., frequency ranges 0-1000 Hz). The force transducer is mounted between the impact tip and the hammer head to register the impact force historically. Fig.A2.1 shows the time domain response of the excitation force on channel 2, and the acceleration on channel 3.

The response of the testpiece can be measured by either a strain gage or piezoelectric accelerometer. The accelerometer has been used throughout the experiment. It turned out that an intensive impact does not produce a better response measure, in fact the opposite is the case. Caution should be paid not to have a bounce when using the impact hammer. Usually, any bounce can be detected by observing the time domain of the excitation as shown in Fig. A2.1.

The computer aided test system, GR2515, is programmed to store the exciter and the response signals and to produce the frequency response function, or transfer function, which contains the real, imaginary, amplitude, and phase information in each increment of frequency. This system yields the Bode diagram both in real-frequency domain, and in imaginary-frequency domain, and the Nyquist plot on real and imaginary coordinates(See Fig. A2.2, A2.3 and A2.4). As is well known, a phase change of 180^{o} occurs at resonance.

A2.2.2 Averaging of Measurement

Practically, it is essential to perform averaging of measurements in the testing. The

idea behind this is that any one measurement is likely to be contaminated by noise, especially in the frequency regions away from resonance where the response levels are likely to be quite low. In this experiment, a 10 times average was carried out. This produced relatively smooth frequency response functions than the ones obtained through one-time measurement as shown in Fig. 6.1b.

A2.3 Transfer Function

A2.3.1 Curve Fitting

As shown in Fig. A2.5, the solid line shows the actual measured curve and the plus sign '++' shows the analytical curve which was derived from the extracted parameters by using the search peak or the complex exponential method. Using the curve fitting method, it is determined that the extracted parameters are well-fitted to the actual measured curve obtained from testing. If the analytical curve is not fitted well, the process should be repeated until the sufficient well-fitted curve is obtained by trial and error. If the analytical curve is well fitted, then modal parameters for the analytical curve may be considered to be acceptable as shown in Fig. A2.5. The result is quite dependent upon the user's ability and experience.

A2.3.2 Consideration of Residuals

The residuals also play important role in the curve fitting. Since the analytical curve basically does not include effects outside frequency region of interests, one might obtain an incorrect result when curve fitting. Therefore, it is necessary to compensate the analytical curve by predicting and including outside effects in the low frequencies region and at higher frequencies using some appropriate methods. In this experiment, the residuals were added to obtain sufficiently correct curve in the curve fitting process. Then, well fitted

curve could be obtained as shown in Fig. A2.6a and Fig. A2.6b.

Finally, the generated analytical curve must be well-fitted with the actual measured curve (FRF), otherwise the process should be repeated with a different set of parameters. Through these process, the resonance frequencies and the modal dampings were obtained.

A2.3.3 Alternative Forms of Frequency Response Function

There are many different forms of the basic FRF concepts, depending on the actual parameters chosen for the input and the output. In addition to the receptance form, which relates displacement response to force excitation, following two alternatives are widely used:

mobility, $Y(\omega)$, which is velocity and

acceleration(or inertance), $In(\omega)$, which is acceleration/force.

Because of the sinusoidal nature of all of the parameters are used, there is a simple relationship between these three different quantities, and the advantage of using one rather than the others are generally based on convenience or availability. These relationships are:

$$Y(\omega) = i\omega\alpha(\omega)$$

and

$$In(\omega) = i\omega Y(\omega) = -\omega^2\alpha(\omega) \qquad \text{(A2.9)}$$

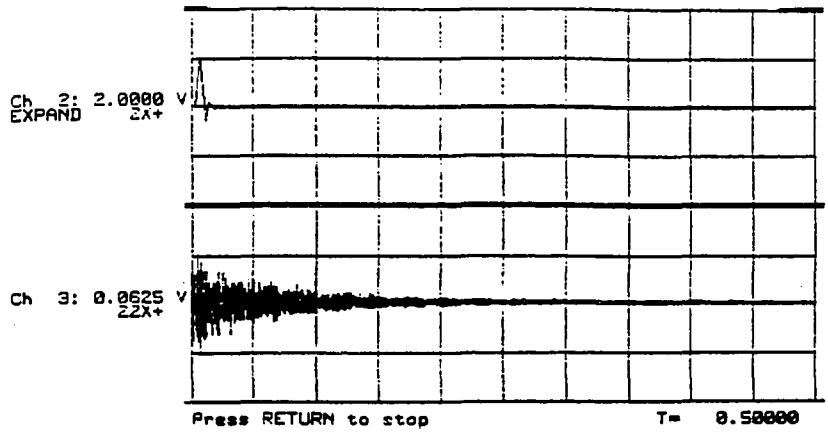

Fig. A2.1 Time Domain for Excitation on Channel 2 and Acceleration on Channel 3

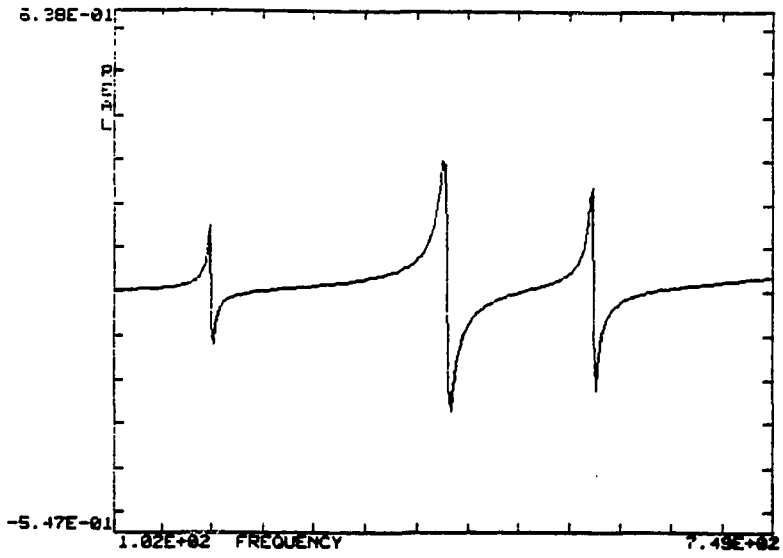

Fig. A2.2 Real vs Frquency Plot for the Point Inertance (2X+ 2X+)

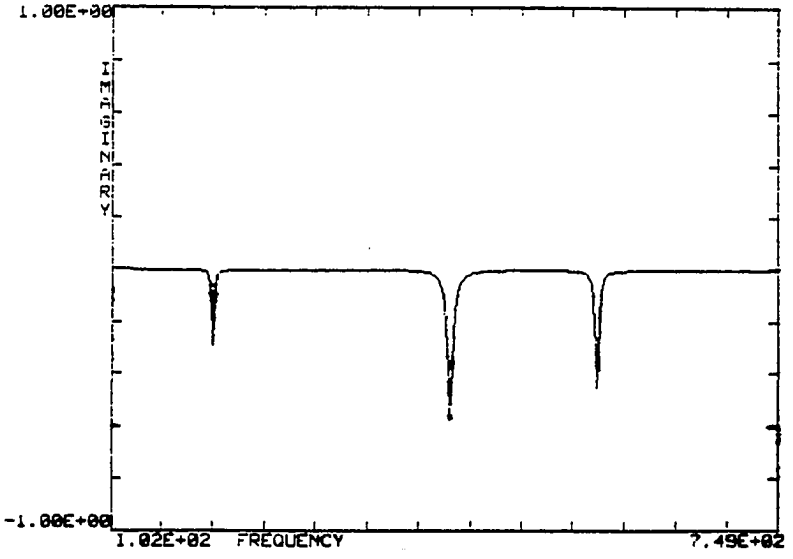

Fig. A2.3 Imaginary vs Frequency Plot

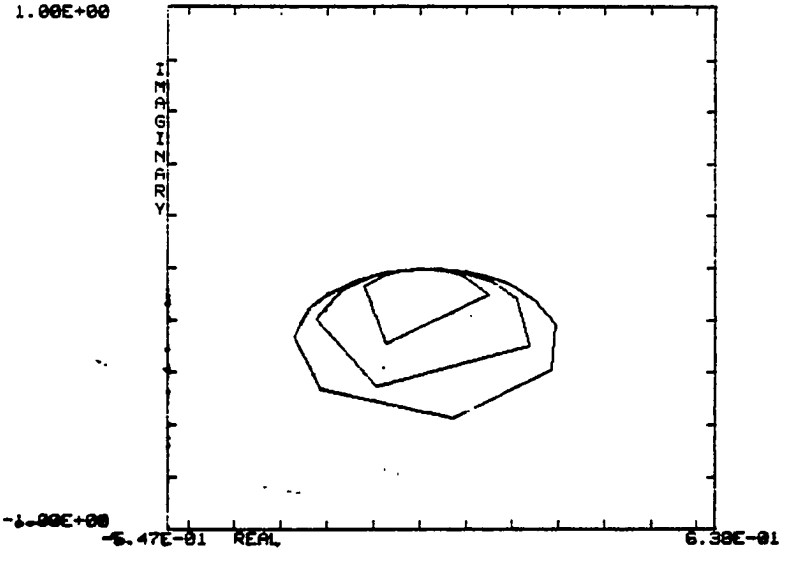

Fig. A2.4 Imaginary vs Real Plot(Nyquist Plot) with Circle Representing Resonances

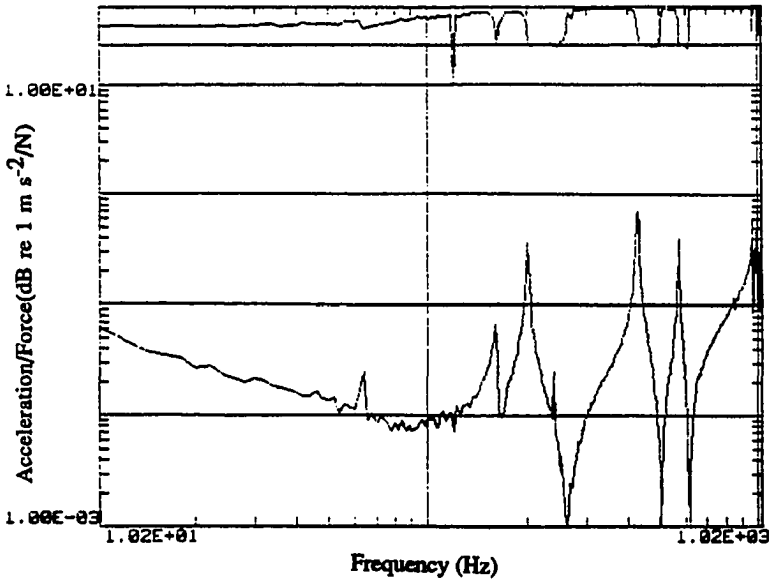

Fig. A2.5 FRF Plot (Bode plot) Measured at the Point Inertance (2X+ 2X+)

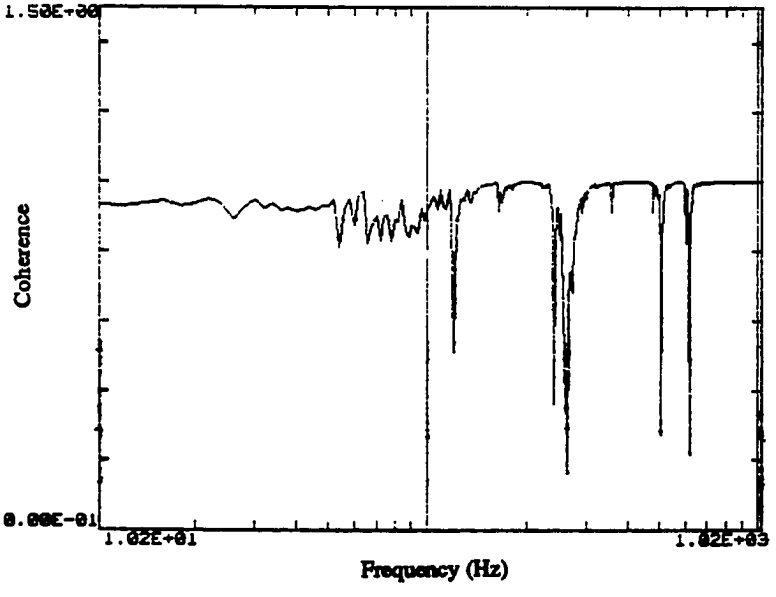

Fig. A2.6 Coherence Spectrum for the FRF Shown in Fig. A2.5, Showing Almost Unity Except in the Vicinity of Each Resonance

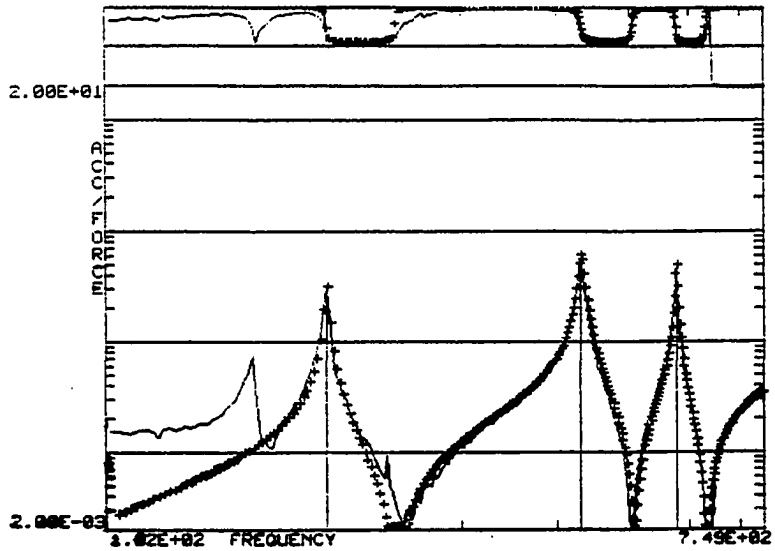

solid line : measured curve
dotted curve : analytic curve with residuals

Fig. A2.7 Curve Fitting Using the Search Peak Method

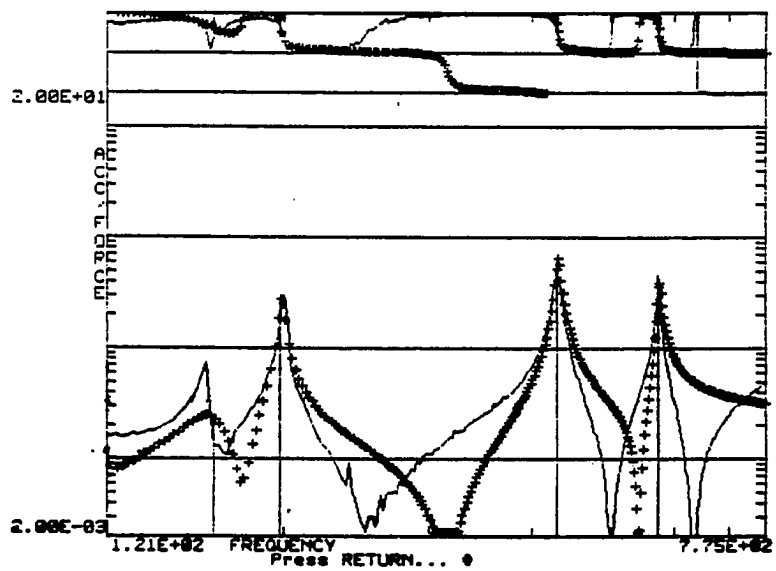

Fig. A2.8 Curve Fitting Using Complex Exponential Method Before Adding the Residuals

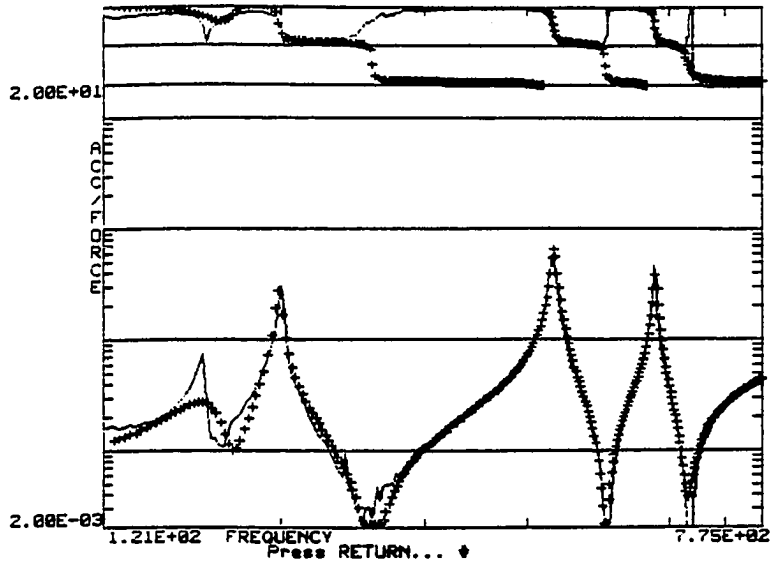

Fig. A2.9 Curve Fitting using Complex Exponential Method with Residuals.

BIBLIOGRAPHY

BIBLIOGRAGHY

1. M. J. Percy, "Vibration Analysis of the NH-250 Valve Cover and Comparison with Its Noise Spectrum", Columbus, Indiana, Cumins Engine Company Inc., 1972.

2. R.S. Lane, S. E. Timour, and G. W. Hawkins, "Analysis Applied to Diesel Engine Noise Reduction", Paper No. 750835 Presented at SAE Conference, Milwaukee, Wisconsin, Sept., 1975.

3. Dean M. Ford, Paul A. Hayes, and Stephen K. Smith, "Engine Noise Reduction by Structural Design Using Advanced Experimental and Finite Element Methods', Paper No. 790366 Presented at SAE Conference, Detroit, Michigan, Feb. 1979.

4. M. E. Moncelle, "Diesel Engine Sound Reduction by Dynamic Modelling", SAE Paper No. 800409 Presented at SAE Conference, Detroit, Michigan, Feb. 1980.

5. I. Nagamaya, Y. Araki, K. Kakuta and Y. Usuba, "Engine Noise Reduction by Structural Study of Cylinder Block", Paper 800441 Presented at SAE Conference, Detroit, Michigan, Feb. 1980.

6. D. M. Croker, N. Lalor and M. Petyt, "The Use of Finite Element Techniques for the Prediction of Engine Noise", Paper C146/79 Presented at the Institute of Mechanical Engineers Conference, London, England, July 1979.

7. R. J. Dejong and N. E. Parsons, "High Frequency Vibration Transmission through the Moving Parts of an Engine", Paper No. 800405 Presented at SAE Conference, Detroit, Michigan, Feb. 1980.

8. P. A. Hayes, "Experimental and Analytical Investigation of Diesel Engine Piston Impact Noise", Master's Thesis, Purdue University, West Lafayette, Indiana, Dec. 1977.

9. N. Lalor, "Computer Optimized Design of Engine Structures for Low Noise Engine", SAE Paper 790364, SAE Congress, Detroit, Jan. 1979.

10. R. J. Tyrrell and D. M. Croker, "Engine Noise: Practicalities and Prediction, Part 2 - Finite Element Analysis", SAE Paper 870978, Noise and Vibration Conference, Traverse City, Michigan, 1987.

11. T. Priede, "Some Studies into Origins of Automotive Diesel Engine Noise and Its Control", FISITA Paper C12, Munchen, 1966.

12. T. Priede, E. C. Grover, and N. Laylor, "Relation between Noise and Basic Structural Vibration between Noise and Vibration of Diesel Engines", SAE Paper 690450, University of Southhampton, England, SAE Conference, Chicago, May 1969.

13. M. F. Russell, "Automotive Diesel Engine Noise and Its Control", SAE Paper 730243 at SAE Congress, Detroit, Jan. 1973.

14. M. F. Russell, "Reduction of Noise from Diesel Engine Surfaces", SAE Paper 720135, Detroit, Michigan, 1972.

15. M. F. Russell, "Diesel Engine Noise: Control at Source", SAE Paper 820238, SAE Conference, Detroit, March 1982.

16. Haddad, S.D., "Mechanical Induced Noise and Vibration in the Automotive Diesel Engine", ASME Paper 77-DET-37, Chicago, 26-30, Sept. 1977.

17. Haddad, S. D., "A Diesel Engine with Lower Mechanical Noise", Inst. of Acoustic Meeting, Cambridge University, 5-7 Apr. 1978.

18. Haddad, S. D., "Analysis of Piston Slap-Induced Noise and Assessment of some methods of Control in Diesel Engines", SAE Presentation 790275, Detroit, Feb. 1979.

19. Haddad, S. D. and Fortescue, P., "Simulating Piston Slap by an Analogue Computer", J. of Sound and Vibration, Vol 52, 791-793, 1977.

20. Koh, B. C. and Kikuchi, N., "New Improved Hourglass Control for Bilinear and Trilinear Elements in Anisotropic Linearly Elasticity", Computer Methods in Applied Mechanics and Engineering,1988.

21. Maenchen, G. and Sack, S., "The Tensor Code", Methods in Computational Physics, Vol.13, Ed. Alder, B., Fernbach, S. and Rotenberg, M., Academic Press, 1964.

22. Belytschko, T., Ong, J. S., Liu, W. K. and Kennedy, J. M., ' Hourglass Control in Linear and Nonlinear Problems," Comp. Meth. Appl. Mech. Engin.,Vol. 43, pp. 251-276, North Holland, 1984.

23. Hallquist, J. O., "DYNA3D," Lawrence Livermore National Laboratories, Livermore, Ca, 1979.

24. Hallquist, J. O., "NIKE3D," Lawrence Livermore National Laboratories, Livermore, Ca.,1981.

25. Hallquist, J. O., "INGRID User's Manual," Lawrence Livermore National Laboratories, Livermore, Ca., 1983.

26. Hallquist, J. O., "TAURUS User's Manual," Lawrence Livermore National Laboratories, Livermore, Ca., 1983.

27. Hughes, T.J.R., and Liu, W.K., "Nonlinear Finite Element Analysis of Shells: Part I, Three-Dimensional Shells", Computer Methods in Applied Mechanics and Engineering", vol. 26(1981), pp331-362.

28. Belytschko, T., and Lin, J.I., "Explicit Algorithm for the Nonlinear Dynamics of Shells", Compter Methods In Applied Mechanics and Engineering", vol.42(1984), pp225-251.

29. E. R. A. Oliveira, " Optimization of Finite Element Solution,' in Precedings Third Conference of Matrix Methods in Structural Mechanics, Wright-Patterson Airforce Base, Dayton, OH, 1971.

30. Caroll, W.E. and Barker, R.M., "A Theorem For Finite Element Idealization", International Journal of Solid and Structures, 9, 1973.

31. Turcke, D.J. and McNeice, G.M., "Guide for Selecting Finite Elements Grid Based on Optimization Study", Computer and Structures, 4, 499-519, 1974.

32. Swell, G., "An Adaptive Computer Program for the Solution Div(P(x,y)Grad U)=F(x,y,U) on a Polygonal Region", in the Mathematics of Finite Elements and Applications, II, MAFELAB, Academic Press, New York, 1975.

33. Prager, W., "A Note on the Optimal Choice of Finite Element Grids, Computer Methods in Applied Mechanics and Engineering, 6, 363-366, 1975.

34. Melosh, R.J. and Marcal, P.V., "An Energy Basis for Mesh Refinements of Structural Continua", International J. for Numerical Methods in Engineering, 11, 1083-1091, 1977.

35. Babuska, I, and Rheinbolt, W. C., "Error Estimates for Adaptive Finite Element Computations, SIAM J. Numer. Anal. 15 (1978) 1736-754.

36. Winslow, A. M. Adaptive Mesh Rezonning by the Equipotential Method, UCID-19062, Lawrence Livermore Laboratory, 1981

37. Arney, David C. and Flaherty, Joseph E., "A Two Dimensional Mesh Moving Technique for Time-Dependent Partial Differential Equations", J. of Comp. Physics 67,124-144(1986).

38. Diaz, A.R., Kikuchi, N. and Taylor, J.E., "A Method of Grid Optimization for Finite Element Methods", Computer Methods in Applied Mechanics and Engineering, 37, 29-46, 1983.

39. Kikuchi, N. "Finite Element Methods in Mechanics," Cambridge Press, 1985.

40. N. Kikuchi, "Adaptive Grid Design Methods for Finite Element Analysis", Computational Methods in Applied Mechanics and Engineering, Vol 55, pp 129-160, 1986

41. N. Kikuchi, K. Y. Chung, T. Torigaki, and J. E. Taylor,"Adaptive Finite Element Methods for Shape Optimization of Linearly Elastic Structures", Computer Methods in Applied Mechanics and Engineering,Vol. 57,pp 67-89,North-Holland, 1986.

42. Kikuchi, N. and Torigaki, T., "Elastic Plastic Impact/Contact Problem by Adaptive Finite Element Method, ASME, Submitted, 1987.

43. Carnahan, B. and et al,"Applied Numerical Methods", Wiley,1969.

44. Beckers, P., " CAD Technology in Optimal Design", Computer Aided Optimal Design , Vol 27., Computer and System Sciences, Series F, Springer Verlag, 1987.

45. Wellen,H.,and Bartholomew, P., "Structural Optimization in Aircraft Construction",Computer Aided Optimal Design , Vol 27., Computer and System Sciences, Series F, Springer Verlag, 1987.

46. T.J.R. Hughes and T. Belytschko, "A Precis of Development in Computational Methods for Transient Analysis", ASME J. Appl. Mech. 50(1983) 1033-1041.

47. K.J. Bathe, Finite Element Procedure in Engineering Analysis (Prentice-Hall, Englewood Cliffs, N.J., 1982).

48. K. C. Park and P.G. Underwood, "A Variable Central Difference Method for Structural Dynamic Analysis- Part 1. Theoretical Aspects", Computational Meths. Appl. Mech. Eng. 22(1980) 241-258.

49. P.G. Underwood and K. C. Park , "A Variable Central Difference Method for Structural Dynamic Analysis- Part 2. Implementation and Performance Evaluation", Computational Meths. Appl. Mech. Eng. 22(1980) 259-279.

50. G. L. Goudreau and R. L. Taylor, "Evaluation of Numerical Integration Methods in Elasto-dynamics", Comp. Meths. Mech. Eng. 2(1973) 69-97.

51. H. M. Hilber, T.J.R. Hughes and P.L. Taylor, "Improved Numerical Dissipation for Time Integration Algorithms in Structural Dynamics", Earthquake Eng. Structural Dynamics 5(1977)

52. H.D. Hibbit and B.I. Karlson, "Analysis of Pipe Whip", ASME Pressure Vessel and Pipe Conference, San Francisco, CA, June 25-29, 1979.

53. L.F. Shampine, "Local Error Control in Codes for Ordinary Differential Equations", Appl. Math. Comp. 3(1977).

54. C.A. Felippa and K.C. Park, "Direct Time Integration Methods in Non-linear Structural Mechanics", Comp. Meths. Appl. Mech. Eng. 17/18(1979) 277-313.

55. P.G. Bergan and E. Mollestad, "An Automatic Time-stepping Algorithm for Dynamic Problems", Comp. Meths. Appl. Mech. Eng. 49(1985) 299-318.

56. T.J.R. Hughes, "Stability, Convergence and Growth and Decay of Energy of the Average Acceleration Method in Non-linear Structural Dynamics", Computers and Structures Vol 6, pp. 313-324(1976).

57. H.M. Hilber and T.J.R. Hughes, "Collocation, Dissipation and 'Overshoot' for Time Integration Schemes in Structural Dynamics", Earthquake Engineering and Structural Dynamics Vol. 6, 99-117(1978).

58. T. Belytschko and T.J.R. Hughes, eds, Computational Methods for Transient Analysis, Vol 1, North-Holland 1983.

59. K.C. Park, "Practical Aspects of Numerical Time Integration", Computers and Structures, vol. 7, pp. 343-353, Pergamon Press, 1977.

60. N.M. Newmark, "A Method of Computation for Structural Dynamics", J. Engng Mech. div. ASCE 85(EM3), 67-94, July 1959.

61. Krieg, R.D., and Key, S.W., "Transient Shell Response by Numerical Time Integration", in Advances in Computational Methods in Structural Mechanics and Design, eds J.C. Oden *et al.*, The Univ. of Alabama Press, Huntsville, pp. 237-257, 1972.

62. Krogh, F.T., "Algorithm for Changing the Step Size by a Multistep Method", Tech. Memo 275, Jet Propulsion Lab., California Institute of Technology, 1971.

63. Brayton, K.R., Gustavson, F.G., and Hachtel, G. D., "A New Efficient Algorithm for Solving Differential-algebraic System Using Implicit Backward Difference Formula", IEEE Proceedings, 60, pp. 98-108, 1972.

64. Zadunaisky, P.E., "On the Estimation of Error Propagated in the Numerical Integration of Ordinary Differential Equation", Numerical Methods, Vol. 27, pp. 21-39, 1976.

65. Wilkinson, J.H., "The Algebraic Eigenvalue Problem", Clarendon Press, Oxford, 1965, pp. 99-101.

66. Bathe, K.J., and Wilson, E. L., "Stability and Accuracy Analysis of Direct Integration Methods", Int. j. Earthquake Engineering and Structural Dynamics, vol.1, pp. 283-291, 1973.

67. Gear, C.W., and Tu, K.W., "The Effects of Variable Time Step Size on the Stability of Multistep Methods", SIAM j. Numerical Analysis, vol. 11, pp. 1025-1043, 1974.

68. Key, S.W., "Transient Response by Time Integration: Review of Implicit and Explicit Operators", In J. Donea(ed.), Advanced Structural Dynamics, Applied Science, London, 1978.

69. Hughes, T.J.R., "Analysis of Transient Algorithm with Particular Reference to Stability Behavior", in T. Belyschko and T.J.R. Hughes(eds.), Computational Methods for Transient Analysis, North-Holland, Amsterdam, 1983, pp. 67-155.

70. Hibbit, H.D., and Karlsonn, B.I., "Analysis of Pipe Whip", Paper 79-PVP-122, ASME, New York,1979.

71. R.E. Nickel, " Direct Integration Methods in Structural Dynamics", J. Eng. Mech. Div., ASCE, vol. 99, EM2, pp. 303-317, 1973.

72. K.C. Park, "Evaluating Time Integration Methods for Nonlinear Dynamic Analysis", in 'Finite Element Analysis of Transient Nonlinear Structural. Behavior", ASME, New York, 1978.

73. J.F. McNamara, "Solution Scheme for Problems of Nonlinear Structural Dynamics", Paper 74-PVP-30, ASME, 1974.

73. R.W.H. Wu and E.A. Witmer, "Nonlinear Transient Response of Structures by the Spatial Finite Element Method", AIAA Journal, Vol. 11, no 8, pp 1110-1117, 1973.

74. J.A. Stricklin, J.E. Martinez, J.R. Tillerson, J.H. Hong and W.E. Haisler, "Nonlinear Dynamic Analysis of Shells of Revolution by the Matrix Displacement Method", AIAA Journal, vol.9, No.4, pp. 629-636, 1971.

75. G.M. Hulbert and T.J.R. Hughes, "An Error Analysis of Truncated Starting Conditions in Step-by-step Time Integration: Consequencies for Structural Dynamics", Earthquake Engineering and Structural Dynamics, vol. 15, pp 901-910, 1987.

76. O.C. Zienkiewicz, W.L. Wood and R.L. Taylor, "An Alternative Single-step Algorithm for Dynamic Problems", Earthquake Engineering and Structural Dynamics, vol. 8, pp 31-40, 1980.

77. T. Belytschko, P. Smolinski, and W.K. Liu, "Stability of Multi-time Step Partitioned Integrator for First-order Finite Element Systems", Computer Methods in Applied Mechanics and Engineering, North-Holland, 49, pp 281-297, 1985.

78. R.W. Clough and J. Penzien, "Dynamics of Structures", McGraw-Hill, New York,1975.

79. I. Babuska, J. Chandra and J. E. Flaherty, eds., Adaptive Computational Method for Partial Differential Method, SIAM, Philadelphia, 1983.

80. Arney, David C. and Flaherty, Joseph E., "A Two Dimensional Mesh Moving Technique for Time-dependent Partial Differential Equations", J. of Comp. Physics 67,124-144(1986).

81. Adjerid, S. and Flahtery, J.,"A Moving-Mesh Finite Element Method with Local Refinement for Parabolic Partial Differential Equations", Comp Methods in Applied Method and Engineering 55, North Holland (1986).

82. Zienkiewicz, O.C. et al., "Hierarchical Finite Element Approaches, Adaptive Refinement and Error Estimates", The mathematics Finite Element Application, ed. J.R. Whitemean, Academic Press, New York, 1982.

83. E. Rank, and I. Babuska, "An Expert System for the Optimal Mesh Design in the Hp-Version of the Finite Element Method", International J. Numerical Methods in Engineering, vol. 24, 2087-2106, 1987.

84. P. Devloo, J.T. Oden and T. Strouboulis, "Implementation of an Adaptive Refinement Technique for the SUPG Algorithm", Computer Methods in Applied Mechanics and Engineering, vol. 61, pp339-358, 1987.

85. B.N. Jiang and G.F. Carey, "Adaptive Refinement for Least-square Finite Elements with Element-by-element Conjugate Gradient Solution", Int. J. Numerical Methods in Engineering, vol 24, 569-580, 1987.

86. I.D. Faux and M.J. Pratt, "Computaional Geometry for Design and Manufature", Ellis Worwood, 1979.

87. S. Braun, Mechanical Signature Analysis, Academic Press,1986.

88. Mark A. Lamontia, "On the Determination and Use of Residual Flexibilities", 1st International Modal Analysis Conference, Nov.1982.

89. Jens Trampe Broch, "Mechanical Vibration and Shoch Measurements', Bruel & Kjer, 1984.

90. William T. Thomson, Theory of Vibration with Applications, Prentice-Hall,Inc, 1981.

91. D.J. Ewins, Modal Testing Theory and Practice, RSP, England, 1986.

92. D.J. Ewins, "Why and Wherefores of Modal Testing",SEE Journal, Sept. 1979.

93. SDRC, Users Manual for Modal Analysis 9.0,U.S.A.